NAVAL POSTGRADUATE SCHOOL

MONTEREY, CALIFORNIA

THESIS

DOUBLY FED INDUCTION MACHINE CONTROL FOR WIND ENERGY CONVERSION

by

Jason G. Massey

June 2009

Thesis Advisor:	Alexander Julian
Second Reader:	Roberto Cristi

THIS PAGE INTENTIONALLY LEFT BLANK

REPORT DOCUMENTATION PAGE			Form Approved OMB No. 0704-0188
Public reporting burden for this collection of information is estimated to average 1 hour per response, including the time for reviewing instruction, searching existing data sources, gathering and maintaining the data needed, and completing and reviewing the collection of information. Send comments regarding this burden estimate or any other aspect of this collection of information, including suggestions for reducing this burden, to Washington headquarters Services, Directorate for Information Operations and Reports, 1215 Jefferson Davis Highway, Suite 1204, Arlington, VA 22202-4302, and to the Office of Management and Budget, Paperwork Reduction Project (0704-0188) Washington DC 20503.			
1. AGENCY USE ONLY *(Leave blank)*	**2. REPORT DATE** June 2009	**3. REPORT TYPE AND DATES COVERED** Master's Thesis	
4. TITLE AND SUBTITLE Doubly Fed Induction Machine Control For Wind Energy Conversion System		**5. FUNDING NUMBERS**	
6. AUTHOR(S) Jason G. Massey			
7. PERFORMING ORGANIZATION NAME(S) AND ADDRESS(ES) Naval Postgraduate School Monterey, CA 93943-5000		**8. PERFORMING ORGANIZATION REPORT NUMBER**	
9. SPONSORING /MONITORING AGENCY NAME(S) AND ADDRESS(ES) N/A		**10. SPONSORING/MONITORING AGENCY REPORT NUMBER**	
11. SUPPLEMENTARY NOTES The views expressed in this thesis are those of the author and do not reflect the official policy or position of the Department of Defense or the U.S. Government.			
12a. DISTRIBUTION / AVAILABILITY STATEMENT Approved for public release; distribution will be unlimited		**12b. DISTRIBUTION CODE**	

13. ABSTRACT (maximum 200 words)

Due to increasing concerns about CO_2 emissions and the shortage of fossil fuels, renewable energy has become a major topic in economic discussions. One renewable source is energy that can be extracted from the wind. This thesis covers the basics of using a doubly-fed induction generator (DFIG) to convert the mechanical energy of the wind into useful electrical power that can be used to supply electricity to any grid. Implementation and simulation results are analyzed in this research. The design implements digital four quadrant control of a DFIG with a direct current (DC) machine serving as the prime mover. Digital control of voltage, current and frequency in the rotor windings is accomplished using a Voltage Source Inverter (VSI), while the stator voltage and frequency is maintained by the grid. Simulation is accomplished using Matlab and Simulink software. The simulations are verified with lab hardware.

14. SUBJECT TERMS Double Fed Induction Generator (DFIG), Voltage Source Inverter (VSI), Space Vector Modulation (SVM), Wind Turbine, Field Programmable Gate Array (FPGA), Wind Energy Conversion System			**15. NUMBER OF PAGES** 115
			16. PRICE CODE
17. SECURITY CLASSIFICATION OF REPORT Unclassified	**18. SECURITY CLASSIFICATION OF THIS PAGE** Unclassified	**19. SECURITY CLASSIFICATION OF ABSTRACT** Unclassified	**20. LIMITATION OF ABSTRACT** UU

NSN 7540-01-280-5500

Standard Form 298 (Rev. 2-89)
Prescribed by ANSI Std. 239-18

THIS PAGE INTENTIONALLY LEFT BLANK

Approved for public release; distribution will be unlimited

DOUBLY FED INDUCTION MACHINE CONTROL FOR WIND ENERGY CONVERSION

Jason G. Massey
Lieutenant, United States Navy
B.S., Clemson University, 1999

Submitted in partial fulfillment of the
requirements for the degree of

MASTER OF SCIENCE IN ELECTRICAL ENGINEERING

from the

NAVAL POSTGRADUATE SCHOOL
June 2009

Author: Jason G. Massey

Approved by: Alexander L. Julian
Thesis Advisor

Roberto Cristi
Second Reader

Jeffrey B. Knorr
Chairman, Department of Electrical and Computer Engineering

THIS PAGE INTENTIONALLY LEFT BLANK

ABSTRACT

Due to increasing concerns about CO_2 emissions and the shortage of fossil fuels, renewable energy has become a major topic in economic discussions. One renewable source is energy that can be extracted from the wind. This thesis covers the basics of using a doubly-fed induction generator (DFIG) to convert the mechanical energy of the wind into useful electrical power that can be used to supply electricity to any grid. Implementation and simulation results are analyzed in this research. The design implements digital four quadrant control of a DFIG with a direct current (DC) machine serving as the prime mover. Digital control of voltage, current, and frequency in the rotor windings is accomplished using a Voltage Source Inverter (VSI), while the stator voltage and frequency is maintained by the grid. Simulation is accomplished using Matlab and Simulink software. The simulations are verified with lab hardware.

THIS PAGE INTENTIONALLY LEFT BLANK

TABLE OF CONTENTS

LIST OF FIGURES

THIS PAGE INTENTIONALLY LEFT BLANK

LIST OF TABLES

THIS PAGE INTENTIONALLY LEFT BLANK

LIST OF ABBREVIATIONS AND ACRONYMS

A/D	Analog to Digital
BNC	Bayonette Neil-Concelman Connector
DC	Direct Current
DFIG	Doubly Fed Induction Generator
FPG	Field Programmable Gate Array
FPGA	Field Programmable Gate Array
IGBT	Insulated Gate Bipolar Transistor
ISE	Integrated Software Environment
NPS	Naval Postgraduate School
PF	Power Factor
PWM	Pulse Width Modulation
SDC	Student Design Center
SVM	Space Vector Modulation
VSI	Voltage Source Inverter

THIS PAGE INTENTIONALLY LEFT BLANK

EXECUTIVE SUMMARY

Due to increasing concerns about CO_2 emissions and the finite supply of fossil fuels, renewable energy has become a major topic across the globe. Wind energy generation has attracted much interest in the last few years. Large wind farms have been planned and installed in various locations around the world. Many of these wind farms are based on the Doubly Fed Induction Generator (DFIG) technology with converter ratings around 30 percent of the generator ratings [1]. DFIGs have some advantages over synchronous and induction generators when used in wind farms, such as variable speed operation, active and reactive power control, and lower converter cost [1].

The objective of this research is to simulate and implement a wind energy conversion system via a DFIG. The control strategy utilizes a Field Programmable Gate Array (FPGA) and a Voltage Source Inverter (VSI) to implement digital four quadrant control of the rotor windings of a DFIG. Matlab/Simulink is the software resource used to design, simulate, and predict the system behavior before actual implementation. A Direct Current (DC) machine is used as mechanical load representing the wind energy source during the implementation.

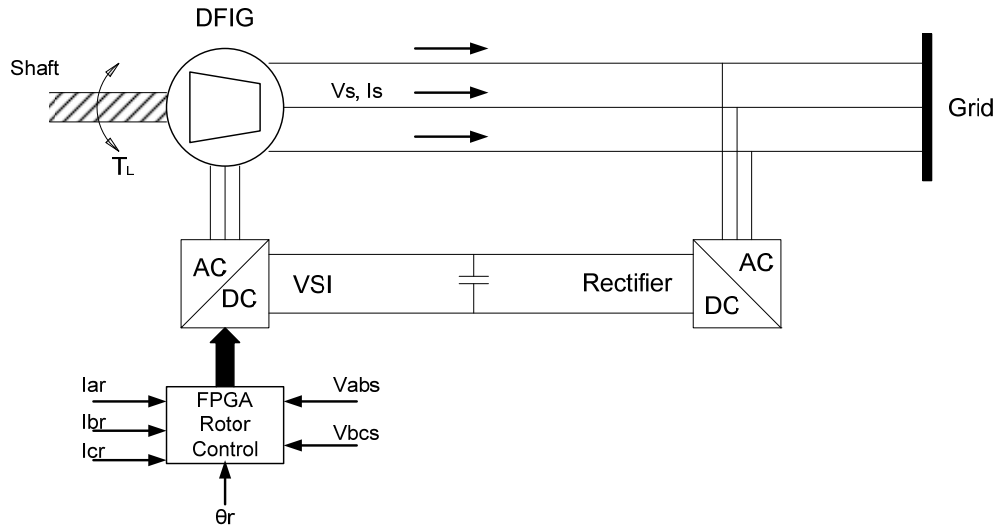

Figure 1. Simplified Circuit of DFIG Control for Wind Energy Conversion.

As seen in Figure 1, the voltage source inverter converts a 3-phase AC source to a controlled DC bus voltage. The DC voltage is then inverted into a 3-phase waveform via a digitally controlled VSI. The digital control for the Insulated Gate Bipolar Transistor (IGBT) network is implemented via a FPGA. The FPGA interface samples the voltage and current of a DFIG and speed of the DC drive through an analog to digital (A/D) converter. An algorithm then calculates the phase and amplitude of the voltage and current needed at the terminals of the rotor circuit. By controlling the phase and amplitude of the currents in the rotor windings various modes of operation and control of the DFIG can be accomplished. Real power flow and reactive power flow can be controlled, as shown in Figure 2, where the variables V_s and I_s represent the stator voltage and stator current.

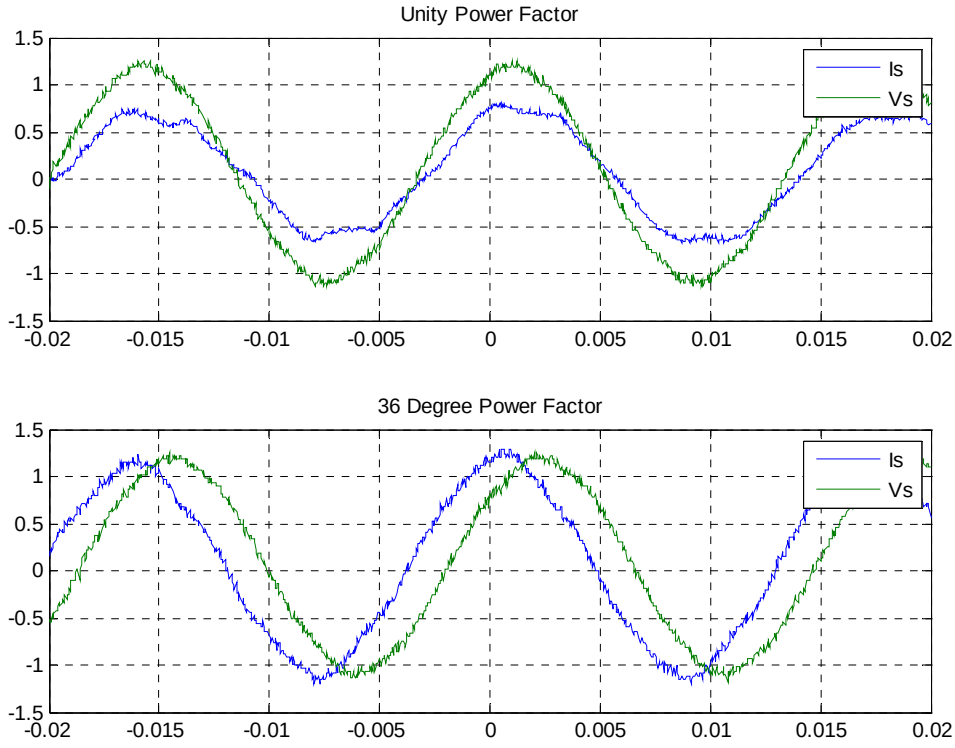

Figure 2. Power Factor Control of the stator circuit is achieved by changing the rotor currents.

A DC machine is used as the prime mover to simulate the wind. By manually controlling the torque produced by the DC machine, variable wind load conditions can be represented. As input torque is increased, the speed of the rotor changes and the position is fed into the algorithm of the FPGA. This corresponding position is then used to define the current in the rotor windings. The increase in input torque increases the output power produced by the system. See variable torque operation in Figure 3 where the stator current increases when the input torque increases. The variables V_s, I_s, and P_s represent the stator voltage, stator current, and average instantaneous output power for one phase multiplied by 3 from the stator.

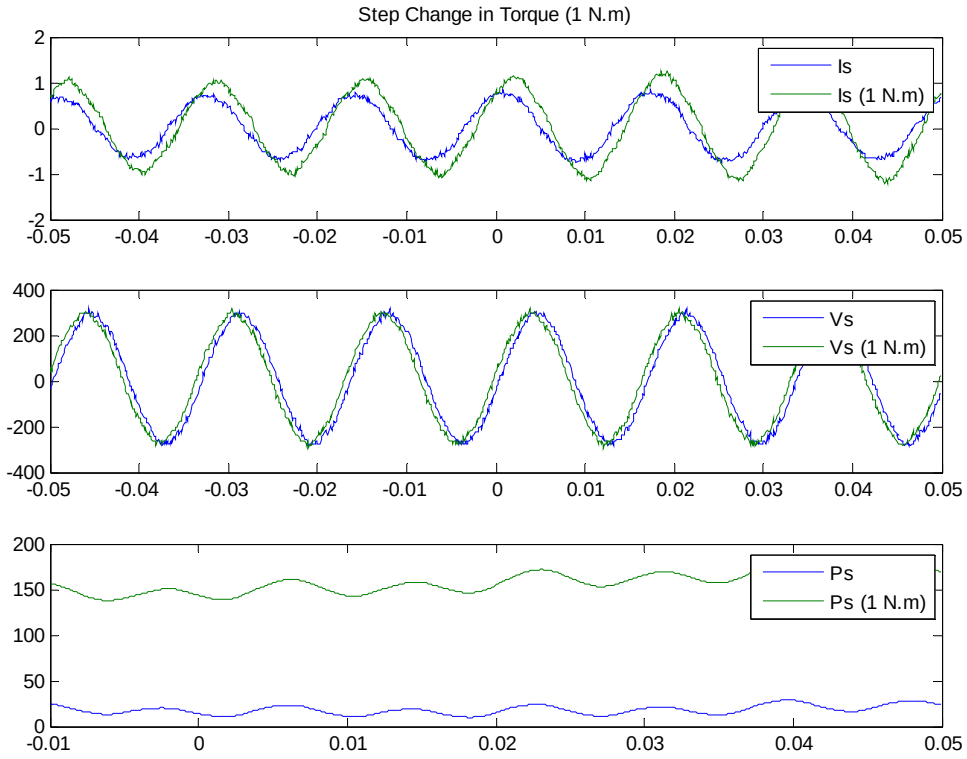

Figure 3. Step Change in Torque after steady state is reached (stator current, stator voltage and average instantaneous stator power).

The rotor current can also be used to control output power from the generator during steady state or transient conditions. An increase in the rotor current during steady state condition will cause a change in the stator current, which results in a change in the output power. Figure 4 shows a step change in rotor current and how it affects the output power for a given load on the shaft. The output power has slightly decreased because the increase in rotor current has caused the power factor to decrease. The variables I_r and P_s represent the rotor current and average instantaneous output power of one phase multiplied by 3 from the stator.

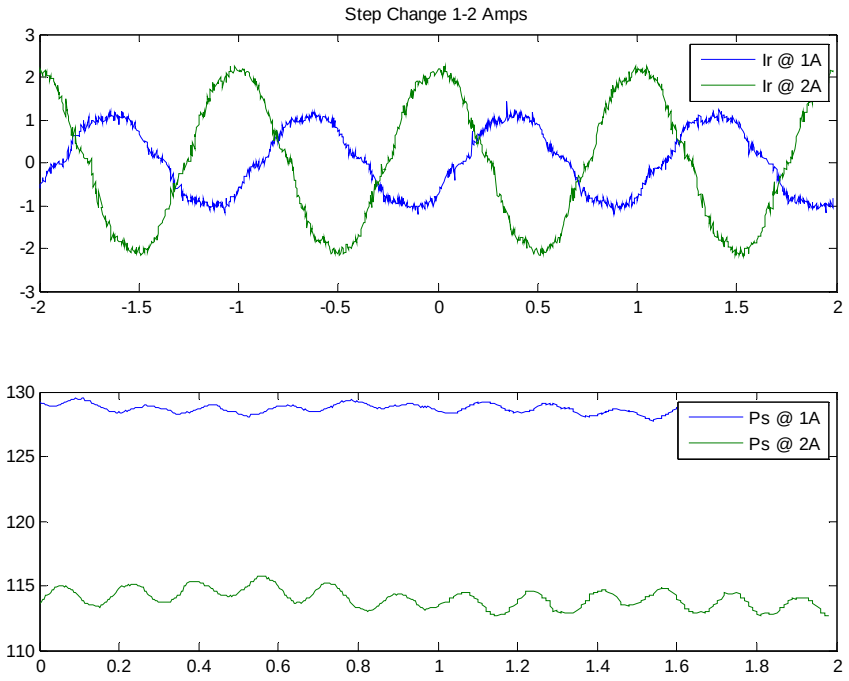

Figure 4. Output Power vs. Step Change Rotor Current after steady state is reached.

The goal of this research was to design an electrical interface for a wind energy conversion system. This thesis covers the simulation and hardware construction of a wind energy conversion system. The simulation results will be used to validate the actual implementation. Future research will investigate control schemes to improve on efficiency, effectiveness, and possibly grid fault analysis.

ACKNOWLEDGEMENTS

I would like to thank the entire faculty and staff at the Naval Postgraduate School for providing me a wonderful experience while attaining a higher education. Thank you to Professor Alexander Julian for your sound advice, knowledge that you passed on to me on digital controls of power systems, and guiding inspiration to research alternative energy sources. Thank you to Warren Rogers for assisting me in a timely matter in the lab with the special tools needed to complete my research. Most importantly, thanks Boosie and Petey for putting up with me.

THIS PAGE INTENTIONALLY LEFT BLANK

I. INTRODUCTION

A. PURPOSE

The mission at the Naval Postgraduate School (NPS) is to provide students with the highest quality and most defense-relevant graduate education available in computer and electrical engineering. The United States President's Agenda on Energy and the Environment encourages the development of energy sources that will increase national security by decreasing our dependence on foreign oil, ensure that 10 percent of our electricity comes from renewable sources by 2012, and 25 percent by 2025 [2]. Wind energy is a very promising renewable energy source of the future and is part of the president's overall strategy to develop a diverse portfolio of domestic energy supplies. This thesis supports the NPS mission and one topic discussed in the President's Agenda on Energy and the Environment by using a wind energy conversion system as a means of increasing national security by harnessing one of nature's renewable energy sources.

B. RESEARCH OBJECTIVE

The goal of this thesis was to build a computer simulation of a Wind Energy Conversion System, based on mathematical equations, through the use of Mathworks' Simulink software. Once the simulation is complete, a fully functioning model of a Wind Energy Conversion System is built, so that various tests on the simulation and the physical system can be performed to compare the simulation results with the physical model. Based on the successful results of the system, we lay the groundwork for future research in the NPS power labs in the field of renewable energy.

C. APPROACH

The first step is to generate a computer simulation of the system, shown in Figure 1. There are numerous ways of simulating a DFIG, but the one used for this thesis is covered in [3]. In particular, a computer model of a DFIG based on mathematical equations is simulated in the rotor reference frame. A current control algorithm is designed in Simulink along with the Xilinx toolbox that controls the rotor currents to

produce the required voltage and frequency needed on the power grid. The wind is simulated via a torque input block. This model allows for representation of various modes of operation, which will be useful for future research, but for this thesis we concentrate on variable load conditions on the rotor, which simulate changes in the wind speed. With a working simulation and the ability to control rotor currents, various modes of operation and control are analyzed through the Simulink software.

The physical system consists of a DFIG, VSI, Student Design Center (SDC) [4], encoder, and a DC drive used to simulate changes in wind speed. The DFIG is connected to the grid via the stator windings and to the VSI via the rotor windings. The SDC is the mechanism by which the control algorithm is implemented. The SDC measures the applicable system parameters and outputs the appropriate control signals to the VSI to control the rotor currents in a fashion that allows for a specific mode of operation. In this research, variable wind speed control, and active and reactive power control are demonstrated.

D. THESIS ORGANIZATION

This thesis is organized as follows. Chapter II covers the theory of induction machines. The equations that represent voltage, flux linkage, and reference frame transformations are discussed. The testing procedure used to measure and calculate the machine parameters used for simulation are also discussed. Lastly, Chapter II explains how the voltage and flux equations and machine parameters are used to model the system. Chapter III is dedicated to the control algorithm. It explains how an algorithm is formulated based on the equations derived in Chapter II and are manipulated to control the simulation and the physical system. Chapter IV displays the results of the working system and compares the actual results to the simulation results. Chapter V discusses the conclusions and the continuation research objectives for this thesis. Appendix A, B, C and D contain Matlab files, data sheets for equipment used, a full schematic layout of all Simulink systems, and transformation derivations used in this thesis.

II. DFIG SIMULATION

A. MATHEMATICAL REPRESENTATION OF DFIG

In order to simulate the Wind Energy Conversion System a proven method is needed to represent the characteristics of a DFIG. The equations used to characterize the DFIG used in this research are obtained from [3]. The rest of this section is devoted to the mathematical equations that describe a DFIG.

The voltage equations to represent a 3-phase induction machine can be expressed as follows,

$$\begin{aligned}\left[v_{abcs}\right] &= \left[r_s\right]\left[i_{abcs}\right] + \rho\left[\lambda_{abcs}\right] \\ \left[v_{abcr}\right] &= \left[r_r\right]\left[i_{abcr}\right] + \rho\left[\lambda_{abcr}\right]\end{aligned} \tag{1}$$

where *v*, *r*, *i*, and λ respectively refer to the voltage, resistance, current, and flux linkage of the phase windings. The subscripts *a*, *b*, and *c* refer to their phase component. The subscripts *r* and *s* refer to the stator and rotor windings. The term ρ represents the derivative$\left(\frac{d}{dt}\right)$. The flux linkages shown in (1) for a linear magnetically coupled circuit are expressed as

$$\begin{bmatrix}\lambda_{abcs} \\ \lambda_{abcr}\end{bmatrix} = \begin{bmatrix}L_s & L_{sr} \\ \left(L_{sr}\right)^T & L_r\end{bmatrix}\begin{bmatrix}i_{abcs} \\ i_{abcr}\end{bmatrix} \tag{2}$$

where *L* refers to the inductance in the respective winding. The subscript *sr* represents the mutual coupling between the stator and rotor windings. Finally, to complete equations that describe an induction machine the winding inductances are defined as

$$L_s = \begin{bmatrix}L_{ls}+L_{ms} & -\frac{1}{2}L_{ms} & -\frac{1}{2}L_{ms} \\ -\frac{1}{2}L_{ms} & L_{ls}+L_{ms} & -\frac{1}{2}L_{ms} \\ -\frac{1}{2}L_{ms} & -\frac{1}{2}L_{ms} & L_{ls}+L_{ms}\end{bmatrix} \tag{3}$$

$$L_r = \begin{bmatrix} L_{lr} + L_{mr} & -\frac{1}{2}L_{mr} & -\frac{1}{2}L_{mr} \\ -\frac{1}{2}L_r & L_{lr} + L_{mr} & -\frac{1}{2}L_{mr} \\ -\frac{1}{2}L_{mr} & -\frac{1}{2}L_{mr} & L_{lr} + L_{mr} \end{bmatrix} \tag{4}$$

$$L_{sr} = L_{sr} \begin{bmatrix} \cos\theta_r & \cos\left(\theta_r + \frac{2\pi}{3}\right) & \cos\left(\theta_r - \frac{2\pi}{3}\right) \\ \cos\left(\theta_r - \frac{2\pi}{3}\right) & \cos\theta_r & \cos\left(\theta_r + \frac{2\pi}{3}\right) \\ \cos\left(\theta_r + \frac{2\pi}{3}\right) & \cos\left(\theta_r - \frac{2\pi}{3}\right) & \cos\theta_r \end{bmatrix} \tag{5}$$

where the variables L_{ls} and L_{ms} are the leakage and magnetizing inductances of the stator windings, L_{lr} and L_{mr} are for the rotor windings. The variable L_{sr} is the amplitude of the mutual inductance between the stator and rotor windings and θ_r is the angular position of the rotor.

As a standard practice and for convenience, the rotor variables are referred to the stator windings by the appropriate turn ratio *N*.

$$i'_{abcr} = \frac{N_r}{N_s} i_{abcr} \tag{6}$$

$$v'_{abcr} = \frac{N_s}{N_r} v_{abcr} \tag{7}$$

$$\lambda'_{abcr} = \frac{N_s}{N_r} \lambda_{abcr} \tag{8}$$

$$r' = \left(\frac{N_s}{N_r}\right)^2 r_r. \tag{9}$$

The magnetizing and mutual inductances are associated with the same magnetic flux path and related by the following equations.

$$L_{ms} = \frac{N_s}{N_r} L_{sr} \tag{10}$$

$$L_r' = \left(\frac{N_s}{N_r}\right)^2 L_r \tag{11}$$

$$L_{lr}' = \left(\frac{N_s}{N_r}\right)^2 L_{lr} \tag{12}$$

By defining $L_{sr}' = \frac{N_s}{N_r} L_{sr}$ and $L_{mr}' = \left(\frac{N_s}{N_r}\right)^2 L_{ms}$ the rotor inductance variables can be referred to the stator windings as

$$L_{sr}' = L_{ms}\begin{bmatrix} \cos\theta_r & \cos\left(\theta_r + \frac{2\pi}{3}\right) & \cos\left(\theta_r - \frac{2\pi}{3}\right) \\ \cos\left(\theta_r - \frac{2\pi}{3}\right) & \cos\theta_r & \cos\left(\theta_r + \frac{2\pi}{3}\right) \\ \cos\left(\theta_r + \frac{2\pi}{3}\right) & \cos\left(\theta_r - \frac{2\pi}{3}\right) & \cos\theta_r \end{bmatrix} \tag{13}$$

$$L_r' = \begin{bmatrix} L_{lr}' + L_{ms} & -\frac{1}{2}L_{ms} & -\frac{1}{2}L_{ms} \\ -\frac{1}{2}L_{ms} & L_{lr}' + L_s & -\frac{1}{2}L_{ms} \\ -\frac{1}{2}L_{ms} & -\frac{1}{2}L_{ms} & L_{lr}' + L_{ms} \end{bmatrix}. \tag{14}$$

Substituting (13 and 14) into (1 and 2), the flux linkage and voltage variables referred to the stator windings, can now be expressed as

$$\begin{bmatrix} \lambda_{abcs} \\ \lambda_{abcr}' \end{bmatrix} = \begin{bmatrix} L_s & L_{sr}' \\ \left(L_{sr}'\right)^T & L_r \end{bmatrix} \begin{bmatrix} i_{abcs} \\ i_{abcr}' \end{bmatrix} \tag{15}$$

$$\begin{aligned} \left[v_{abcs}\right] &= \left[r_s\right]\left[i_{abcs}\right] + \rho\left[\lambda_{abcs}\right] \\ \left[v_{abcr}'\right] &= \left[r_r'\right]\left[i_{abcr}'\right] + \rho\left[\lambda_{abcr}'\right]. \end{aligned} \tag{16}$$

The voltages and flux linkages in (15 and 16) describe the behavior of a DFIG and have components that vary with time and rotor position. A change of variables is used to reduce the complexity of these differential equations. A change of variables that formulates a transformation of balanced 3-phase equations to a new reference frame may be expressed as

$$\begin{bmatrix} f_{qd0s}^{x} \end{bmatrix} = K_s^x \begin{bmatrix} f_{abcs} \end{bmatrix}$$
$$\begin{bmatrix} f'^{x}_{qd0r} \end{bmatrix} = K_r^x \begin{bmatrix} f'_{abcr} \end{bmatrix} \tag{17}$$

where the matrix K_s for stator variables and K_r for rotor variables is expressed as

$$K_s = \frac{2}{3}\begin{bmatrix} \cos\theta & \cos\left(\theta - \frac{2\pi}{3}\right) & \cos\left(\theta + \frac{2\pi}{3}\right) \\ \sin\theta & \sin\left(\theta - \frac{2\pi}{3}\right) & \sin\left(\theta + \frac{2\pi}{3}\right) \\ \frac{1}{2} & \frac{1}{2} & \frac{1}{2} \end{bmatrix} \tag{18}$$

$$K_r = \frac{2}{3}\begin{bmatrix} \cos\beta & \cos\left(\beta - \frac{2\pi}{3}\right) & \cos\left(\beta + \frac{2\pi}{3}\right) \\ \sin\beta & \sin\left(\beta - \frac{2\pi}{3}\right) & \sin\left(\beta + \frac{2\pi}{3}\right) \\ \frac{1}{2} & \frac{1}{2} & \frac{1}{2} \end{bmatrix}. \tag{19}$$

The variable θ in (18 and 19) is the position of the reference frame for the f_{abc} variables and $\beta = \theta - \theta_r$. The x in (17) represents the particular frame of reference that the variables are transformed while *f* represents the voltage, current, or flux linkages in the stator or rotor windings. In the remaining equations in this chapter the absence of a variable in the place holder of x represents an arbitrary frame of reference.

$${}^{x}K^{y} = \begin{bmatrix} \cos\left(\theta_y - \theta_x\right) & \sin\left(\theta_y - \theta_x\right) & 0 \\ -\sin\left(\theta_y - \theta_x\right) & \cos\left(\theta_y - \theta_x\right) & 0 \\ 0 & 0 & 1 \end{bmatrix} \tag{20}$$

To transform between reference frames use (20) where y represents the new frame of reference. Utilizing a little trigonometry, and performing the transformation in (17) on each component in the matrices on the right hand side of (16), the voltage equations can now be expressed in the arbitrary reference frame as

$$
\begin{aligned}
v_{qs} &= r_s i_{qs} + \omega\lambda_{qs} + \rho\lambda_{qs} \\
v_{ds} &= r_s i_{ds} - \omega\lambda_{ds} + \rho\lambda_{ds} \\
v_{0s} &= r_s i_{0s} + \rho\lambda'_{0r} \\
v'_{qr} &= r'_s i'_{qs} + (\omega - \omega_r)\lambda'_{qs} + \rho\lambda'_{qs} \\
v'_{dr} &= r'_s i'_{ds} - (\omega - \omega_r)\lambda'_{ds} + \rho\lambda'_{ds} \\
v'_{0r} &= r'_s i'_{0s} + \rho\lambda'_{0r}
\end{aligned} \tag{21}
$$

where ω_r is the rotational speed of the rotor and ω is the speed of the reference frame that the variables are transformed in radians per second. The next step is to express the inductance component of the flux linkages in (21) as a reactance instead of as an inductance. This is convenient because in the next section (Induction Motor Test) the actual machine parameters are measured and calculated in ohms. The inductance is converted to reactance at a base frequency (ω_b) of 377 radians per second and (21) is rewritten as

$$
\begin{aligned}
v_{qs} &= r_s i_{qs} + \frac{\omega}{\omega_b}\psi_{ds} + \frac{\rho}{\omega_b}\psi_{qs} \\
v_{ds} &= r_s i_{ds} - \frac{\omega}{\omega_b}\psi_{qs} + \frac{\rho}{\omega_b}\psi_{ds} \\
v_{0s} &= r_s i_{0s} + \frac{\rho}{\omega_b}\psi_{0s} \\
v'_{qr} &= r'_r i'_{qr} + \frac{(\omega - \omega_r)}{\omega_b}\psi'_{dr} + \frac{\rho}{\omega_b}\psi'_{qr} \\
v'_{dr} &= r'_r i'_{dr} - \frac{(\omega - \omega_r)}{\omega_b}\psi'_{qr} + \frac{\rho}{\omega_b}\psi'_{dr} \\
v'_{0r} &= r'_r i'_{0r} + \frac{\rho}{\omega_b}\psi'_{0r}.
\end{aligned} \tag{22}
$$

The flux linkage component of (21) now has units of flux linkage per second and represented by the symbol ψ. For ease of understanding the flux linkages in (21) and flux linkage per second in (22) are compared

$$
\begin{aligned}
\lambda_{qs} &= L_{ls} i_{qs} + L_{ms}(i_{qs} + i'_{qr}) \\
\lambda_{ds} &= L_{ls} i_{ds} + L_{ms}(i_{ds} + i'_{dr}) \\
\lambda_{0s} &= L_{ls} i_{0s} \\
\lambda'_{qr} &= L_{lr} i_{qr} + L_{ms}\left(i_{qs} + i'_{qr}\right) \\
\lambda'_{dr} &= L_{lr} i_{dr} + L_{ms}\left(i_{ds} + i'_{dr}\right) \\
\lambda'_{0r} &= L_{lr} i'_{0r}
\end{aligned}
\tag{23}
$$

$$
\begin{aligned}
\psi_{qs} &= X_{ls} i_{qs} + X_{ms}(i_{qs} + i'_{qr}) \\
\psi_{ds} &= X_{ls} i_{ds} + X_{ms}(i_{ds} + i'_{dr}) \\
\psi_{0s} &= X_{ls} i_{0s} \\
\psi'_{qr} &= X'_{lr} i_{qr} + X_{ms}\left(i_{qs} + i'_{qr}\right) \\
\psi'_{dr} &= X'_{lr} i_{dr} + X_{ms}\left(i_{ds} + i'_{dr}\right) \\
\psi'_{0r} &= X'_{lr} i'_{0r}.
\end{aligned}
\tag{24}
$$

Equations (21 and 22) are derived in this section and mathematically represent the behavior of a DFIG. The next section discusses how to measure and calculate the parameters of the actual machine used in this thesis.

B. INDUCTION MOTOR TEST

In order to efficiently model the system in Matlab and Simulink, the physical machines parameters are used for the simulation. The DFIG, model 8231, used for this research is part of the Lab-Volt Electro-Mechanical System (EMS) and consists of a 4-pole, 0.25 horsepower, 120 volt, 60 hertz, wave wound rotor machine. The stator consists of a set of 3-phase wye-connected windings with turns N_s and resistance R_s. The rotor consists of a set of 3-phase wye-connected windings with turns N_r and resistance R_r. The induction motor test performed is carried out as in [5].

The steady state operating characteristics of the DFIG was analyzed using a per-phase equivalent circuit shown in Figure 5. The DFIG was converted to an Induction machine for the parameter test by short circuiting the rotor winding terminals in a wye-configuration. The variables V_s, R_s and X_{ls} represent the voltage, resistance, and leakage reactance of the stator. The variables V_r', R_r', and X_{lr}' represent the voltage, resistance and leakage reactance of the rotor referred to the stator. X_{ms} represents the stator magnetizing reactance and s is the slip.

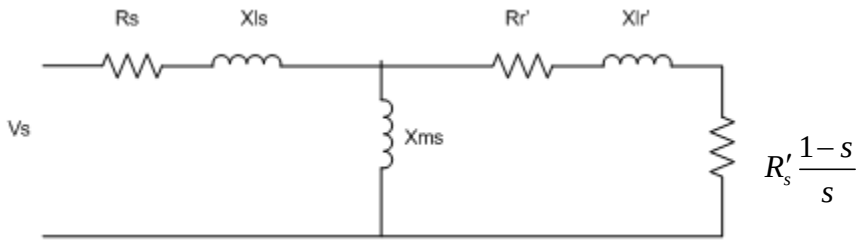

Figure 5. Induction Motor Equivalent Circuit (From [5]).

1. DC Test

The first parameter test ran was to calculate the stator winding resistance for each phase. This test consisted of applying a known DC voltage to the stator terminals and measuring the current flow through the windings. The DC test on the stator windings is useful because it does not induce a voltage in the stator or rotor windings and eliminates the need to measure or calculate any reactance caused by induced voltages. The only circuit parameter limiting current flow is R_s. The measured voltage and current values are inserted into (25) and the stator resistance R_s is calculated. This test is performed on each phase of the stator windings and the three values are averaged together.

$$R_s = \frac{V_{dc}}{I_{dc}} \tag{25}$$

2. No Load Test

A no-load test is performed to measure the rotational losses and other equivalent circuit parameters needed in the blocked rotor test. In this test, rated voltage and frequency is applied to the stator while the machine is running at no load. The input power, phase voltage, and phase current are measured for each phase and averaged. At no load, the slip is very small and the rotor branch impedance is very large. Therefore, all the real power is dissipated in the stator resistance. The machine at no load is very inductive, so the input impedance is expressed as

$$\frac{\left|V_{a,nL}\right|}{\left|I_{a,nL}\right|} = \sqrt{R_s^{\,2} + \left(X_{ms} + X_{ls}\right)^2}. \tag{26}$$

From this equation, we can solve for the quantity $X_{ms} + X_{ls}$, which is used in the blocked rotor test.

3. Blocked Rotor Test

The blocked rotor test is performed to calculate the remaining circuit parameters. In this test, the rotor of the induction machine is blocked and a reduced voltage is applied to the terminals so that rated current flows through the stator windings of the machine. The input power, voltage, and current are measured and averaged. When the rotor is blocked, the slip is equal to one. As a result, the rotor branch impedance is very small and the magnetizing impedance is ignored. Real power is only consumed by the stator and rotor resistances. The sum of the stator and rotor resistances can be solved as

$$R_s + R_r' = \frac{\left(P_{in}\right)}{3\left|I_a\right|^2}. \tag{27}$$

The input impedance is expressed as

$$\frac{\left|V_{a,br}\right|}{\left|I_{a,br}\right|} = \sqrt{\left(R_s + R_r'\right)^2 + \left(X_{ls} + X_{lr}'\right)^2} \tag{28}$$

where it is assumed that $X_{ls} = X_{lr}$. Substituting the result of (27) into (28) allows us to solve for the numerical quantities of X_{ls} and X_{lr}. From this point X_{ms} can be calculated by substituting the stator leakage reactance value into equation (26). Table 1 below is a summary of parameters calculated from the DFIG used for this thesis.

Parameters (Ω)	
Stator Resistance $\left(r_s\right)$	12
Stator Leakage Reactance $\left(X_{ls}\right)$	9.1
Rotor Resistance $\left(r_r'\right)$	15
Rotor Reactance $\left(X_{lr}'\right)$	9.1
Magnetizing Reactance $\left(X_{ms}\right)$	126

Table 1. DFIG Measured Values at 60 Hz.

C. DFIG COMPUTER MODEL

The equations (22 and 24) are the basis for simulating the DFIG. A block diagram of the simulation setup is shown in Figure 6. The model simulates the DFIG in the rotor reference frame. Although the equations that represent a DFIG have been defined, they still need to put in a form that is useful for computer simulation. We also need to define the torque, power, and rotor speed equations, which are needed for simulating the machine.

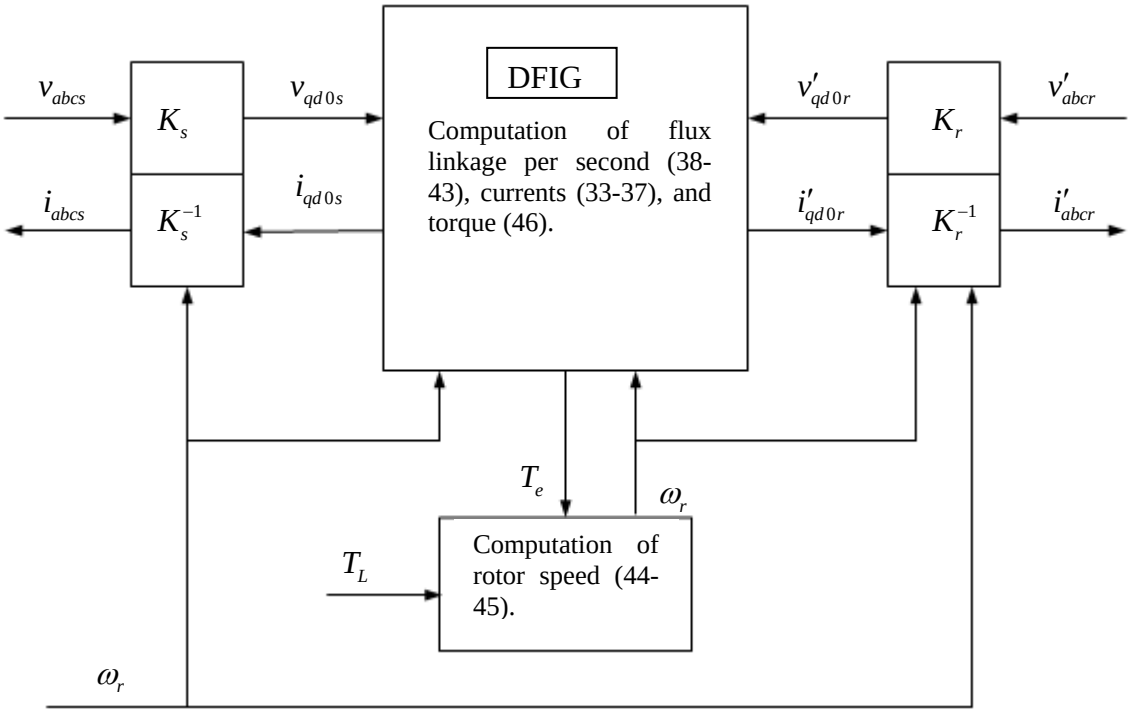

Figure 6. DFIG Computer Model in Block Form (After [3]).

The first step is to solve the flux linkage per second equations of (22) for current. We do this by defining four new variables in terms of quantities calculated in the induction motor test

$$\psi_{mq} = X_{ms}\left(i_{qs} + i'_{qr}\right) = X_{aq}\left(\frac{\psi_{qs}}{X_{ls}} + \frac{\psi'_{qr}}{X'_{lr}}\right) \tag{29}$$

$$\psi_{md} = X_{ms}\left(i_{ds} + i'_{dr}\right) = X_{ad}\left(\frac{\psi_{ds}}{X_{ls}} + \frac{\psi'_{dr}}{X'_{lr}}\right) \tag{30}$$

where

$$X_{aq} = X_{ad} = \left(\frac{1}{X_{ms}} + \frac{1}{X_{ls}} + \frac{1}{X'_{lr}}\right). \tag{31}$$

The currents are now defined as

$$i_{qs} = \frac{1}{X_{ls}}\left(\psi_{qs} - \psi_{mq}\right) \tag{32}$$

$$i_{ds} = \frac{1}{X_{ls}}\left(\psi_{ds} - \psi_{md}\right) \tag{33}$$

$$i_{0s} = \frac{1}{X_{ls}}\psi_{0s} \tag{34}$$

$$i'_{qr} = \frac{1}{X'_{lr}}\left(\psi'_{qr} - \psi_{mq}\right) \tag{35}$$

$$i'_{dr} = \frac{1}{X'_{lr}}\left(\psi'_{dr} - \psi_{md}\right) \tag{36}$$

$$i'_{0r} = \frac{1}{X'_{lr}}\left(\psi'_{0r}\right). \tag{37}$$

Now that the current equations have been defined, the flux linkage per second equations in (22) are rewritten as integral equations defined in terms of the four new variables from (29-31). The final form of the flux linkage equations that are used to simulate the DFIG shown in Figure 6 are represented as

$$\psi_{qs} = \omega_b \int \left[v_{qs} - \frac{\omega}{\omega_b}\psi_{ds} + \frac{r_s}{X_{ls}}\left(\psi_{mq} - \psi_{qs}\right) \right] \tag{38}$$

$$\psi_{ds} = \omega_b \int \left[v_{ds} + \frac{\omega}{\omega_b}\psi_{qs} + \frac{r_s}{X_{ls}}\left(\psi_{md} - \psi_{ds}\right) \right] \tag{39}$$

$$\psi_{0s} = \omega_b \int \left[v_{0s} - \frac{r_s}{X_{ls}}\psi_{0s} \right] \tag{40}$$

$$\psi'_{qr} = \omega_b \int \left[v'_{qr} - \left(\frac{\omega - \omega_r}{\omega_b} \right) \psi'_{dr} + \frac{r_r}{X'_{lr}} \left(\psi_{mq} - \psi'_{qr} \right) \right] \tag{41}$$

$$\psi'_{dr} = \omega_b \int \left[v'_{dr} + \left(\frac{\omega - \omega_r}{\omega_b} \right) \psi'_{dr} + \frac{r_r}{X'_{lr}} \left(\psi_{md} - \psi'_{dr} \right) \right] \tag{42}$$

$$\psi'_{0r} = \omega_b \int \left[v'_{0r} - \frac{r'}{X'_{lr}} \psi'_{0r} \right]. \tag{43}$$

The rotor position, which is needed to transform the equations to the respective frame of reference, is

$$\omega_r = \int \frac{\left(T_e - T_L \right) P}{2J} \, dt \tag{44}$$

where T_e and T_I, represent the electrical torque generated in the machine and input torque on the shaft of the rotor. The variables P and J are the number of machine poles and the inertia of rotor. Once the speed of the rotor is obtained, the position is calculated as

$$\theta_r = \int \omega_r \, dt. \tag{45}$$

The electrical torque and the power equations are defined as

$$T_e = \left(\frac{3}{2} \right) \left(\frac{P}{2} \right) \left(\psi_{ds} i_{qs} - \psi_{qs} i_{ds} \right) \tag{46}$$

$$P = \left(\frac{3}{2} \right) \left(v_{qs} i_{qs} + v_{ds} i_{ds} \right). \tag{47}$$

D. SIMULINK IMPLEMENTATION OF DFIG

The DFIG from Figure 6 is implemented with Simulink Software. The following Figures 7 and 8 show how (38-46) are implemented using the Simulink software to represent the DFIG.

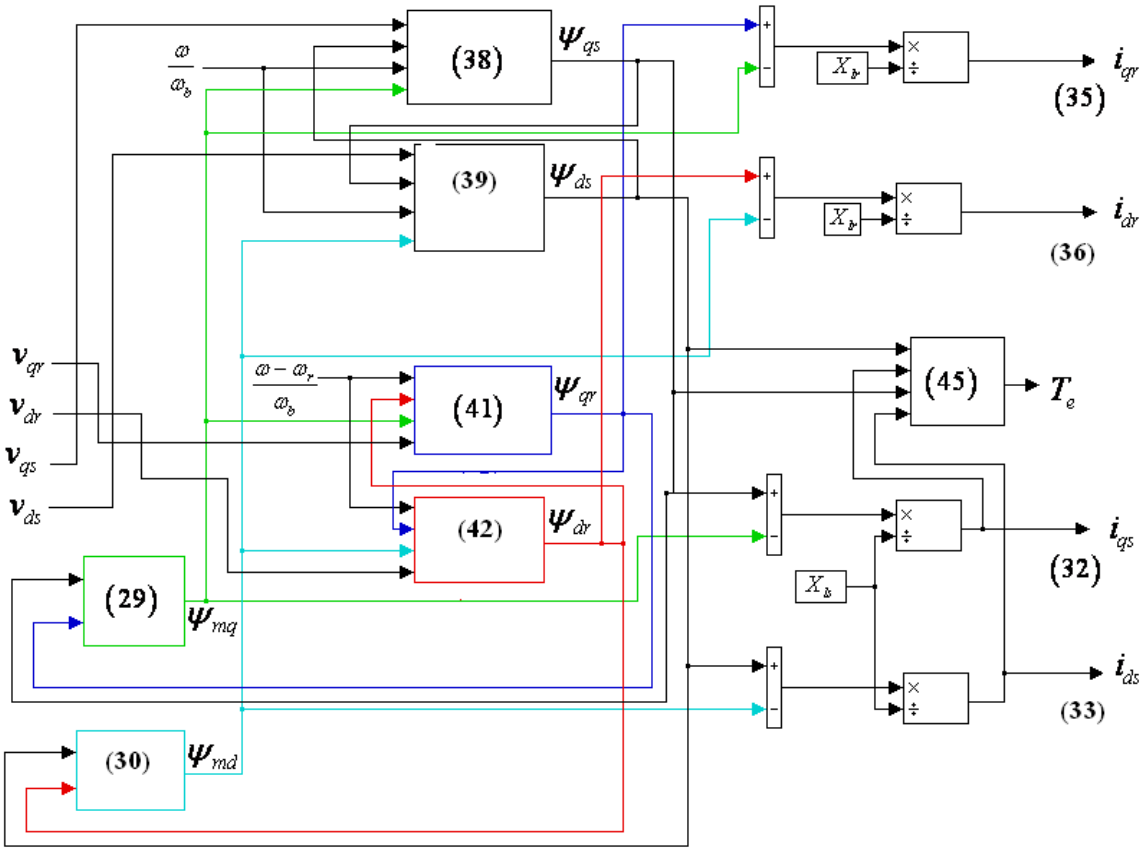

Figure 7. DFIG Simulink Simulation (From [6]).

Figure 7 shows the blocks where the flux linkage per second equations are implemented, and how they are used to compute the rotor and stator currents. The respective equation number is annotated on each block along with the associated input and output. Figure 8 is a drill down into the block that represents (38) the stator flux linkage per second on the q-axis. As seen in Figure 7, there are four inputs and one output, which also serve as an input to the same block. Using the basic mathematical operators in the Simulink library (38) is represented as shown in Figure 8. The remaining blocks for each equation that represent the DFIG are built the same way and can be found in Appendix C.

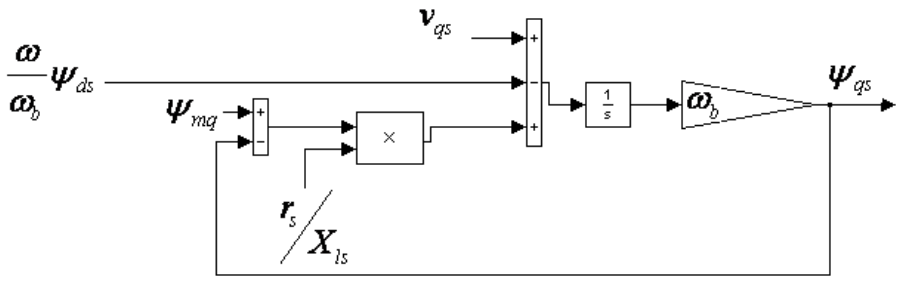

Figure 8. Equation 38.

In conclusion, this chapter described the methods in which to simulate the DFIG used in this thesis. The next chapter will discuss the methodology used to control the Wind Energy Conversion System.

III. CONTROLLER

A. CONTROLLER TOPOLOGY

As stated earlier, one of the components of the wind energy conversion system is the rectifier and VSI. The VSI and rectifier used for this research are a combined package manufactured by SEMIKRON and called a SEMISTACK. The SEMISTACK consists of a three phase rectifier and three phase inverter. The inverters inside the SEMISTACK are made of SKM 50 GB 123D IGBTs that are controlled by SEMIKRON SKHI 22 gate drivers. The VSI is used to control the magnitude, frequency, and phase angle of the currents in the rotor. The rectifier produces a constant DC voltage to the VSIs. The control for each IGBT in the SEMISTACK is implemented through the SDC. The SDC utilizes a Xilinx Field Programmable Gate Array (FPGA) chip and a control board that has various inputs and outputs that interface with the SEMISTACK and DFIG. One of the inputs is an 8-channel, 12-bit A/D converter used to measure the voltage and current signals from the DFIG. Another input samples the rotor speed. The pre-programmed FPGA chip, based on the sampled inputs, outputs the desired gate signals to the control board. The control board has BNC (Bayonette Neil-Concelman) connecters that connect to the SEMISTACK's gate drivers. The gate drive signals activate the IGBTs in a fashion that will produce the desired 3-phase current in the rotor windings. The SDC has many parts and functions, which make it useful as a design and analysis tool. The procedure for using the SDC, architecture of internal components, and the benefits of using a FPGA for digital control of power systems are discussed in [4].

Figure 9 is a Simulink block diagram of the Wind Energy Conversion System. The diagram shows where the controller samples each input and the corresponding outputs that go to the DFIG. The controller is physically located inside the SDC for the hardware design. It is important to note that the same controller logic used for simulation is used in the hardware design; therefore, the input/output blocks shown in the simulation block diagram symbolize actual connections to the SDC from the grid and the DFIG.

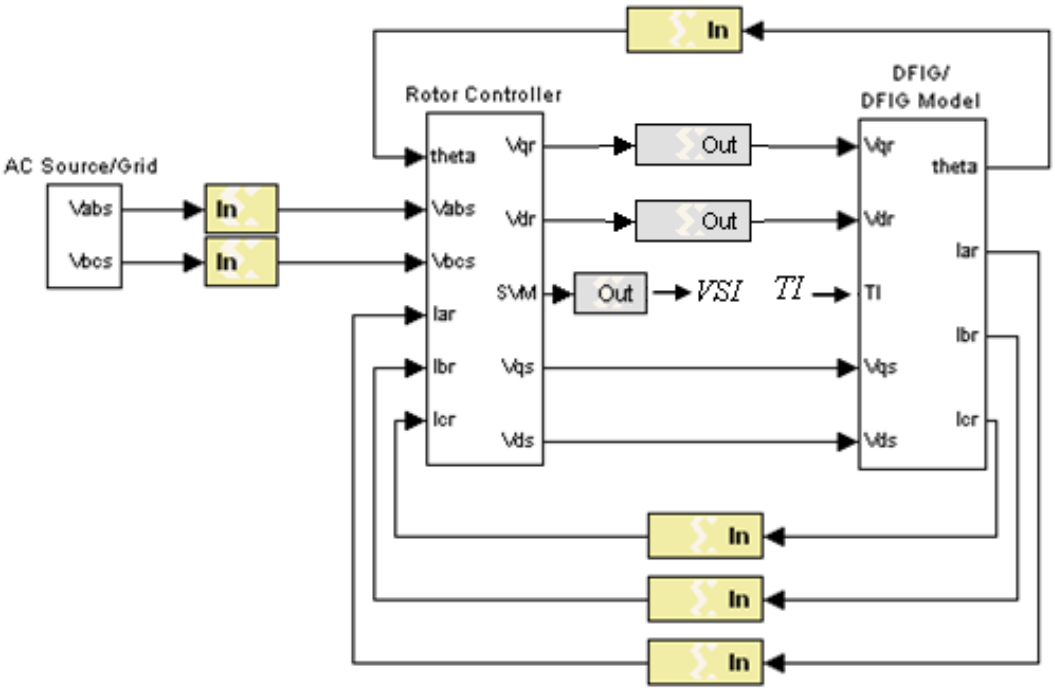

Figure 9. Simulation of DFIG Control for Wind Energy Conversion.

Figure 10 is a drill down of the Rotor Controller Block. The same logic blocks used in the simulation to control the DFIG model are used in the hardware configuration to control the DFIG with one exception. An additional set of logic blocks is added to implement Space Vector Modulation (SVM) which is one of many techniques that can be implemented on a VSI to create sinusoidal 3-phase waveforms and will be discussed more in Section B.7. For now, it is important to know that inside the rotor controller there is a separate SVM block that is not needed for simulation. Figure 10 shows how the rotor controller is used for the simulation and hardware design. The next section explains how each of the components in Figure 10 is used to control the rotor current.

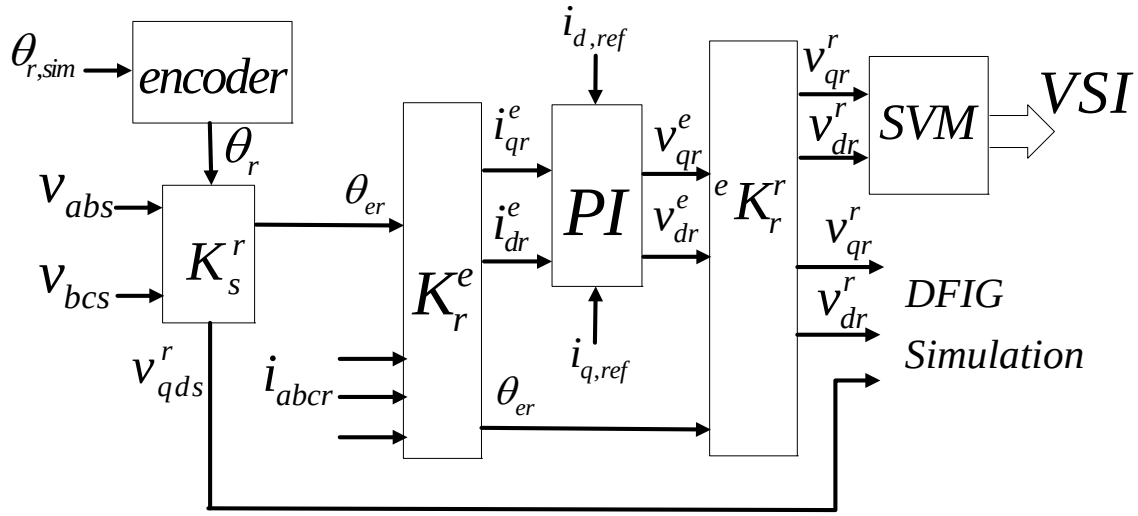

Figure 10. Rotor Controller Block Diagram.

B. CONTROLLER COMPONENTS

1. Voltage Source Simulation

The simulation required a voltage block to simulate the voltages on the grid. The design of the source is shown in Figure 11. The voltage block models the rated parameters of the DFIG used for this thesis. The voltage block produces three sinusoidal waveforms at 60 hertz with peak amplitude of $120*\sqrt{2}$ and displaced equally 120 degrees apart. The controller setup requires only two voltage inputs so the line to line values are extracted as shown.

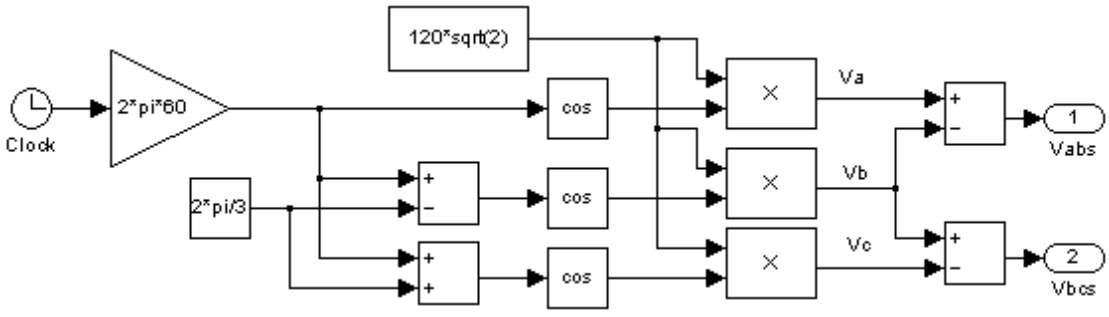

Figure 11. Voltage Source Simulation.

2. Transformation of Stator Voltage

As seen in Figure 10, the stator voltages are fed into the rotor controller where they are transformed to the rotor reference frame. The transformation $\left[f_{qd0s} \right] = K_s \left[f_{abcs} \right]$ in (17) is slightly modified to transform the line-to-line voltages v_{abs} and v_{bcs} to the rotor reference frame (See Appendix D). Figure 12 demonstrates how the transformation is performed with the Xilinx library set. The constant 85 in Figure 12 corresponds to a 30 degree phase shift from the transformation in Appendix D. The sin and cosine blocks from the Xilinx library use a 10 bit lockup table to represent angles from 0-360 degrees. The angle θ_{er} is obtained by taking the angle from arctangent of the transformed voltages and represents the electrical position of the currents in the rotor. This angle is used to transform the rotor currents to the synchronously rotating reference frame. The voltage d-axis component is inverted before taking the arctangent to account for the d-axis being 180 degrees out of phase from the y-axis.

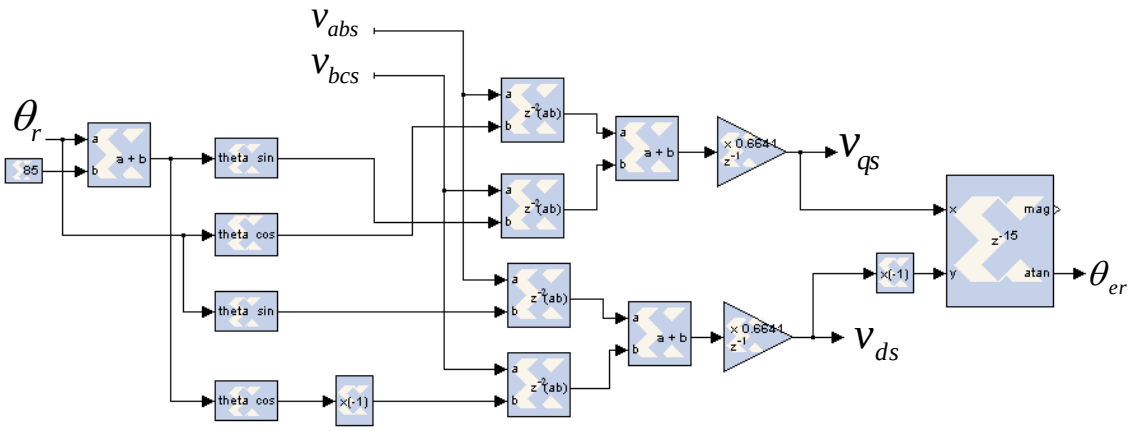

Figure 12. Stator Voltage Transformation to Rotor Reference Frame.

3. Transformation of Rotor Currents

The rotor currents i_{abc}, shown in Figure 13, are also fed into the controller where they are transformed using (17) to the variables i^e_{qdr}. This notation represents a transformation of the rotor currents to the synchronously rotating reference frame. This

transformation produces a constant value, if the currents are in steady state condition, which is useful in the next block. The constant 341.33 represents a 120 degree phase shift used in (17-19).

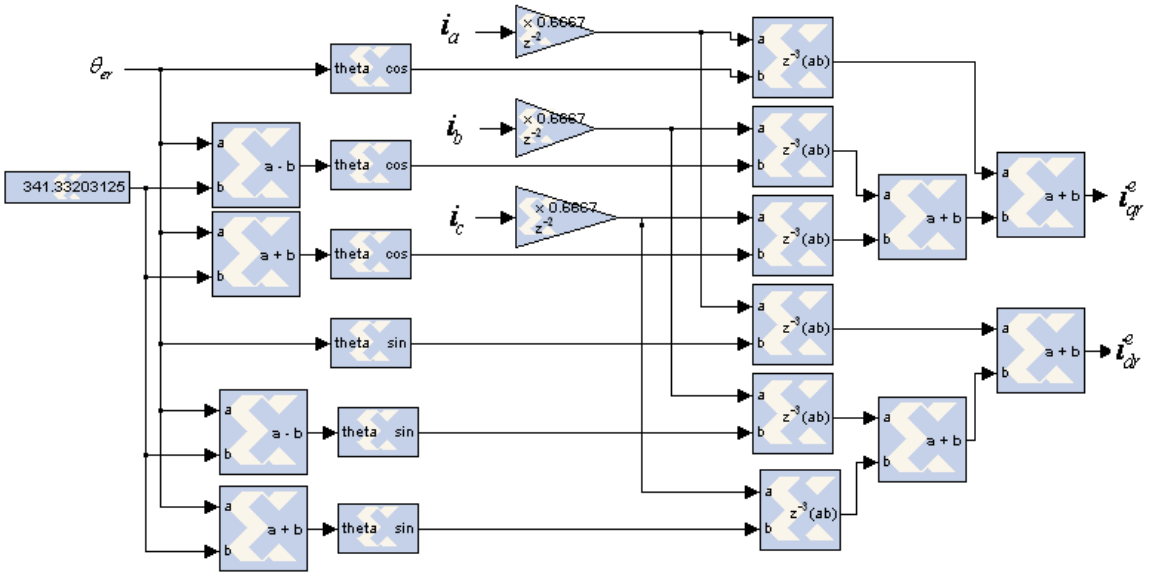

Figure 13. Rotor Current Transformations.

4. Proportional /Integral (PI) Gain

The transformation of balanced 3-phase variables to the $qd0$ axis will only produce components on the qd axis. Additionally, if the transformation is to the synchronously rotating reference frame, the q component will have constant amplitude equal to the amplitude of the phase variables and the d component will have amplitude of zero. This property is useful in the PI control algorithm for driving the steady state error to zero. Figure 14 contains the logic used for a proportional and integral gain controller designed with the Xilinx library block set. By transforming the rotor currents to the synchronously rotating reference frame two constants are produced as discussed above. Setting the reference i_q to the desired output value and the reference i_d to zero allows for full control of the output. The Integral part of the PI controller is built with an

accumulator so a reset is added to set the accumulator to zero when desired. The currents in the rotor windings are controlled by adjusting the voltage at the rotor terminals; therefore, the output from the current PI controller is a voltage.

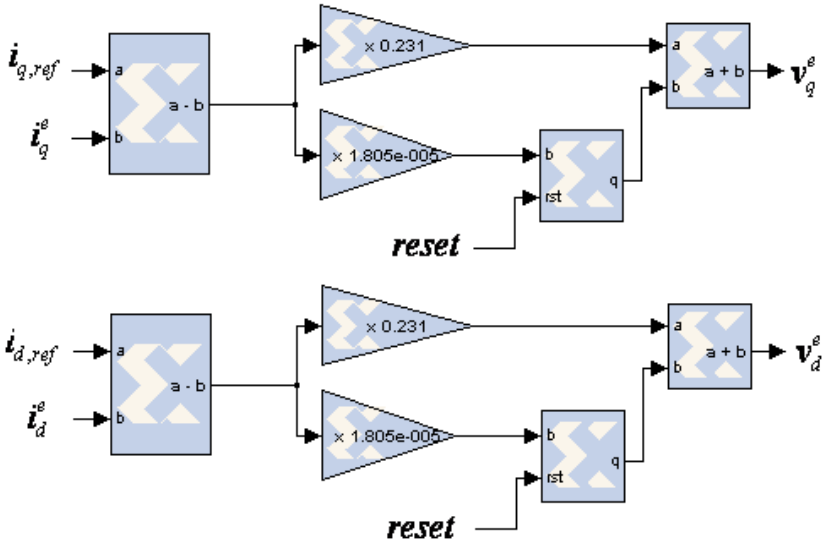

Figure 14. PI Current Controller.

5. Transformation of Rotor Voltages to Rotor Reference Frame

The rotor voltages v_q^e and v_d^e are transformed from the synchronously rotating reference frame to the rotor reference frame as shown in Figure 15. This transformation utilizes equation (20), which is useful for transforming variables between frames of reference. The input to the VSI in Figure 10 is normalized to the value of the DC voltage produced by the rectifier on the SEMISTACK. This normalization takes place in the last logic block of Figure 15.

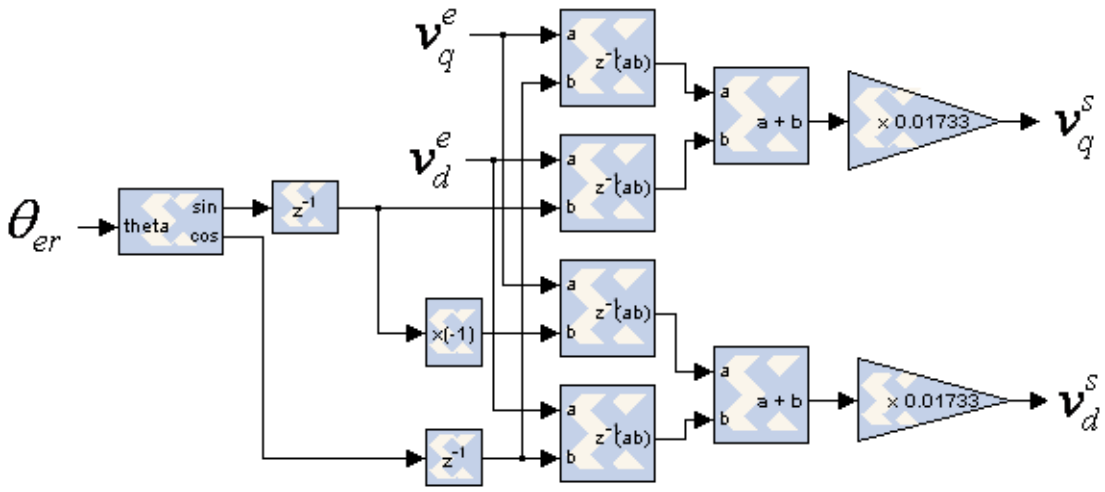

Figure 15. Transformation Between Reference Frames.

6. Rotor Encoder

The encoder used for this thesis is an MES20 (Type C) incremental shaft encoder. The encoder provides a digital input to the SDC. The control circuitry inside the SDC interprets the digital signals from the encoder and produces both rotor speed and position. The encoder software used in this thesis is discussed in detail in [7]. One modification, shown in Figure 16, was added to the design in [7], which was used to adjust rotor position and speed for a 4-pole machine. See Appendix C for complete encoder layout.

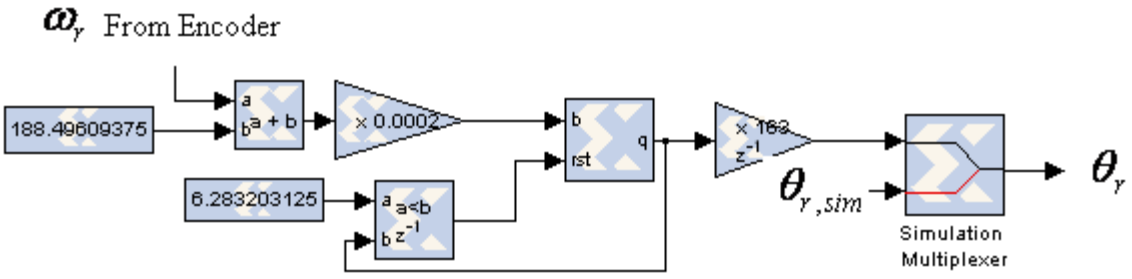

Figure 16. Rotor Encoder Addition.

7. Space Vector Modulation

One well-known way of creating 3-phase waveforms from a VSI is via SVM. SVM is a form of Pulse Width Modulation (PWM) in which an algorithm involving space vectors is used to control the on and off times of pulsed signals. The pulsed signals then drive the input signals to a VSI allowing the user to create any magnitude and frequency of signal desired. The SVM approach utilized in this controller is obtained from [7].

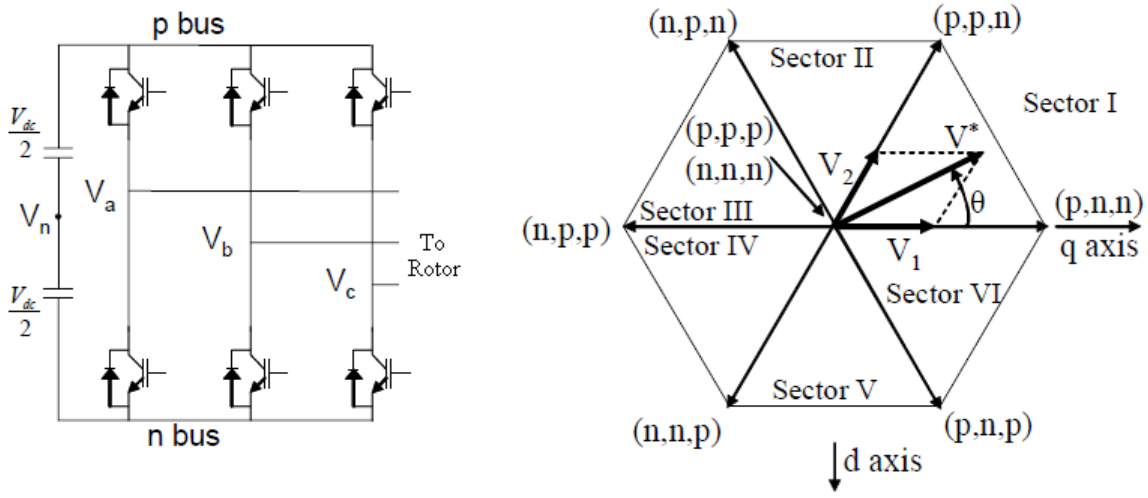

Figure 17. VSI and SVM Hexagon (From [7]).

The VSI produces a three phase output voltage that is controlled by turning on and off the six IGBTs on the VSI diagram in Figure 17. The on and off switching states are based on the SVM Hexagon also shown in Figure 17. The qd axis is overlaid on the SVM Hexagon and represents the axis of the variables v_{qr}^s and v_{dr}^s, which are shown entering the SVM block in Figure 10. The magnitude of the vectors v_{qr}^s and v_{dr}^s is equal to the vector $V*$ and θ is equal to the arctangent of the two vectors.

There are six sectors on the hexagon and eight possible on and off states that are used to produce the vectors $V*$. The vectors V_1 and V_2 when summed are also equal to the vector $V*$. In Sector I, V_1 and V_2, correspond to the states (p,n,n) and (p,p,n). The

p and n correspond to the positive or negative IGBT bus signals for the respective phases V_a, V_b, and V_c. The zero vectors, which are represented by the states (p, p, p) and (n, n, n) are not shown but represented as vectors into and out of the page. The magnitude of the vectors V_1 and V_2 correspond to the amount of time spent on the switching states in each sector. The duty cycles T_1 and T_2 are the times spent on each cycle for the vectors V_1 and V_2. The total time spent for one switching period is T_s.

$$V_1 = \frac{2T_1 V_{dc}}{3T_s} \tag{48}$$

$$V_2 = \frac{2T_2 V_{dc}}{3T_s}. \tag{49}$$

Applying the law of sines to any one of the sectors in the SVM Hexagon will produce

$$\frac{2V^*}{\sqrt{3}} = \frac{V_1}{\sin\left(60^o - \theta\right)} = \frac{V_2}{\sin\left(\theta\right)} \tag{50}$$

Substituting (48 and 49) into (50) is used to find the time of the duty cycles for the vectors V_1 and V_2.

$$T_1 = \frac{V^*\sqrt{3}}{V_{dc}} T_s \sin\left(60^o - \theta\right) \tag{51}$$

$$T_2 = \frac{V^*\sqrt{3}}{V_{dc}} T_s \sin\left(\theta\right) \tag{52}$$

$$T_s = T_1 + T_2 + T_0 \tag{53}$$

SVM has the ability to minimize switching loss and harmonic distortion by controlling the order in which the states are applied [8]. The switching pattern for each state and sector used in this thesis is shown in Table 2. The SVM algorithm is implemented inside

the SDC center where it is oversampled to converge on the performance of a true continuous sinusoidal signal. The digital implementation of the SVM scheme used for this thesis is discussed in detail in [9] and the schematic diagrams can be found in Appendix C. Figure 18 is a block diagram of the functions for each process in the SVM block.

	a	b	c	d	e	
Sector I	nnn	pnn	ppn	ppp	ppn	pnn	nnn
	$\frac{T_0}{4}$	$\frac{T_1}{2}$	$\frac{T_2}{2}$	$\frac{T_0}{2}$	$\frac{T_2}{2}$	$\frac{T_1}{2}$	$\frac{T_0}{4}$
Sector II	nnn	npn	ppn	ppp	ppn	npn	nnn
	$\frac{T_0}{4}$	$\frac{T_2}{2}$	$\frac{T_1}{2}$	$\frac{T_0}{2}$	$\frac{T_1}{2}$	$\frac{T_2}{2}$	$\frac{T_0}{4}$
Sector III	nnn	npn	npp	ppp	npp	npn	nnn
	$\frac{T_0}{4}$	$\frac{T_1}{2}$	$\frac{T_2}{2}$	$\frac{T_0}{2}$	$\frac{T_2}{2}$	$\frac{T_1}{2}$	$\frac{T_0}{4}$
Sector IV	nnn	nnp	npp	ppp	npp	nnp	nnn
	$\frac{T_0}{4}$	$\frac{T_2}{2}$	$\frac{T_1}{2}$	$\frac{T_0}{2}$	$\frac{T_1}{2}$	$\frac{T_2}{2}$	$\frac{T_0}{4}$
Sector V	nnn	nnp	npp	ppp	npp	nnp	nnn
	$\frac{T_0}{4}$	$\frac{T_1}{2}$	$\frac{T_2}{2}$	$\frac{T_0}{2}$	$\frac{T_2}{2}$	$\frac{T_1}{2}$	$\frac{T_0}{4}$
Sector VI	nnn	pnn	pnp	ppp	pnp	pnn	nnn
	$\frac{T_0}{4}$	$\frac{T_2}{2}$	$\frac{T_1}{2}$	$\frac{T_0}{2}$	$\frac{T_1}{2}$	$\frac{T_2}{2}$	$\frac{T_0}{4}$

Table 2. Space Vector Modulation Switching Pattern (From [9]).

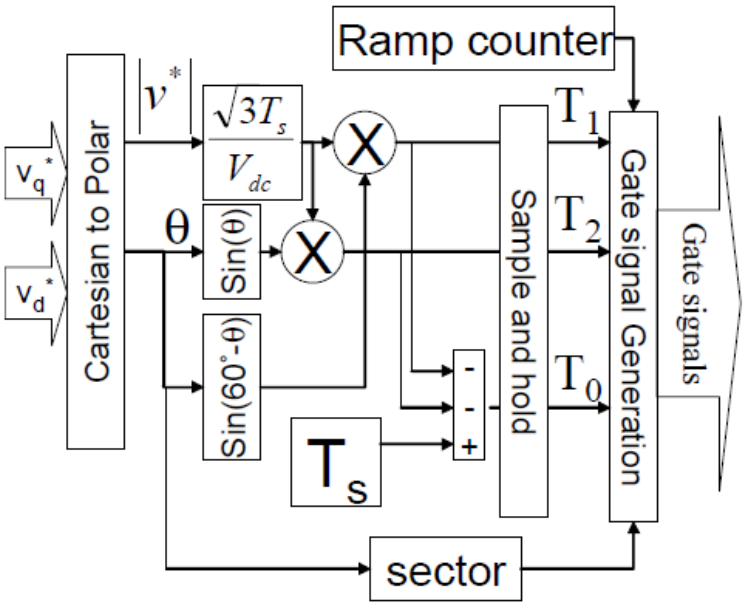

Figure 18. SVM Digital Implementation (From [9]).

In Conclusion, this chapter described the methodology used to control the DFIG for simulation and hardware design. The next chapter discusses the test performed to verify the operation of the system.

THIS PAGE INTENTIONALLY LEFT BLANK

IV. RESULTS AND ANALYSIS

A. VOLTAGE AND CURRENT COMPARISON

Several tests were performed to verify the operation of the wind energy conversion system. The first test is used to verify that the system can produce rated stator voltage and frequency on the grid. Figure 19 is a comparison of the physical system to the simulation with the rotor current set at 1A. The simulation closely matches the physical system and produces a 170V peak to peak signal at 60 Hz. The variables Vs, and Vs,sim represent the stator voltage and stator simulation voltage. The variable Ir represents the rotor current. The variable Pout represents the average instantaneous output power from one phase multiplied by 3 delivered from the stator terminals to the grid. This notation is followed for all the graphs in the results section.

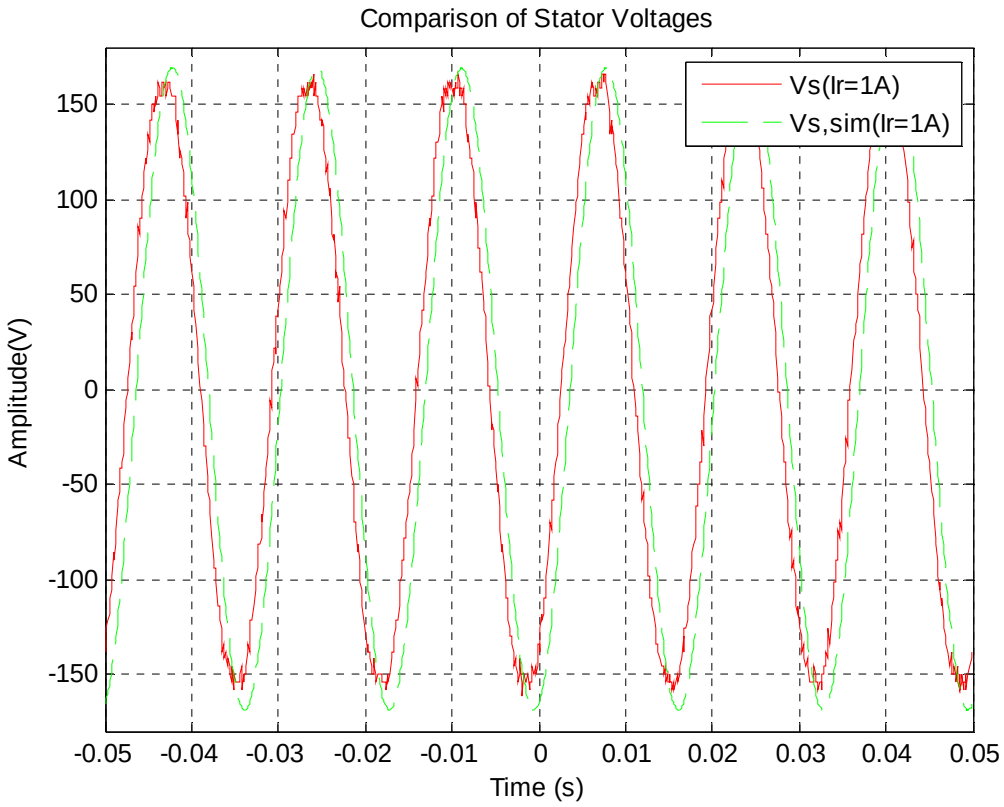

Figure 19. Comparison of Grid Stator Voltage to Simulation Source.

The second test was to verify the operation of the system for various changes in rotor current. The control algorithm allows the user to specify the amplitude of the rotor current. The benefits of controlling the amplitude of the current are discussed in the next section. This test is just to prove that the system functions similarly to the simulation for changes in rotor current. The results are shown in Figure 20.

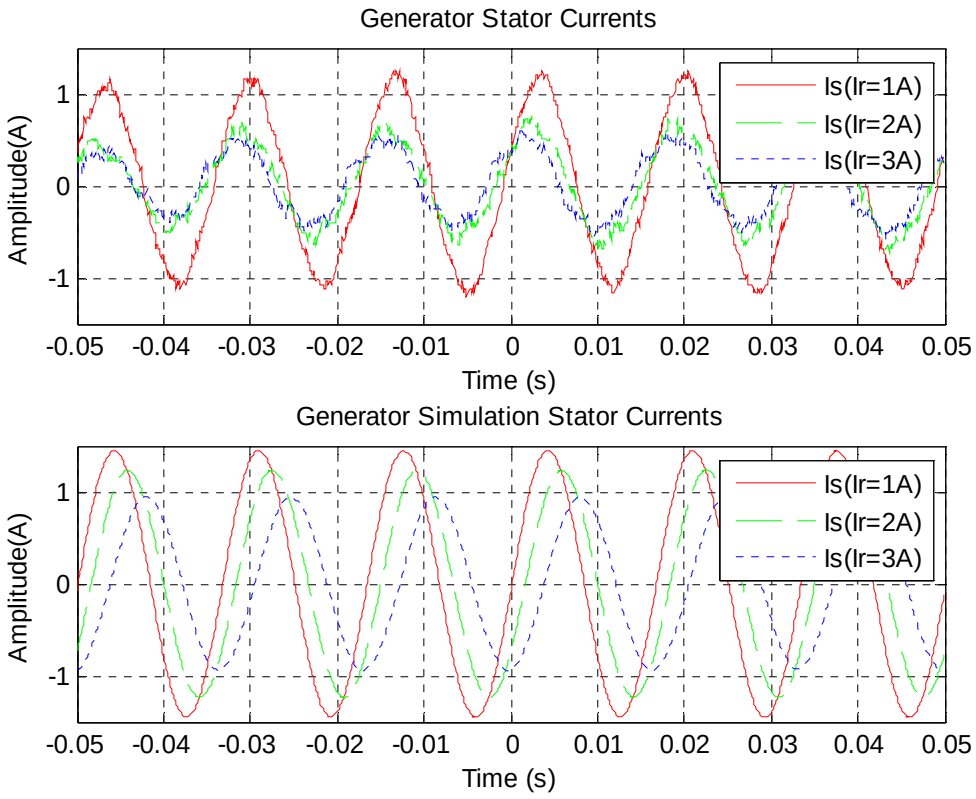

Figure 20. Comparison of Stator Currents to the Stator Simulation Currents.

From Figure 20, one can see that as the rotor current is increased in amplitude, the stator current reduces in amplitude. The simulation does not produce as much change in stator current amplitude as the physical system for equal changes in rotor current. This is not a problem; the system still produces voltage and current at 60Hz.

B. POWER FACTOR AND OUTPUT POWER COMPARISONS

The next test demonstrates the usefulness of having the ability to control the amplitude of the rotor currents. A Wind Energy Conversion System can only output as much power as the wind inputs into to the turbine blades. A specific amount of torque on the turbine blades will generate a certain amount of apparent power in the machine. Controlling the amplitude of the rotor currents allows the user to determine how much real power is abstracted from the total amount of apparent power generated in the machine. This technique is known as power factor control and shown in Figure 21. The voltage and current values below are normalized to the DFIG ratings.

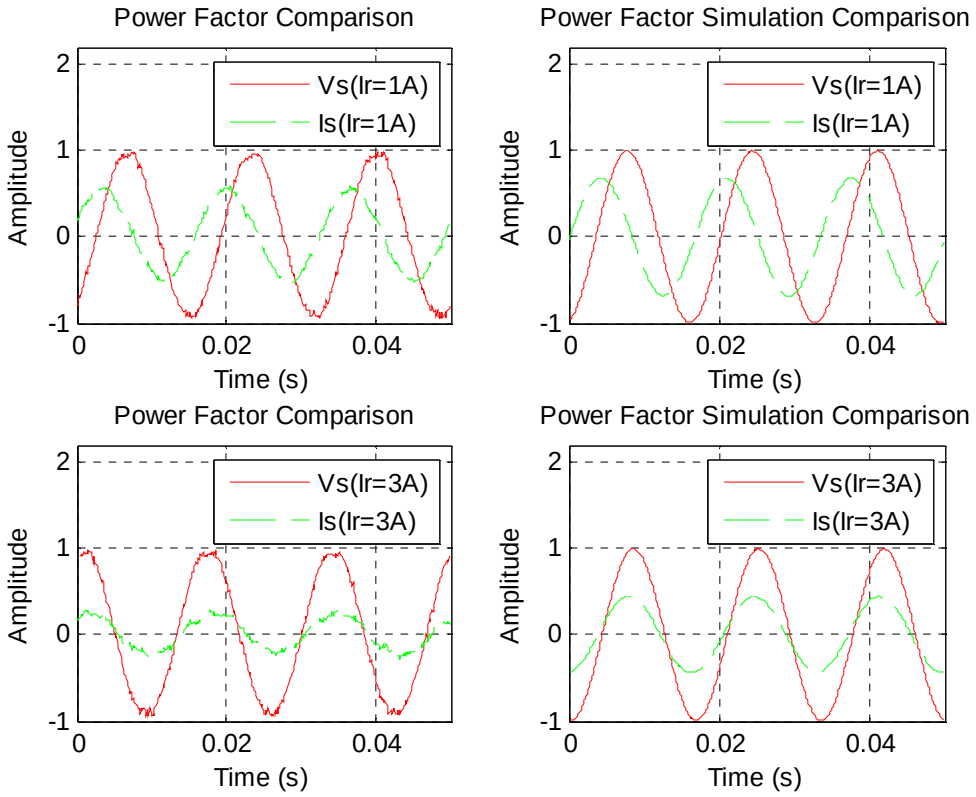

Figure 21. Power Factor Comparison.

Figure 21 compares the power factor adjustment for the physical system with the simulation. The rotor current is adjusted from 1 to 3 amps and the stator voltage and

currents are graphed. One can see that the angle between the voltage and current are almost in phase, as the rotor current is shifted from 1 to 3 amps.

Figure 22 is a display of how the power factor affects real power delivered to the grid for changes in rotor current. The power factor for rotor currents of 1A, 2A, and 3A respectively are calculated as 0.3, 0.71, and 0 .94 for the physical system and 0.28, 0.69, and 0.97 for the simulation.

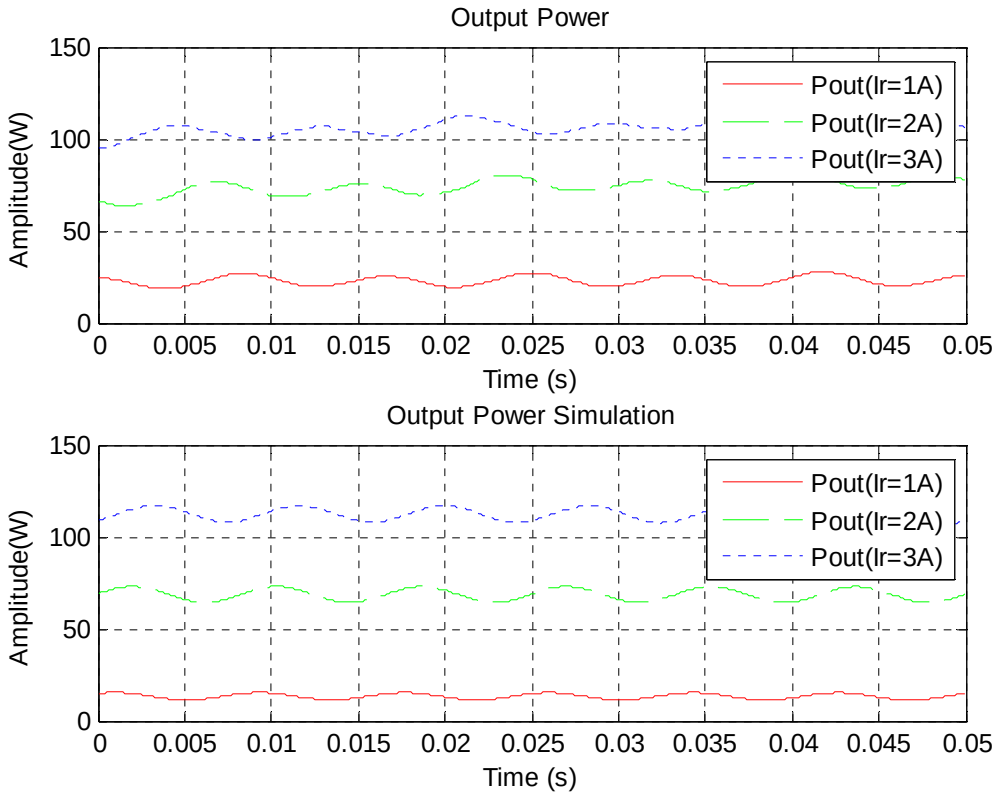

Figure 22. Comparison of Output Power for Changes in Rotor Current

The last test is used to verify that the system can operate under various changes in load. A DC machine is used to simulate a change in wind speed by increasing the amount of torque delivered to the DFIG shaft. A step change of 1 Newton is applied by the DC drive, which is equivalent to 175 watts at rated speed. The results, shown in Figure 23,

prove that the system is capable of delivering constant power to the grid as wind speed changes. The physical system produces slightly less output power than the simulation due to mechanical coupling losses from the DC drive to the DFIG.

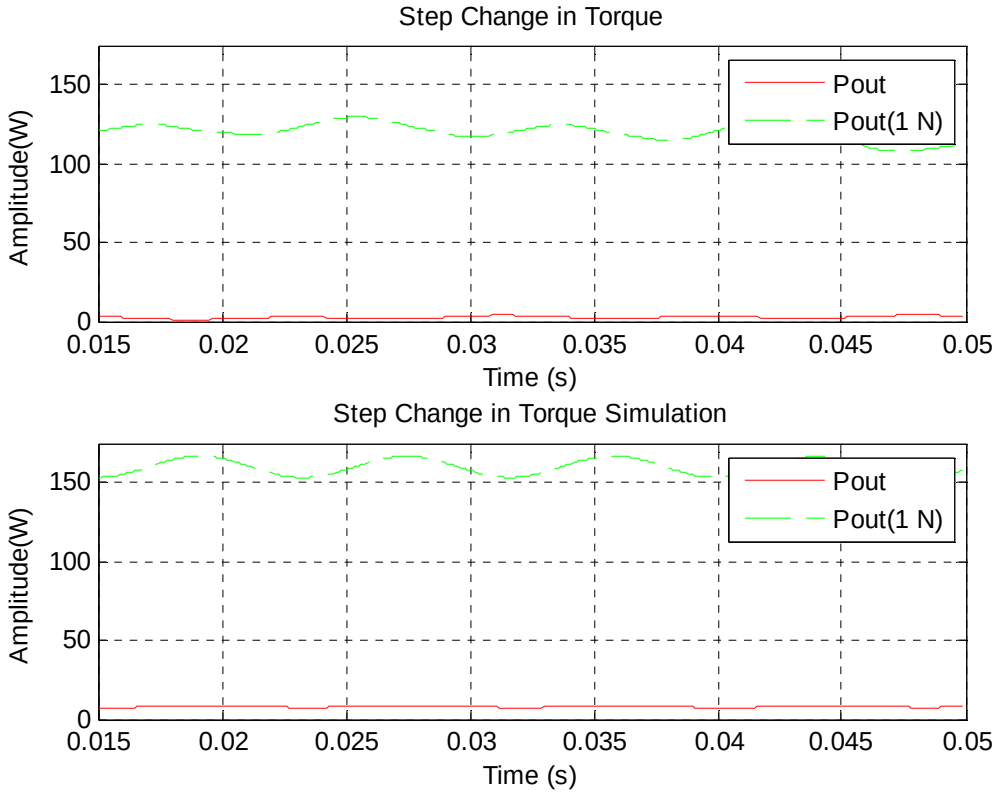

Figure 23. Comparison for Step Change in Torque

This chapter covered the results for each test performed that compared the operation of the simulation to physical system. The next chapter will discuss the results and conclusions.

THIS PAGE INTENTIONALLY LEFT BLANK

V. CONCLUSIONS AND SUGGESTIONS

A. CONCLUSIONS

A Wind Energy Conversion System was designed, simulated, and constructed using the methods discussed. A series of tests were conducted to validate the design. The system was designed to work under various load conditions, which in this scenario simulates changes in wind speed. The ability to control the rotor currents provides the user with functionality to adjust power factor thereby increasing the efficiency of power delivered to the grid. The response of the Wind Energy Conversion system was compared to the simulation. The results show that the physical system behaved as predicted by the simulation.

A successful Wind Energy Conversion system demonstrates the ability to transform mechanical energy delivered by the wind into electrical energy that can be used to power any electrical grid. The Wind Energy Conversion System successfully transformed mechanical torque on the shaft into electrical power.

B. FUTURE RESEARCH OBJECTIVES

This thesis dealt with simulation and operation of a Wind Energy Conversion System. Future research will be on various control strategies to improve overall efficiency.

One area of research currently being explored is the ability to extract power from both the rotor and stator windings when the machine is operating at super-synchronous speed. This design will require two VSI and control software that will allow for bi-directional flow of current through the rotor windings for sub-synchronous and super-synchronous operation. Delivering power from the rotor and stator windings will improve the overall efficiency of the system.

The other area of research currently being explored is a continuation of controlling the power factor angle. The rotor side converter will be used to control active

and reactive power of the DFIG by controlling the amplitude of the rotor currents. The amplitude of the rotor currents will follow a tracking characteristic that adjusts generator speed for optimal power generation depending on wind speed.

APPENDIX A: DATASHEETS

SEMISTACK - IGBT

SEMITRANS Stack[1)]

Three-phase rectifier + inverter with brake chopper

SEMITEACH - IGBT
SKM 50 GB 123D
SKD 51
P3/250F

Features

- Multi-function IGBT converter
- Transparent enclosure to allow visualization of every part
- IP2x protection to minimize safety hazards
- External banana/BNC type connectors for all devices
- Integrated drive unit offering short-circuit detection/cut-off, power supply failure detection, interlock of IGBTs + galvanic isolation of the user
- Forced-air cooled heatsink

Typical Applications

- Education: One stack can simulate almost all existing industrial applications:
- 3-phase inverter+brake chopper
- Buck or boost converter
- Single phase inverter
- Single or 3-phase rectifier

[1)] Photo non-contractual

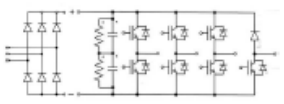

B6U + B6CI + E1CIKF

Circuit	I_{rms} (A)	V_{ac} / V_{dcmax}	Types
B6CI	30	440 / 750	SEMITEACH - IGBT

Symbol	Conditions	Values	Units
I_{rms}	no overload	30	A
	IGBT - 4x SKM 50 GB 123D		
V_{CES}		1200	V
$V_{CE(SAT)}$	I_C= 50A, V_{GE}= 15V, chip level; T_j= 25(125)°C	2,7 (3,5)	V
V_{GES}		±20	V
I_C	T_{case}= 25 (80)°C	50 (40)	A
I_{CM}	T_{case}= 25 (80)°C; t_p= 1ms	100 (80)	A
	Rectifier - 1x SKD 51/14		
$V_{in(max)}$	without filter	3 x 480	V
	with filter	3 x 380	V
	DC Capacitor bank - Electrolytic 2x 2200µF/400V		
C_{eqvl}	total equivalent capacitance	1100 / 800	µF / V
V_{DCmax}	max. DC voltage applied to the capacitor bank	750	V
	Driver - 4x SKHI 22		
Power supply		0 / 15	V
Current consumption	max; per driver	16	mA
Thermal trip	Normally Open type (NO)	71	°C

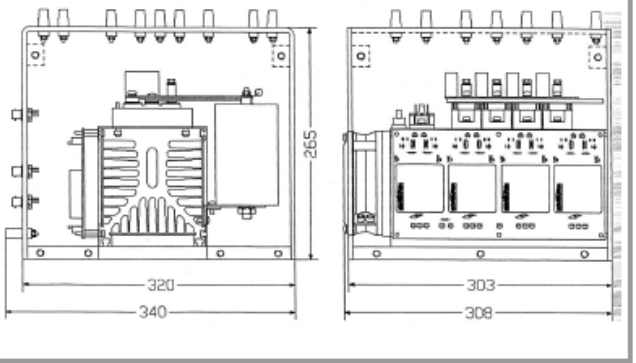

General dimensions

This technical information specifies semiconductor devices but promises no characteristics. No warranty or guarantee expressed or implied is made regarding delivery, performance or suitability.

Model 8211 DC Motor/Generator

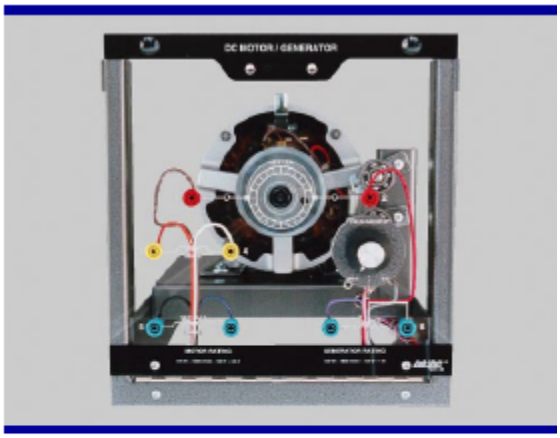

This machine can be run independently as a DC motor or a DC generator. The armature, shunt field, and series field windings are terminated separately on the faceplate to permit long and short shunt as well as cumulatively and differentially compounded motor and generator connections. This machine is fitted with exposed movable brushes to allow students to study the effect of armature reaction and commutation while the machine is operating under load. An independent, circuit- breaker protected, shunt-field rheostat is mounted on the faceplate for motor speed control or generator output voltage adjustment.

Model 8231 Three-Phase Wound-Rotor Induction Motor

Each phase of the stator windings of this motor is independently terminated and identified on the faceplate to permit operation in either delta or star (wye) configuration. The rotor windings are brought out to the faceplate via external slip rings and brushes. This machine can be used as a wound-rotor induction motor, phase shifter, single-phase variable coupling transformer, three-phase transformer, selsyn control, frequency converter or asynchronous induction generator. The speed of this machine can be controlled through the use of the Three-Phase Rheostat (Model 8731).

SPECIFICATIONS

Model 8211 DC Motor/Generator		**120/208 V – 60 Hz**	**220/380 V – 50 Hz**	**240/415 V – 50 Hz**
Power Requirement		120/208 V	220/380 V	240/415 V
Rating	Motor Output Power	175 W		
	Generator Output Power	120 W	110 W	120 W
	Armature Voltage	120 V – DC	220 V – DC	240 V – DC
	Shunt Field Voltage	120 V – DC	220 V – DC	240 V – DC
	Full Load Speed	1800 r/min	1500 r/min	1500 r/min
	Full Load Motor Current	2.8 A	1.3 A	1.1 A
	Full Load Generator Current	1 A	0.5 A	0.5 A
Physical Characteristics	Dimensions (H x W x D)	308 x 291 x 440 mm (12.1 x 11.5 x 17.3 in)		
	Net Weight	14.1 kg (31 lb)		
Model 8221 Four-Pole Squirrel-Cage Induction Motor		**120/208 V – 60 Hz**	**220/380 V – 50 Hz**	**240/415 V – 50 Hz**
Power Requirement		120/208 V	220/380 V	240/415 V
Rating	Output Power	175 W		
	Stator Voltage	120/208 V, 3-phase	220/380 V, 3-phase	240/415 V, 3-phase
	Full Load Speed	1670 r/min	1360 r/min	1395 r/min
	Full Load Current	1.2 A	0.52 A	0.46 A
Physical Characteristics	Dimensions (H x W x D)	308 x 291 x 440 mm (12.1 x 11.5 x 17.3 in)		
	Net Weight	13.5 kg (29.7 lb)		
Model 8231 Three-Phase Wound-Rotor Induction Motor		**120/208 V – 60 Hz**	**220/380 V – 50 Hz**	**240/415 V – 50 Hz**
Power Requirement		120/208 V	220/380 V	240/415 V
Rating	Output Power	175 W		
	Stator Voltage	120/208 V, 3-phase	220/380 V, 3-phase	240/415 V, 3-phase
	Rotor Voltage	60/104 V, 3-phase	110/190 V, 3-phase	120/208 V, 3-phase
	Full Load Speed	1500 r/min	1240 r/min	1315 r/min
	Full Load Current	1.3 A	0.53 A	0.48 A
Physical Characteristics	Dimensions (H x W x D)	308 x 291 x 440 mm (12.1 x 11.5 x 17.3 in)		
	Net Weight	14 kg (30.8 lb)		

POWER SUPPLY
MODEL 8821

The Power Supply provides fixed and variable AC and DC voltage sources, all terminated by color-coded 4 mm safety sockets. Independent circuit breakers, reset at the front panel, protect the input to and output from the Power Supply. Indicator lamps monitor the presence of input voltage in each phase. When a phase leg of the site's power service is out, the lamp goes off to reflect this condition.

A voltmeter, connected through a selector switch, monitors the variable AC and DC outputs and fixed DC output. A 24 V AC output provides a low-voltage supply required to operate other EMS equipment such as metering modules and modules used in the Power Electronics Training System.

SPECIFICATIONS

Model 8821 – Power Supply		120/208 V – 60 Hz	220/380 V – 50 Hz	240/415 V – 50 Hz
Input	Line Voltage	120/208 V	220/380 V	240/415 V
	Line Current	15 A	10 A	
	Service Installation	20 A, 3-phase, 5 wires, star (Wye)- connected, including neutral and ground		
Outputs	Fixed AC 3-Phase	120/208 V – 15 A	220/380 V – 10 A	240/415 V – 10 A
	Variable AC 3-Phase	0-120/208 V – 5 A	0-220/380 V – 3 A	0-240/415 V – 3 A
	Variable DC	0-120 V – 8 A	0-220 V – 5 A	0-240 V – 5 A
	Fixed DC	120 V – 2 A	220 V – 1 A	240 V – 1 A
	Low Power AC	24 V – 3 A		
Wall Outlet included		NEMA L21-20	NEMA L22-20	CLIPSAL 56SO520
Power Cord		3 m (10 ft)		
Physical Characteristics	Dimensions (H x W x D)	308 x 287 x 500 mm (12.1 x 11.3 x 19.7 in)		
	Net Weight	18.4 kg (40.5 lb)		

THIS PAGE INTENTIONALLY LEFT BLANK

APPENDIX B: MATLAB M-FILES

A. MATLAB INITIAL CONDITIONS FILE

Dbl_Fed_Ind.m

```
clc,clear
Vdc=150;              %Bus voltage maintained for Capacitor on VSI
DC_Bus_Prot=200;      %Secure firing circuit at 200Vdc.
omega_b = 2*pi*60;    % Base Frequency in radians/second
oversample=2;         % Determine oversampling rate in SVM block
pulsect = 1800/oversample;
step_ct=1;
clock_freq=25e6;
tstep=.0004;           % only to speed up simulation.
%tstep=step_ct/clock_freq; %When compiling software us this line

%More constants used for simulation
twopiby3 = 2*pi/3;
poles = 4;
polesby2J=poles*12/2/.089;
TL=.25*746/(2/poles*omega_b);

%Calculated constants from Induction motor test.
rs=12;
rr =15;
Xls =9.1;
Xm =126;
Xlr =9.1;

%D=(Xls+Xm)*(Xlr+Xm)-Xm^2;   Defined in book for per unit values of
Inertia.
rsbyXls = rs/Xls;
rrbyXlr = rr/Xlr;
Xaq = 1/(1/Xm+1/Xls+1/Xlr);
Xad = Xaq;
XaqbyXls = Xaq/Xls;
XaqbyXlr = Xaq/Xlr;
XadbyXls = Xad/Xls;
XadbyXlr = Xad/Xlr;
XaqbyXm = Xaq/Xm;
XadbyXm = Xad/Xm;

psi_qsic=0;
psi_dsic=0;
psi_qric=0;
psi_dric=0;
omegar_ic =omega_b; %Set the initial condition speed of rotor to 1800
rpm.

Kp_i=.231;            %current Proportional gain
```

```
Ki_i=415.7*1.042;    %Current Integral gain

%Used for Mealy State Machine in A/D Current simulation.

F_mat = [0 0 0 1;1 1 2 0;2 2 3 0;3 3 0 0];
O_mat = F_mat;


%Everything below this line is used for the encoder controls
               %fvtool(output1,output2)

t_square=2e-4/10;%2e-4 produces 1500RPM...4e-4 produces 750RPM
%8e-4 = 374RPM...10e-4=300RPM
%there is 400 1/2 pulses per rotation therefore:
%60sec/(400* 1/2*t_square)= correct RPM
RPM=60/(200*t_square);
Hz=RPM/60;

sw_freq=15000;
% sw_counter=round(f_clock/sw_freq-mod(f_clock/sw_freq,10));
%Counter for sawtooth for switching modulo 10 used so step_ct can be 10
Total_Rotations=6;

%Ctr=[1:2^8]/2^8/tstep/400*50;%16,000,000
%reciprocal=1./Ctr;%1/16,000,000=244.1406
Ctr=[1:2^11];
reciprocal=360/30/1./Ctr;%360/30/1./Ctr

%                  [Pk, Nk, 0k]
output_vec=[0;...%Nothing is occurring with [0,0,0]
            5;...%3Motor is turning in the CCW direction and crossing
the
                  %zero pt with [0,1,1]
            0;...%0Nothing is occurring with [0,0,0]
            4;...%2Motor is turning in the CCW direction with [0,1,0]
            0;...%0Nothing is occurring with [0,0,0]
            3;...%5[1,0,1] indicates CW rotation and resets rotation
                  %counter
            0;...%0Nothing is occurring with [0,0,0]
            2;...%4[1,0,0] indicates CW rotation
            3;...%5[1,0,1] indicates CW rotation and resets rotation
                 %counter
            0;...%0Nothing is occurring with [0,0,0]
            2;...%4[1,0,0] indicates CW rotation
            0;...%0Nothing is occurring with [0,0,0]
            5;...%3[0,1,1] indicates CCW direction and resets rotation
                 %counter
            0;...%0Nothing is occurring with [0,0,0]
            4;...%2 Motor is turning in the CCW direction with [0,1,0]
            0];  %0 Nothing is occurring with [0,0,0]

        next = [0,0,1,0;1,0,1,0];
output=next;
```

B. MATLAB M-FILE USED FOR SPACE VECTOR MODULATION

cverflow3.m

```
function [sector1, sector2, sector3, sector4, sector5, sector6, z] =
overflow3(x)
%gain = xfix({xlUnsigned,10,7},2.359296/3);%for 60 hz
gain = xfix({xlUnsigned,10,7},2.359296);%for 180 hz
%tempv=gain*x;
tempv=x;
if tempv<=171-1
    sector1=xfix({xlBoolean},1);
    sector2=xfix({xlBoolean},0);
    sector3=xfix({xlBoolean},0);
    sector4=xfix({xlBoolean},0);
    sector5=xfix({xlBoolean},0);
    sector6=xfix({xlBoolean},0);
    z=xfix({xlUnsigned,10,0},tempv);
elseif tempv<=2*171-1
    sector1=xfix({xlBoolean},0);
    sector2=xfix({xlBoolean},1);
    sector3=xfix({xlBoolean},0);
    sector4=xfix({xlBoolean},0);
    sector5=xfix({xlBoolean},0);
    sector6=xfix({xlBoolean},0);
    z=xfix({xlUnsigned,10,0},tempv-171);
elseif tempv<=3*171-1
    sector1=xfix({xlBoolean},0);
    sector2=xfix({xlBoolean},0);
    sector3=xfix({xlBoolean},1);
    sector4=xfix({xlBoolean},0);
    sector5=xfix({xlBoolean},0);
    sector6=xfix({xlBoolean},0);
    z=xfix({xlUnsigned,10,0},tempv-2*171);
elseif tempv<=4*171-1
    sector1=xfix({xlBoolean},0);
    sector2=xfix({xlBoolean},0);
    sector3=xfix({xlBoolean},0);
    sector4=xfix({xlBoolean},1);
    sector5=xfix({xlBoolean},0);
    sector6=xfix({xlBoolean},0);
    z=xfix({xlUnsigned,10,0},tempv-3*171);
elseif tempv<=5*171-1
    sector1=xfix({xlBoolean},0);
    sector2=xfix({xlBoolean},0);
    sector3=xfix({xlBoolean},0);
    sector4=xfix({xlBoolean},0);
    sector5=xfix({xlBoolean},1);
    sector6=xfix({xlBoolean},0);
    z=xfix({xlUnsigned,10,0},tempv-4*171);
else
    sector1=xfix({xlBoolean},0);
    sector2=xfix({xlBoolean},0);
    sector3=xfix({xlBoolean},0);
```

```
    sector4=xfix({xlBoolean},0);
    sector5=xfix({xlBoolean},0);
    sector6=xfix({xlBoolean},1);
    z=xfix({xlUnsigned,10,0},tempv-5*171);
end
```

ramp2mod.m

```
function z = ramp2(x)
gain=xfix({xlSigned,20,19},1/1800)
z=xfix({xlSigned,14,13},x*gain);
```

thetaconv2.m

```
function [y] = thetaconv(x)
gain1 = xfix({xlSigned,14,10},2*3.14);
gain2 = xfix({xlSigned,14,10},1/gain1)
if x<0
y=xfix({xlUnsigned,10,0},(x+gain1)*gain2*1024);
else
y=xfix({xlUnsigned,10,0},x*gain2*1024);
end
```

C. MATLAB M-FILES USED FOR ENCODER

mcode5A.m

```
function [NewRotation, NewValue, Direction] = mcode5A(Pk, Nk, Zk,
OldRotation, OldValue)
%This fuction records CW and CCW rotations via matlab MCODE simulation
%block. It also records 360 degrees of rotation and total degrees
traveled
%Author: LT Andrew M LaValley
%Last Modified: 14 APR 08

if Pk && ~Zk && ~Nk %Increments the # of pulses produced in the CW
rotation

        Direction=0;%indicates positive direction

    if OldValue==399 %this keeps the value positive if the value is
zero.

        NewValue=xfix({xlSigned,15,0},0);
        NewRotation=xfix({xlSigned,15,0},OldRotation+1);

    else
        NewValue=xfix({xlSigned,15,0},OldValue+1);
        NewRotation=xfix({xlSigned,15,0},OldRotation);
```

```
    end
elseif Nk && ~Zk && ~Pk %Decrements the # of pulses produced in the CCW
rotation if not zero

        Direction=1;%Indicates negitive direction

    if OldValue==0 %this keeps the value positive if the value is zero.

        NewValue=xfix({xlSigned,15,0},399);
        NewRotation=xfix({xlSigned,15,0},OldRotation-1);
        %Direction=1;
    else
        NewValue=xfix({xlSigned,15,0},OldValue-1);
        NewRotation=xfix({xlSigned,15,0},OldRotation);

    end


else %OldValue will equal NewValue and OldRotation will equal NewRotion
if
     %the above if/else statements do not apply.
        Direction=0;%default direction
        NewValue=xfix({xlSigned,15,0},OldValue);
        NewRotation=xfix({xlSigned,15,0},OldRotation);

end
```

D. MATLAB M-FILES FOR CHIPSCOPE INTERFACE

Black_box_dc_machine2_config.m

```
function code_config(this_block)

  % Revision History:
  %
  %   18-Dec-2008  (15:15 hours):
  %         Original code was machine generated by Xilinx's System
Generator
  %     after parsing H:\Docs\work_files\Docs\classes\EC3130_2009\DC
  %     machine lab\black_box_dc_machine2.vhd

  this_block.setTopLevelLanguage('VHDL');

  this_block.setEntityName('code');

  %  System  Generator  has  to  assume  that  your  entity    has  a
combinational
  % feed through;
  %   if it  doesn't, then comment out the following line:
```

```
  this_block.tagAsCombinational;

  this_block.addSimulinkInport('ind');
  this_block.addSimulinkInport('ila_clock');
  this_block.addSimulinkInport('ind2');

  this_block.addSimulinkOutport('outd');
  this_block.addSimulinkOutport('open_loop');
  this_block.addSimulinkOutport('speed');

  outd_port = this_block.port('outd');
  outd_port.setType('UFix_1_0');
  open_loop_port = this_block.port('open_loop');
  open_loop_port.setType('UFix_1_0');
  speed_port = this_block.port('speed');
  speed_port.setType('UFix_8_0');

  % ------------------------------
  if (this_block.inputTypesKnown)
    % do input type checking, dynamic output type and generic setup in
% this code block.

    if (this_block.port('ind').width ~= 1);
      this_block.setError('Input data type for port "ind" must have
width=1.');
    end

    this_block.port('ind').useHDLVector(false);

    if (this_block.port('ila_clock').width ~= 1);
      this_block.setError('Input data type for port "ila_clock" must
have width=1.');
    end

    this_block.port('ila_clock').useHDLVector(false);

    if (this_block.port('ind2').width ~= 48);
      this_block.setError('Input data type for port "ind2" must have
width=48.');
    end

  end  % if(inputTypesKnown)
  % ------------------------------

  % ------------------------------
   if (this_block.inputRatesKnown)
     setup_as_single_rate(this_block,'clk','ce')
   end  % if(inputRatesKnown)
  % ------------------------------


  % Add addtional source files as needed.
```

```
  %  |------------- | Add files in the order in which they should be
  %  compiled. | If two files "a.vhd" and "b.vhd" contain the entities
  %  entity_a and entity_b, and entity_a contains a | component of type
  %  entity_b, the correct sequence of | addFile() calls would be: |
  %  this_block.addFile('b.vhd'); |    this_block.addFile('a.vhd');
  %  |-------------

  %    this_block.addFile(''); this_block.addFile('');
  this_block.addFile('black_box_dc_machine2.vhd');

return;


% ------------------------------------------------------------

function setup_as_single_rate(block,clkname,cename)
  inputRates = block.inputRates;
  uniqueInputRates = unique(inputRates);
  if (length(uniqueInputRates)==1 & uniqueInputRates(1)==Inf)
    block.setError('The inputs to this block cannot all be constant.');
    return;
  end
  if (uniqueInputRates(end) == Inf)
     hasConstantInput = true;
     uniqueInputRates = uniqueInputRates(1:end-1);
  end
  if (length(uniqueInputRates) ~= 1)
    block.setError('The inputs to this block must run at a single
rate.');
    return;
  end
  theInputRate = uniqueInputRates(1);
  for i = 1:block.numSimulinkOutports
     block.outport(i).setRate(theInputRate);
  end
  block.addClkCEPair(clkname,cename,theInputRate);
  return;

% ------------------------------------------------------------
```

THIS PAGE INTENTIONALLY LEFT BLANK

APPENDIX C: SIMULINK/ XILINX MODEL OF WIND ENERGY CONVERSION SYSTEM

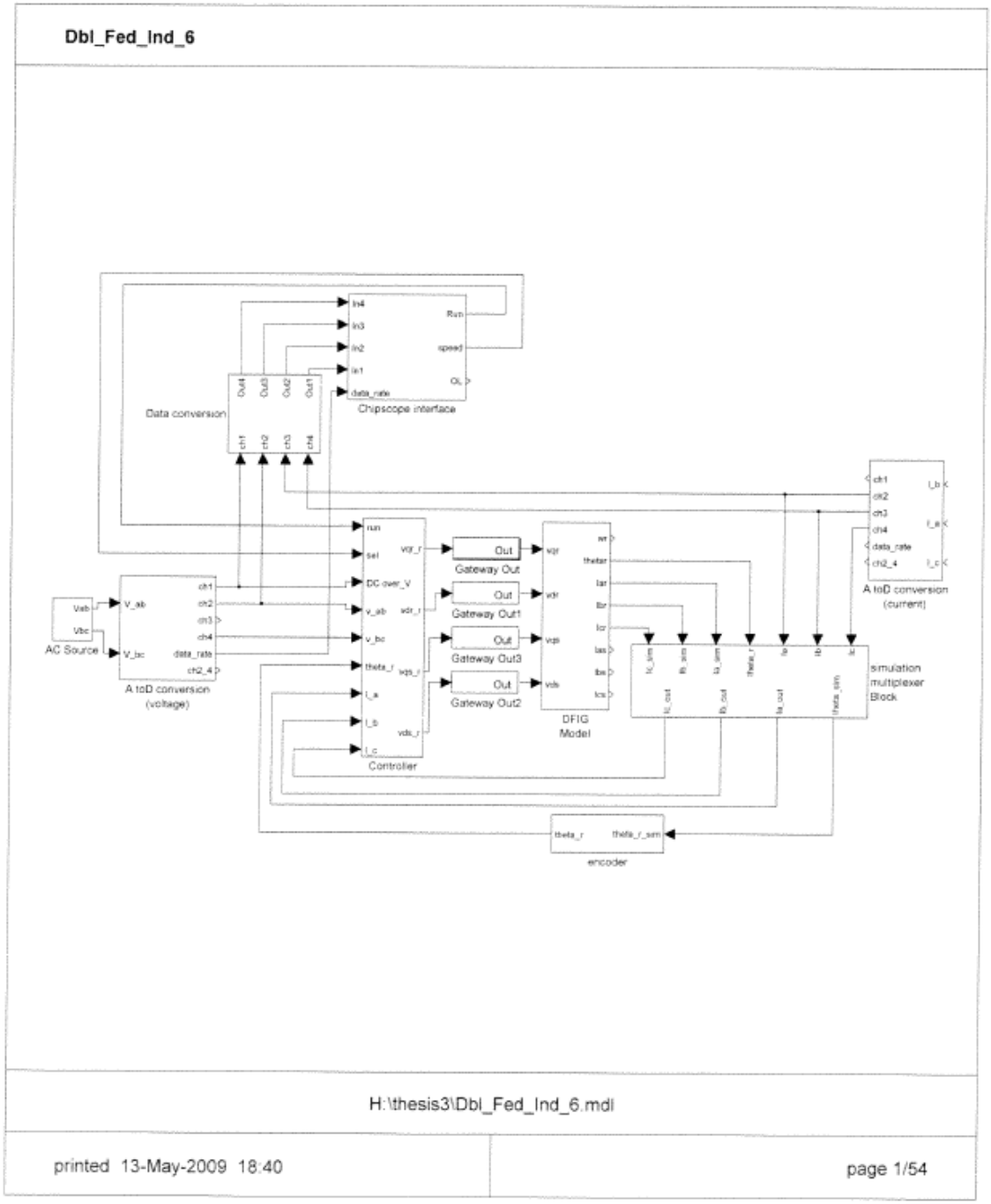

Dbl_Fed_Ind_6/A toD conversion (current)

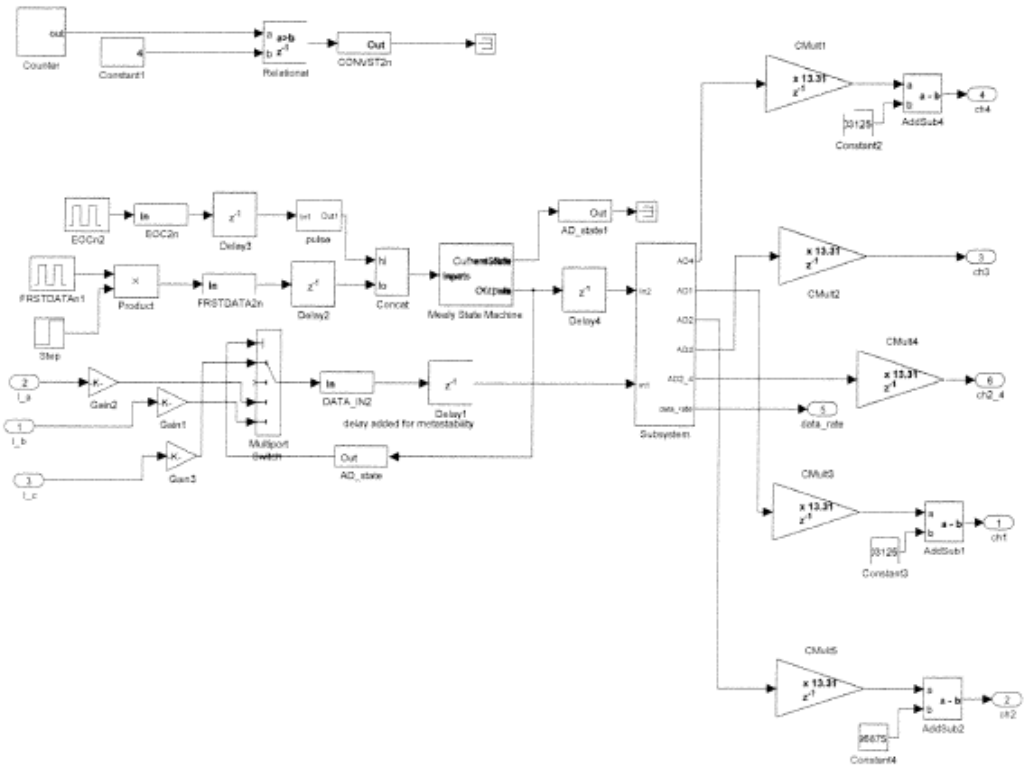

H:\thesis3\Dbl_Fed_Ind_6.mdl

printed 13-May-2009 18:40

page 2/54

Dbl_Fed_Ind_6/A toD conversion (current)/Subsystem

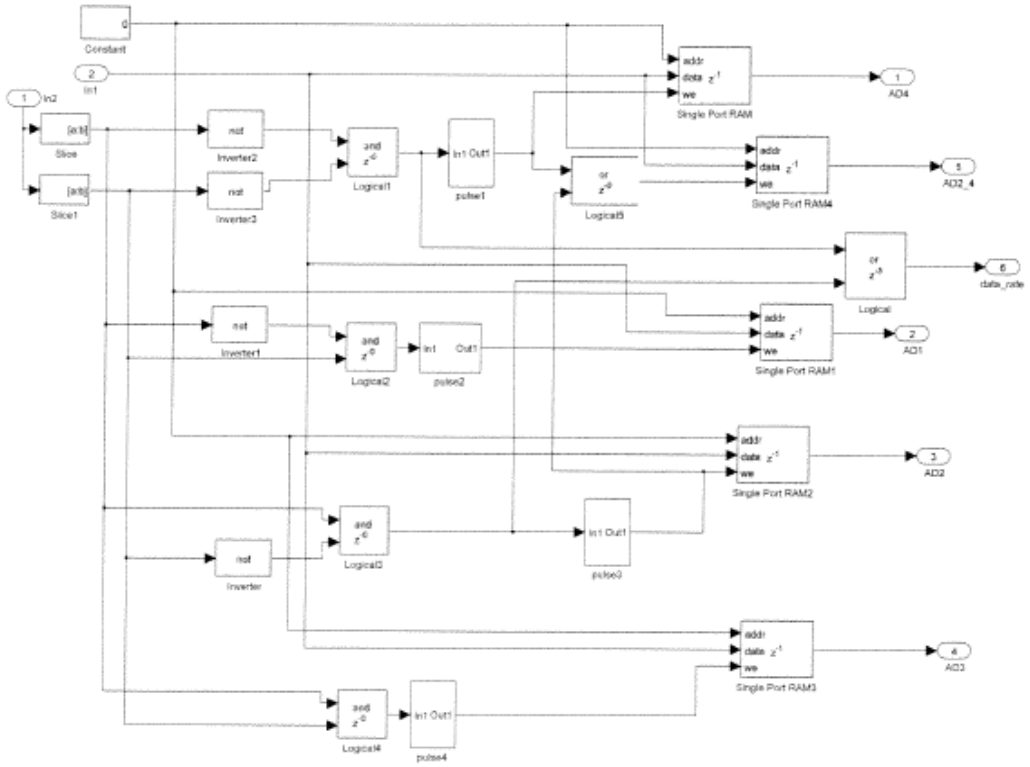

H:\thesis3\Dbl_Fed_Ind_6.mdl

printed 13-May-2009 18:40

page 3/54

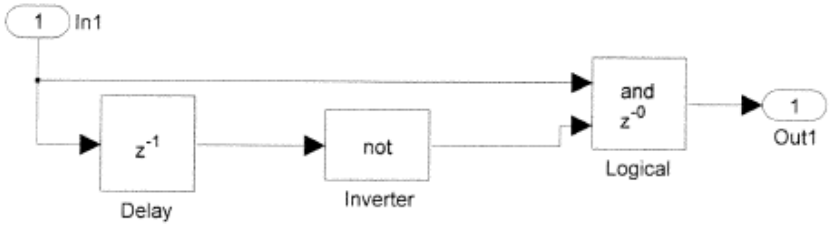
1
In1
z-1
Delay
not
Inverter
and
z-0
Logical
1
Out1

Dbl_Fed_Ind_6/A toD conversion (voltage)

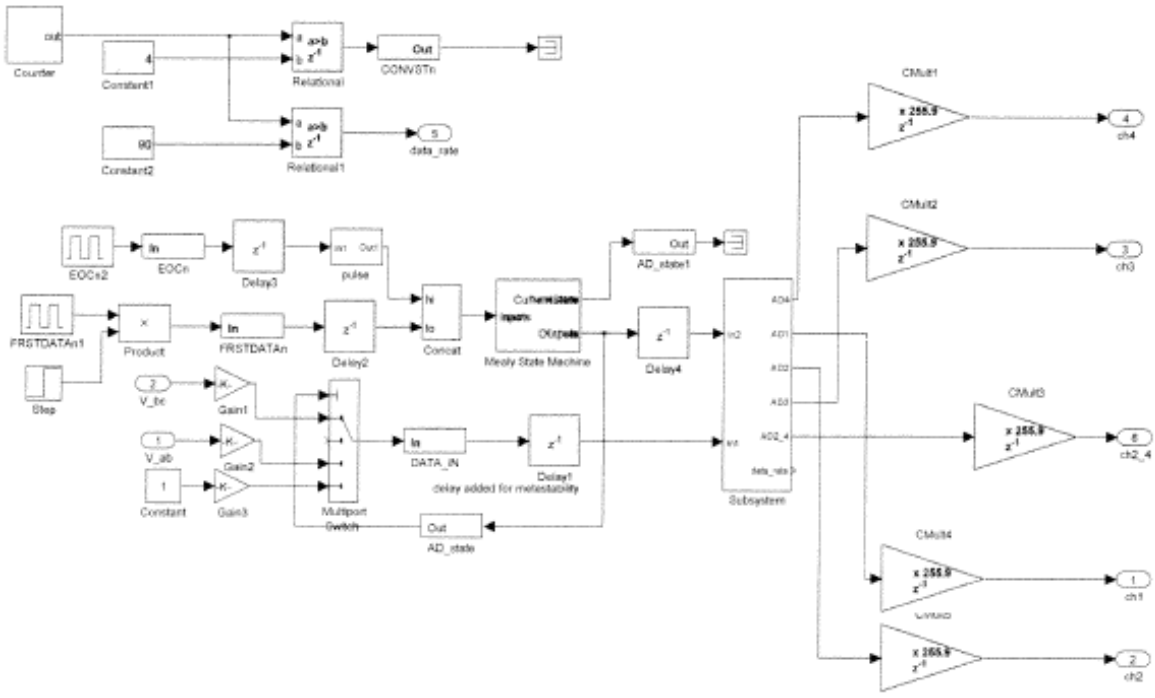

H:\thesis3\Dbl_Fed_Ind_6.mdl

printed 13-May-2009 18:40

page 9/54

Dbl_Fed_Ind_6/A toD conversion (voltage)/Subsystem

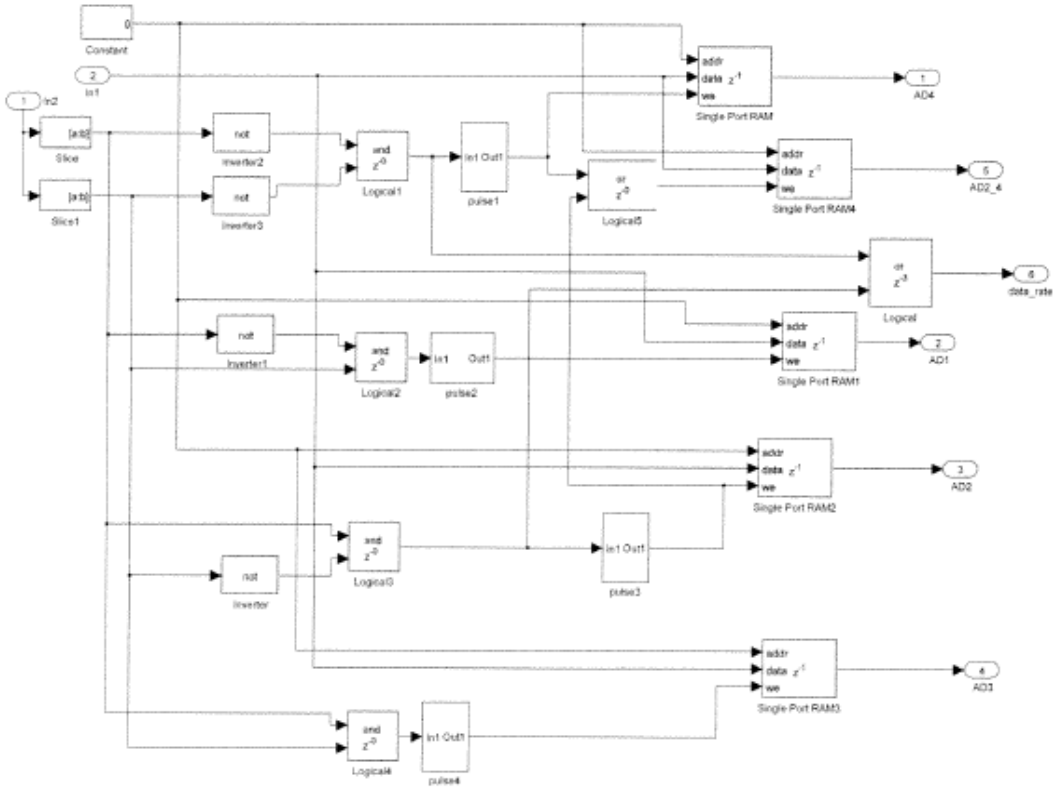

H:\thesis3\Dbl_Fed_Ind_6.mdl

printed 13-May-2009 18:40

page 10/54

Dbl_Fed_Ind_6/AC Source

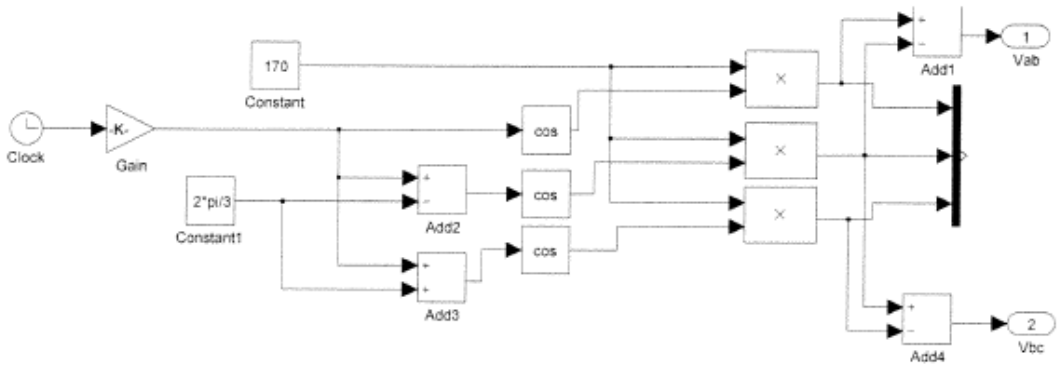

H:\thesis3\Dbl_Fed_Ind_6.mdl

printed 13-May-2009 18:40

page 16/54

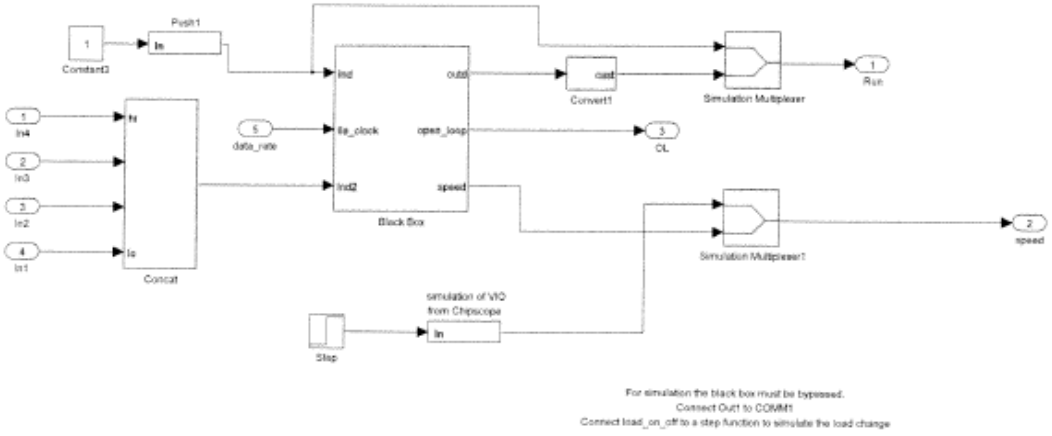
Push1
In
Constant3
ind
outd
cast
Convert1
Simulation Multiplexer
1
Run
1
In4
2
In3
3
In2
4
In1
In
Io
Concat
5
data_rate
fix_clock
open_loop
ind2
speed
Black Box
3
CL
2
speed
Simulation Multiplexer1
simulation of VIO
from Chipscope
In
Step
For simulation the black box must be bypassed.
Connect Out1 to COMM1
Connect load_on_off to a step function to simulate the load change

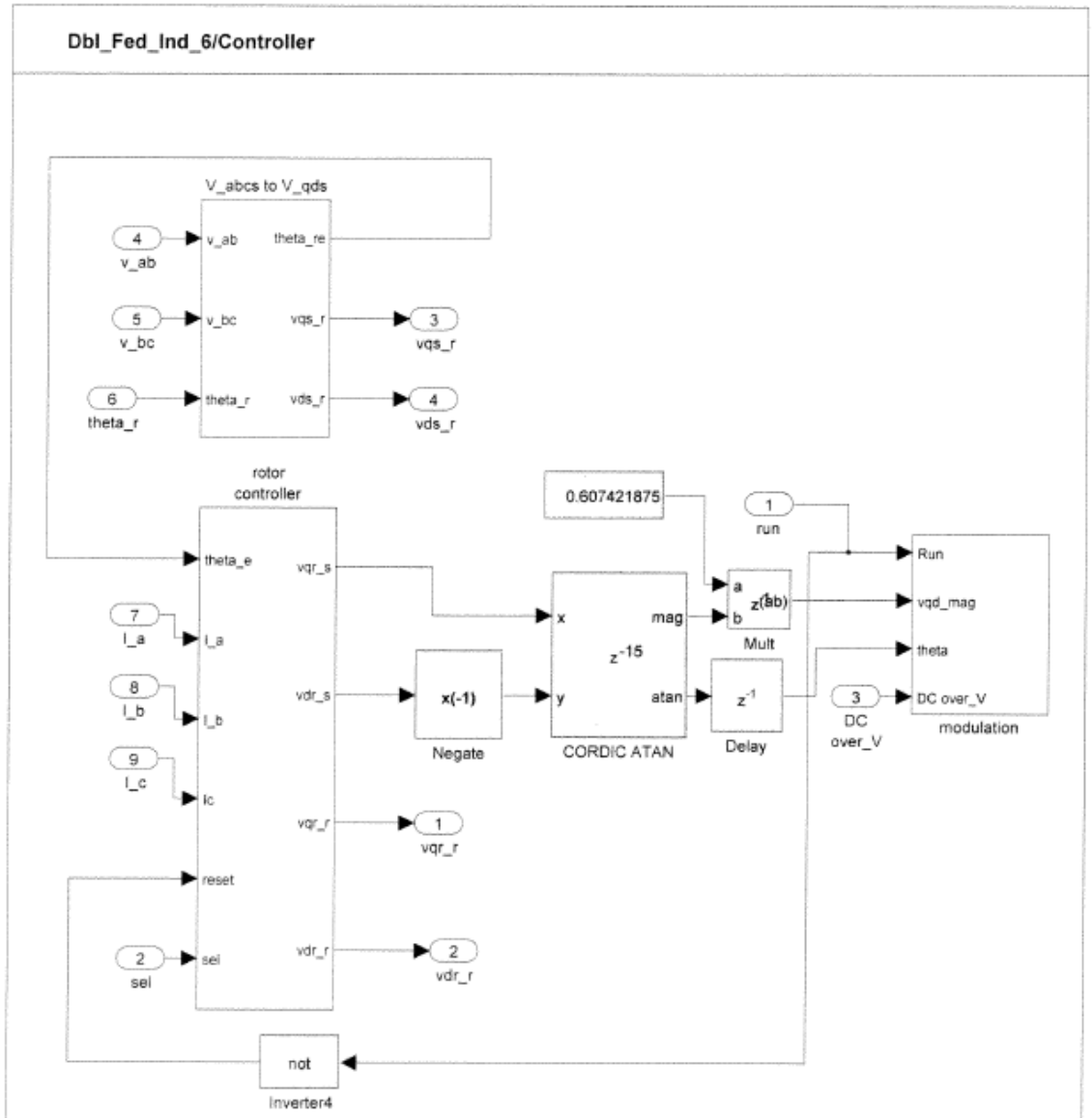
Dbl_Fed_Ind_6/Controller
V_abcs to V_qds
4
v_ab
v_ab
theta_re
5
v_bc
v_bc
vqs_r
3
vqs_r
6
theta_r
theta_r
vds_r
4
vds_r
rotor
controller
0.607421875
1
run
theta_e
vqr_s
a
b
z(ab)
Mult
Run
7
I_a
I_a
x
mag
z-15
vqd_mag
8
I_b
I_b
vdr_s
x(-1)
Negate
y
atan
CORDIC ATAN
z-1
Delay
theta
3
DC
over_V
DC over_V
modulation
9
I_c
Ic
vqr_r
1
vqr_r
reset
2
sel
sel
vdr_r
2
vdr_r
not
Inverter4
H:\thesis3\Dbl_Fed_Ind_6.mdl
printed 13-May-2009 18:40
page 18/54

Dbl_Fed_Ind_6/Controller/V_abcs to V_qds

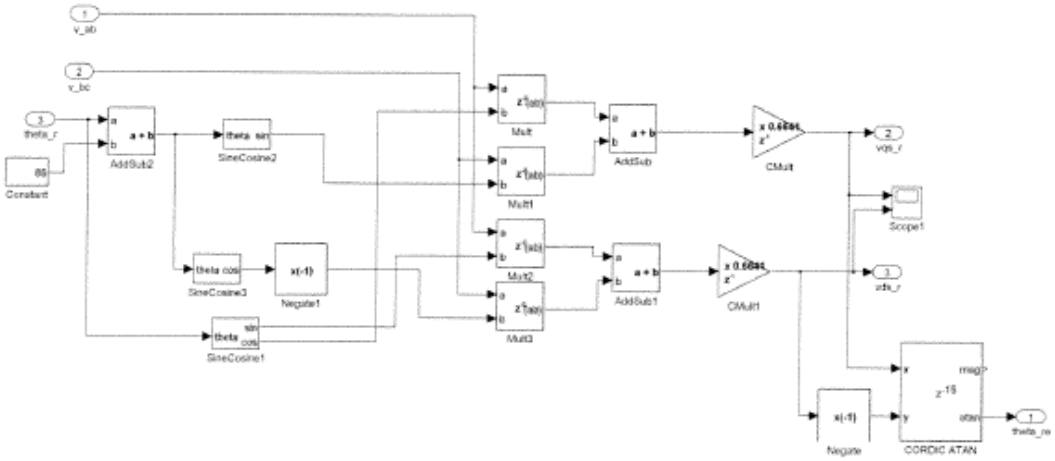

H:\thesis3\Dbl_Fed_Ind_6.mdl

printed 13-May-2009 18:40

page 19/54

Dbl_Fed_Ind_6/Controller/modulation

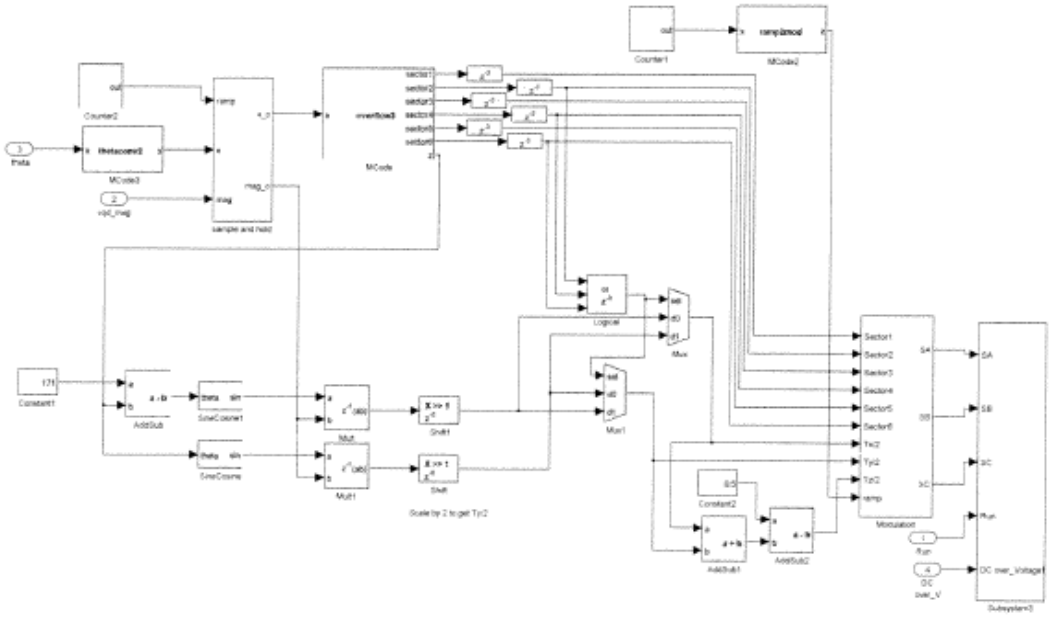

H:\thesis3\Dbl_Fed_Ind_6.mdl

printed 13-May-2009 18:40

page 20/54

Dbl_Fed_Ind_6/Controller/modulation/Modulation

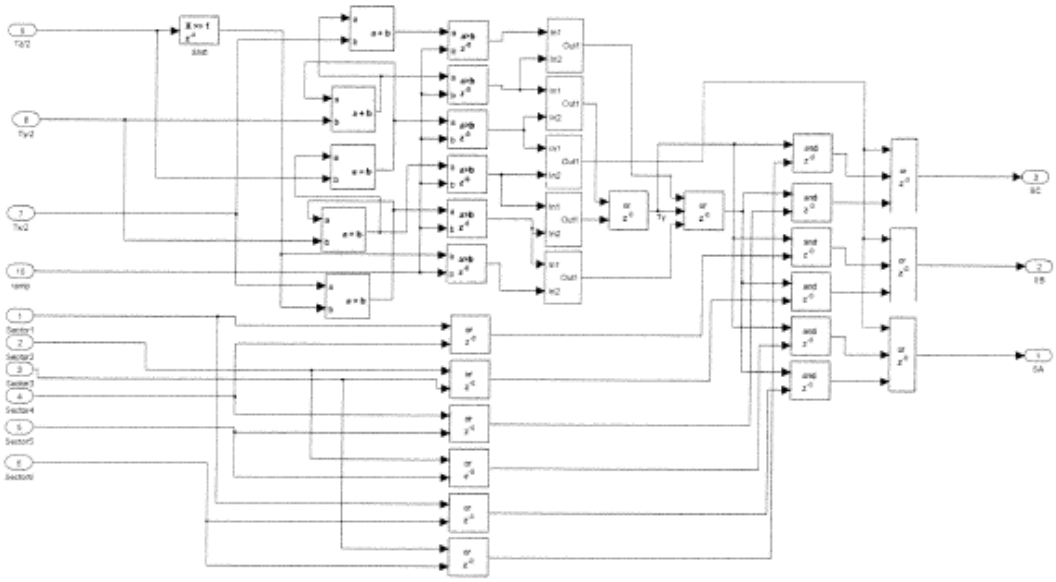

H:\thesis3\Dbl_Fed_Ind_6.mdl

printed 13-May-2009 18:40

page 21/54

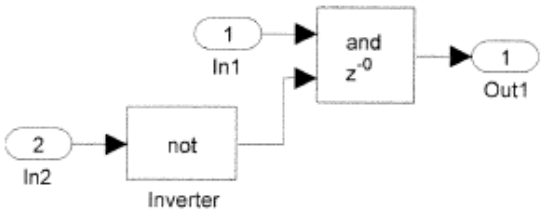
1
In1
and
z-0
1
Out1
2
In2
not
Inverter

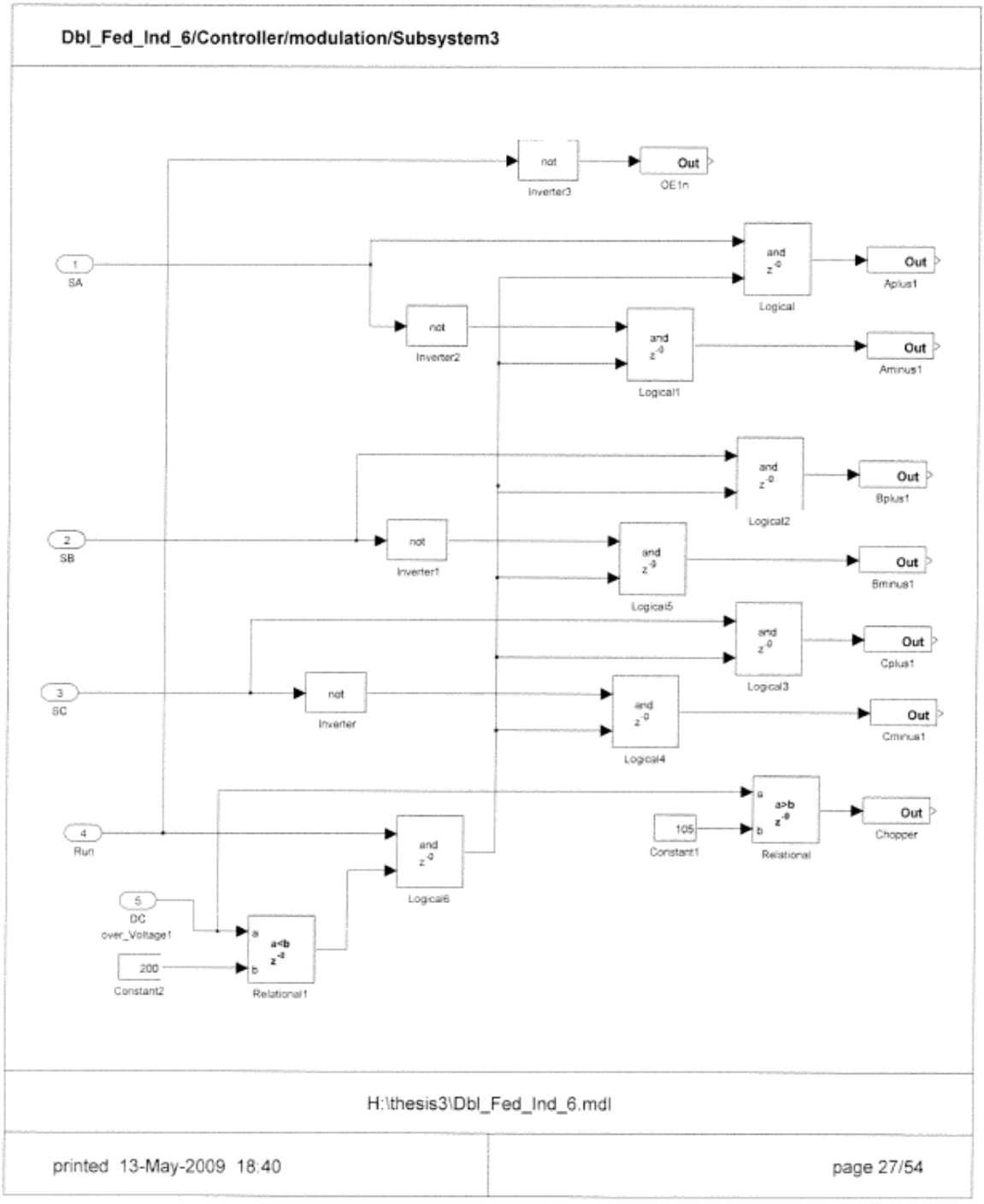
Dbl_Fed_Ind_6/Controller/modulation/Subsystem3
not
Inverter3
Out
OE1n
1
SA
and
Logical
Out
Aplus1
not
Inverter2
and
Logical1
Out
Aminus1
and
Logical2
Out
Bplus1
2
SB
not
Inverter1
and
Logical5
Out
Bminus1
and
Logical3
Out
Cplus1
3
SC
not
Inverter
and
Logical4
Out
Cminus1
4
Run
and
Logical6
105
Constant1
a>b
Relational
Out
Chopper
5
DC
over_Voltage1
a<b
200
Constant2
Relational1
H:\thesis3\Dbl_Fed_Ind_6.mdl
printed 13-May-2009 18:40
page 27/54

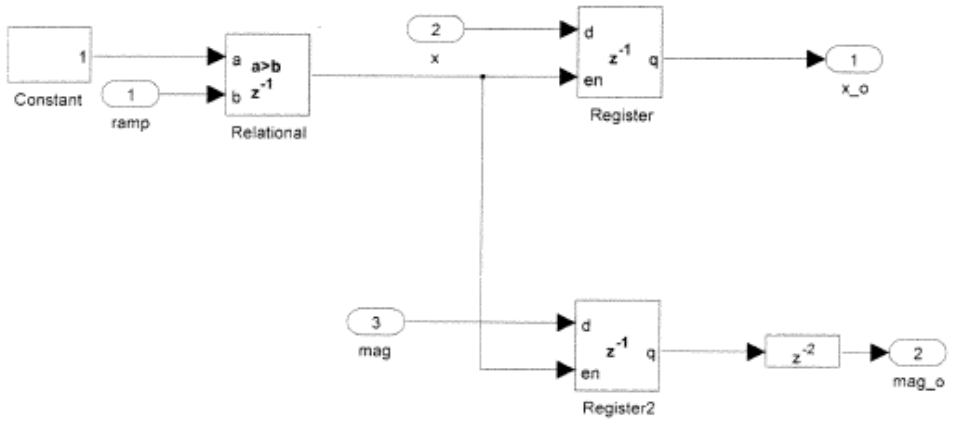
1
Constant
1
ramp
a
a>b
b
z-1
Relational
2
x
d
z-1
q
en
Register
1
x_o
3
mag
d
z-1
q
en
Register2
z-2
2
mag_o

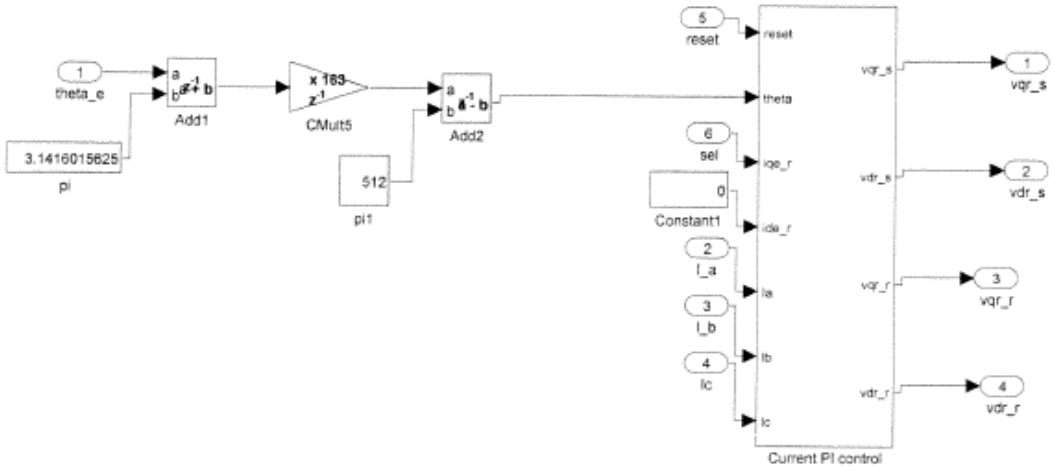
1
theta_e
3.1416015625
pi
Add1
x 183
z-1
CMult5
512
pi1
Add2
5
reset
6
sel
0
Constant1
2
I_a
3
I_b
4
Ic
reset
theta
iqe_r
ide_r
Ia
Ib
Ic
vqr_s
vdr_s
vqr_r
vdr_r
Current PI control
1
vqr_s
2
vdr_s
3
vqr_r
4
vdr_r

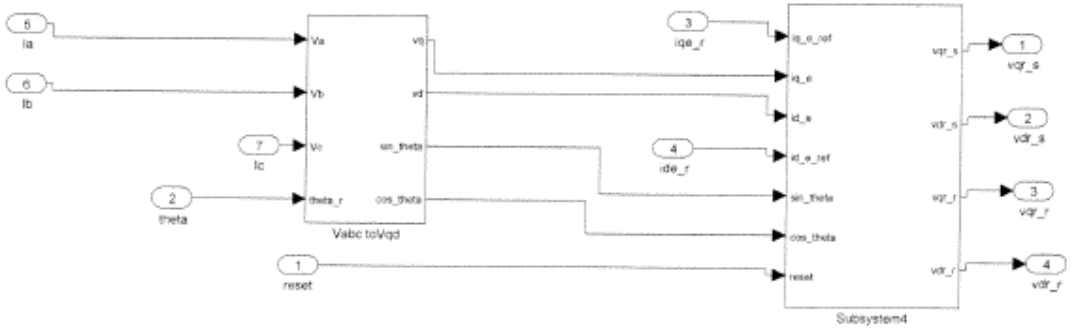
5
Ia
6
Ib
7
Ic
2
theta
Va
Vb
Vc
theta_r
vq
vd
sin_theta
cos_theta
Vabc toVqd
1
reset
3
iqe_f
4
ide_f
iq_e_ref
iq_e
id_e
id_e_ref
sin_theta
cos_theta
reset
vqr_s
vdr_s
vqr_r
vdr_r
Subsystem4
1
vqr_s
2
vdr_s
3
vqr_r
4
vdr_r

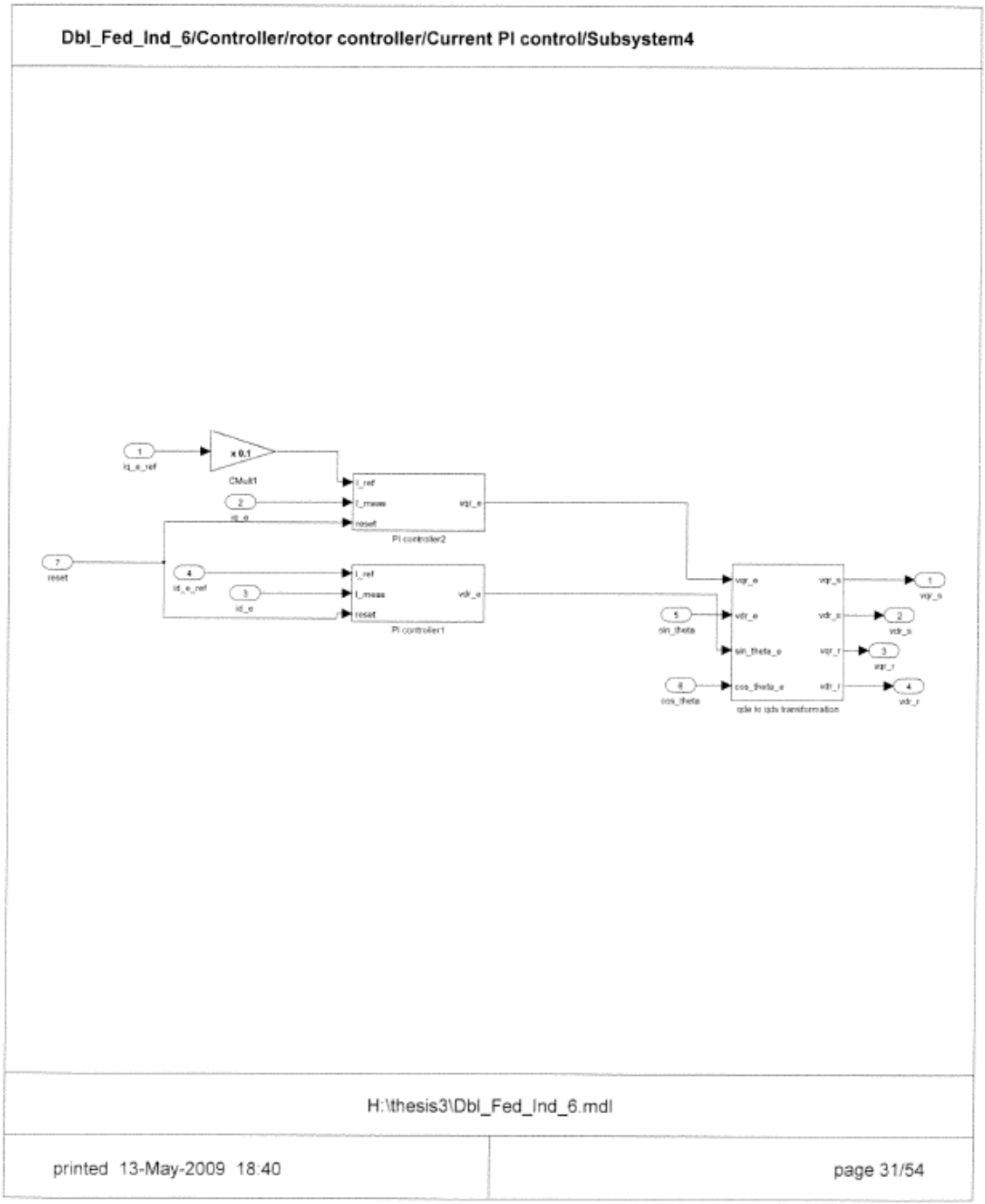
Dbl_Fed_Ind_6/Controller/rotor controller/Current PI control/Subsystem4
1
id_e_ref
x 0.1
CMult1
2
id_e
I_ref
I_meas
reset
vqr_e
PI controller2
7
reset
4
id_e_ref
3
id_e
I_ref
I_meas
reset
vdr_e
PI controller1
vqr_e
vdr_e
sin_theta
sin_theta_e
cos_theta
cos_theta_e
vqr_s
vdr_s
vqr_r
vdr_r
qde to qds transformation
1
vqr_s
5
sin_theta
2
vdr_s
3
vqr_r
6
cos_theta
4
vdr_r
H:\thesis3\Dbl_Fed_Ind_6.mdl
printed 13-May-2009 18:40
page 31/54

Dbl_Fed_Ind_6/Controller/rotor controller/Current PI control/Subsystem4/PI controller1

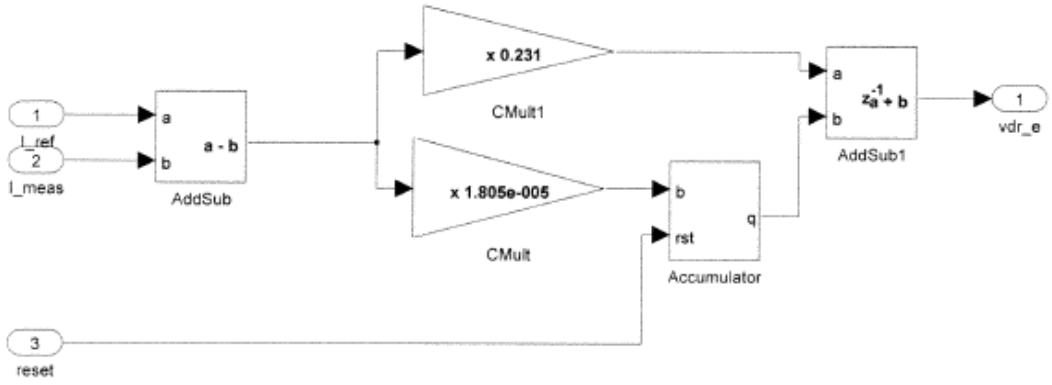

-12 is IC

H:\thesis3\Dbl_Fed_Ind_6.mdl

printed 13-May-2009 18:40

page 32/54

Dbl_Fed_Ind_6/Controller/rotor controller/Current PI control/Subsystem4/PI controller2

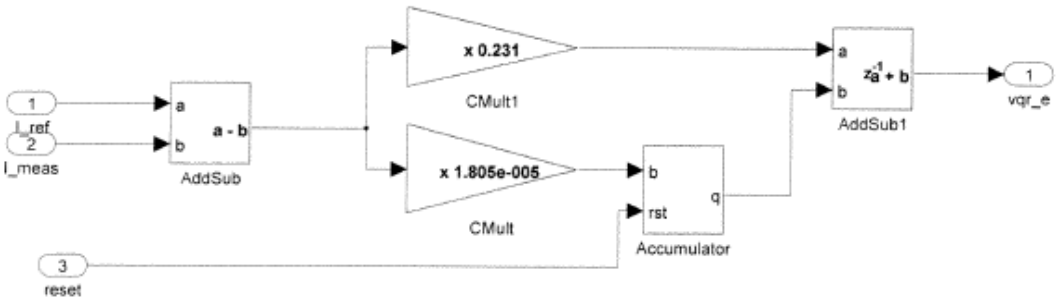

H:\thesis3\Dbl_Fed_Ind_6.mdl

printed 13-May-2009 18:40 | page 33/54

Dbl_Fed_Ind_6/Controller/rotor controller/Current PI control/Subsystem4/qde to qds transformation

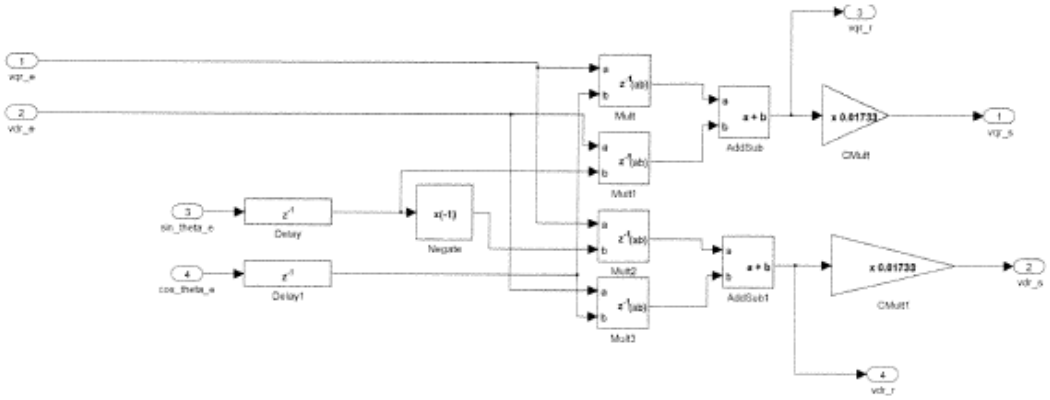

H:\thesis3\Dbl_Fed_Ind_6.mdl

printed 13-May-2009 18:40

page 34/54

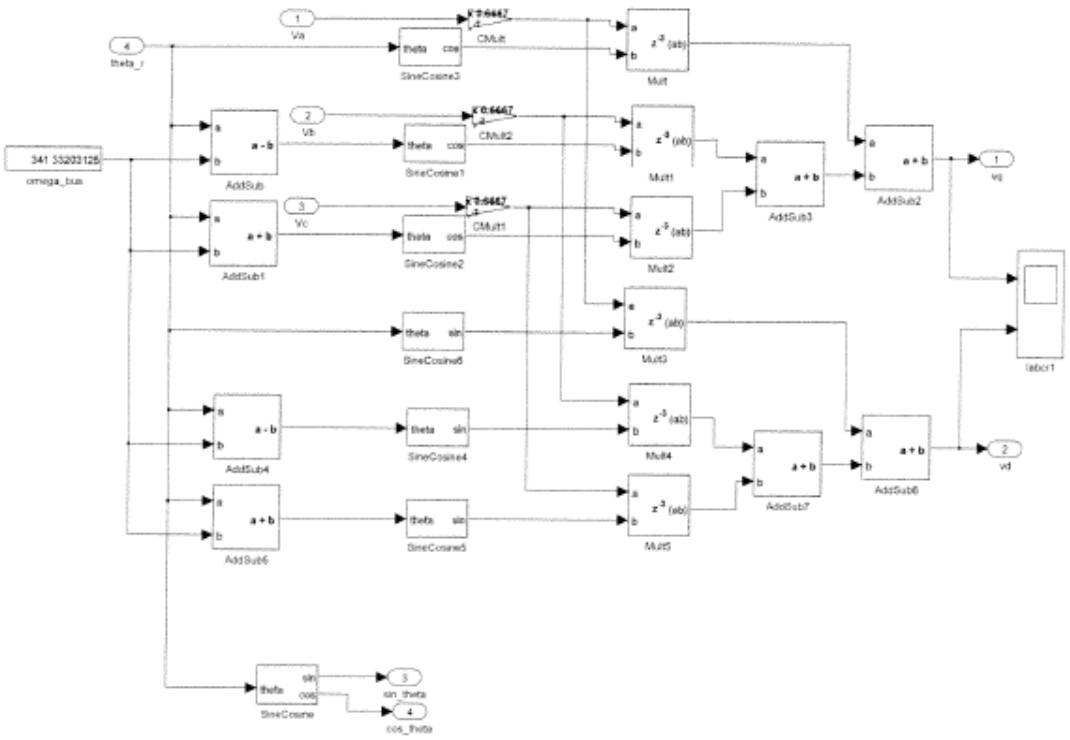
Va
Vb
Vc
theta_r
omega_bus
SineCosine3
SineCosine1
SineCosine2
SineCosine6
SineCosine4
SineCosine5
SineCosine
CMult
CMult2
CMult1
Mult
Mult1
Mult2
Mult3
Mult4
Mult5
AddSub
AddSub1
AddSub2
AddSub3
AddSub4
AddSub5
AddSub6
AddSub7
sin_theta
cos_theta
vq
vd

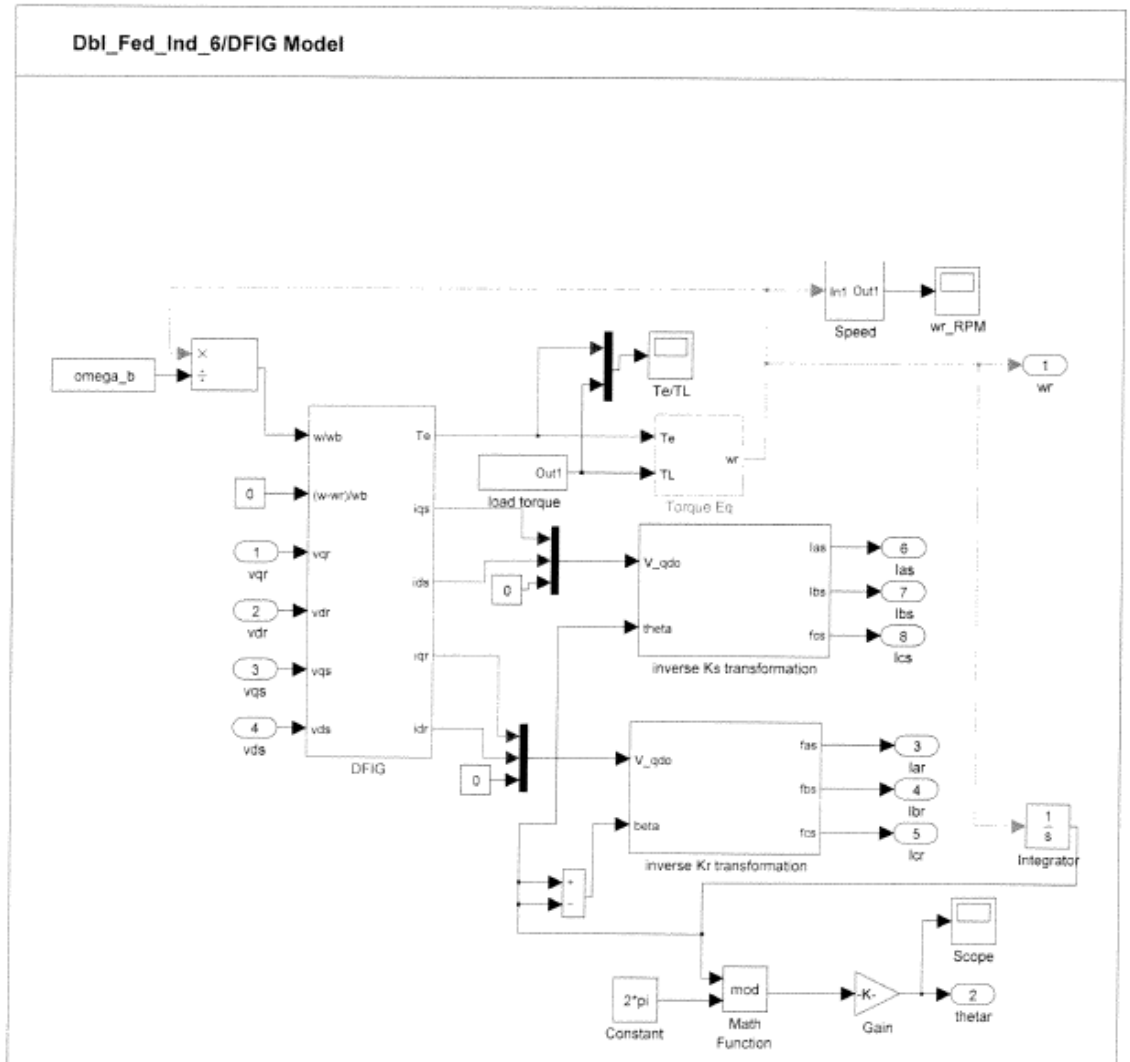
Dbl_Fed_Ind_6/DFIG Model
In1 Out1
Speed
wr_RPM
omega_b
Te/TL
1
wr
w/wb
Te
Te
wr
TL
Torque Eq
Out1
load torque
0
(w-wr)/wb
iqs
1
vqr
vqr
ids
V_qdo
Ias
6
Ias
2
vdr
vdr
0
theta
Ibs
7
Ibs
3
vqs
vqs
iqr
fcs
8
Ics
inverse Ks transformation
4
vds
vds
idr
DFIG
0
V_qdo
fas
3
Iar
fbs
4
Ibr
beta
fcs
5
Icr
inverse Kr transformation
1
s
Integrator
Scope
2*pi
Constant
mod
Math
Function
-K-
Gain
2
thetar
H:\thesis3\Dbl_Fed_Ind_6.mdl
printed 13-May-2009 18:40
page 36/54

Dbl_Fed_Ind_6/DFIG Model/DFIG

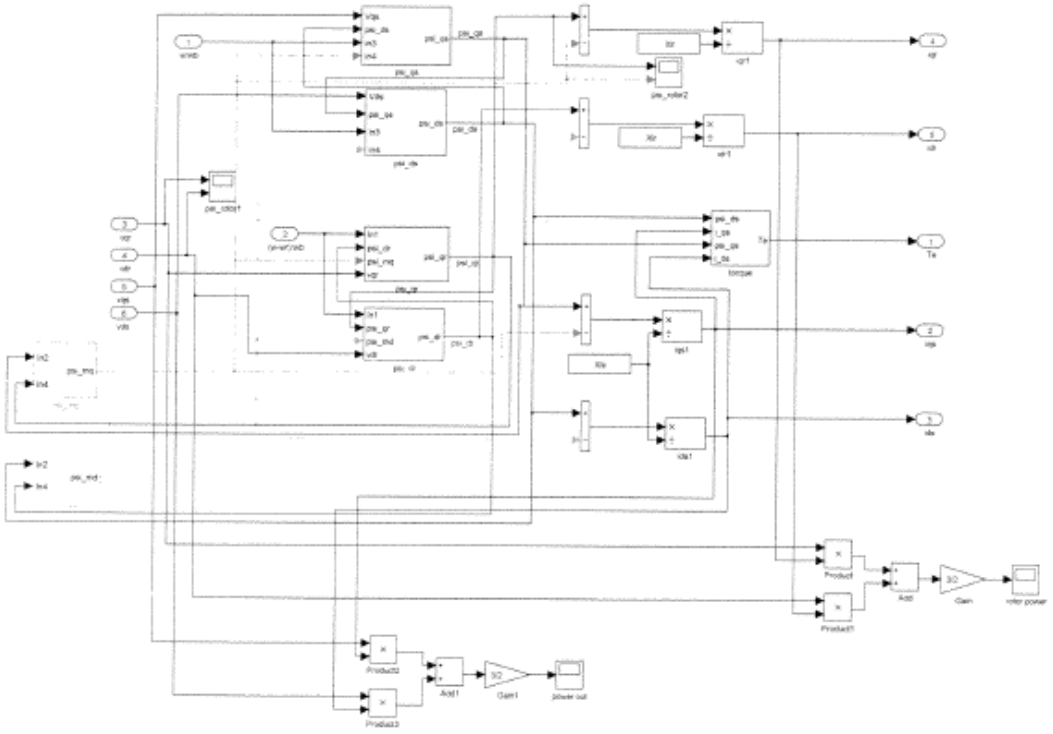

H:\thesis3\Dbl_Fed_Ind_6.mdl

printed 13-May-2009 18:40

page 37/54

Dbl_Fed_Ind_6/DFIG Model/DFIG/psi_dr

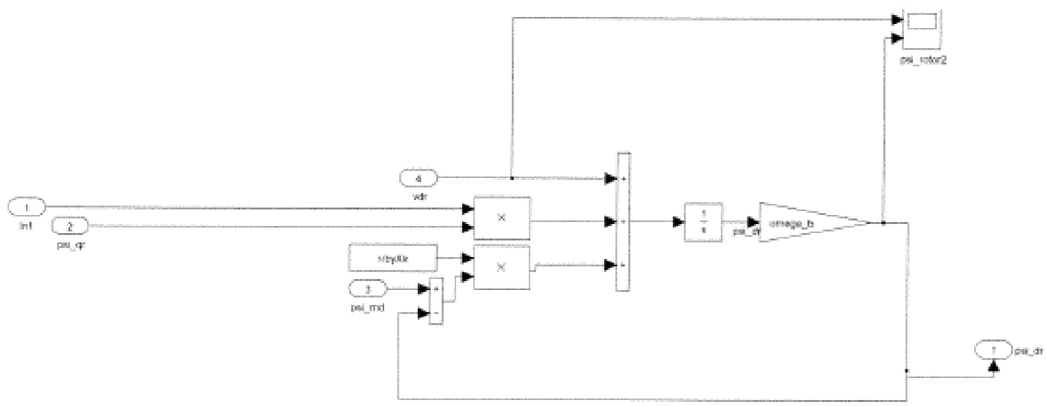

H:\thesis3\Dbl_Fed_Ind_6.mdl

printed 13-May-2009 18:40

page 38/54

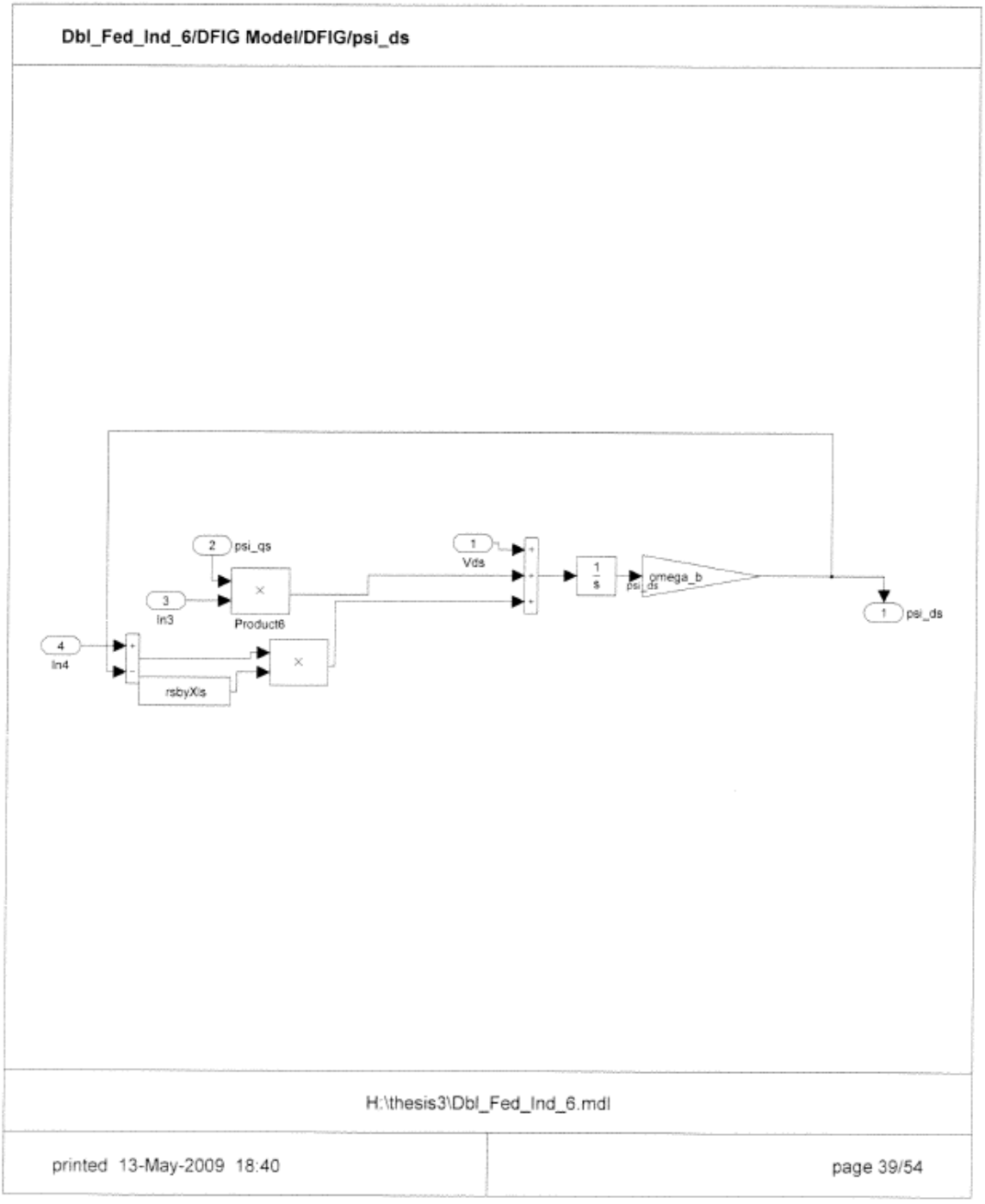
Dbl_Fed_Ind_6/DFIG Model/DFIG/psi_ds
2
psi_qs
3
In3
Product6
1
Vds
1
s
psi_ds
omega_b
1
psi_ds
4
In4
rsbyXls
H:\thesis3\Dbl_Fed_Ind_6.mdl
printed 13-May-2009 18:40
page 39/54

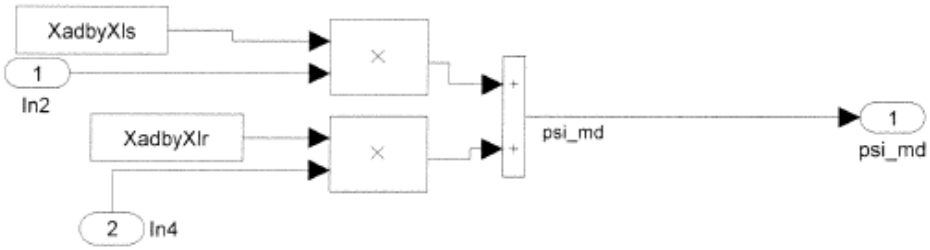
XadbyXls
1
In2
XadbyXlr
2
In4
psi_md
1
psi_md

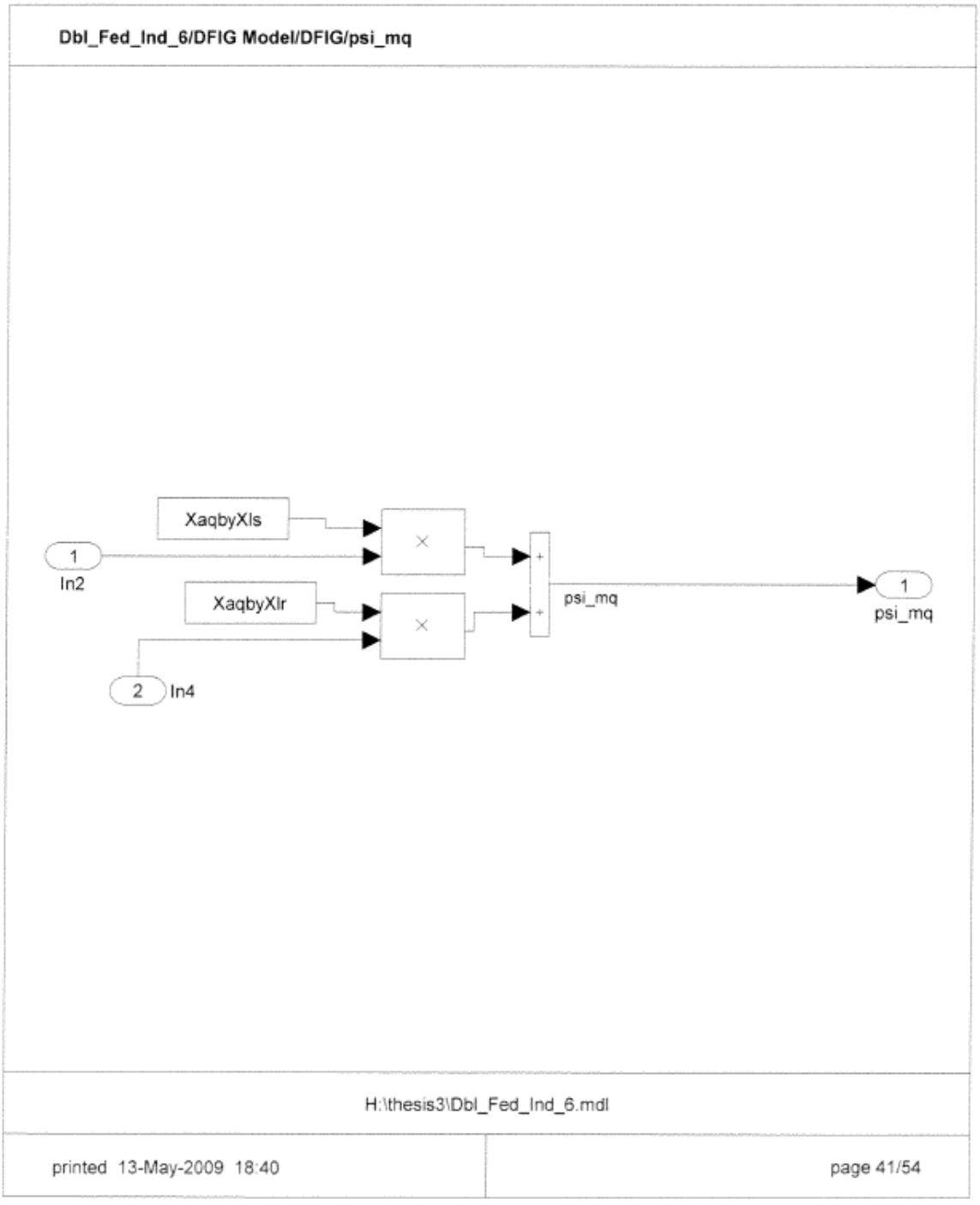
Dbl_Fed_Ind_6/DFIG Model/DFIG/psi_mq
XaqbyXls
1
In2
XaqbyXlr
2
In4
psi_mq
1
psi_mq
H:\thesis3\Dbl_Fed_Ind_6.mdl
printed 13-May-2009 18:40
page 41/54

Dbl_Fed_Ind_6/DFIG Model/DFIG/psi_qr

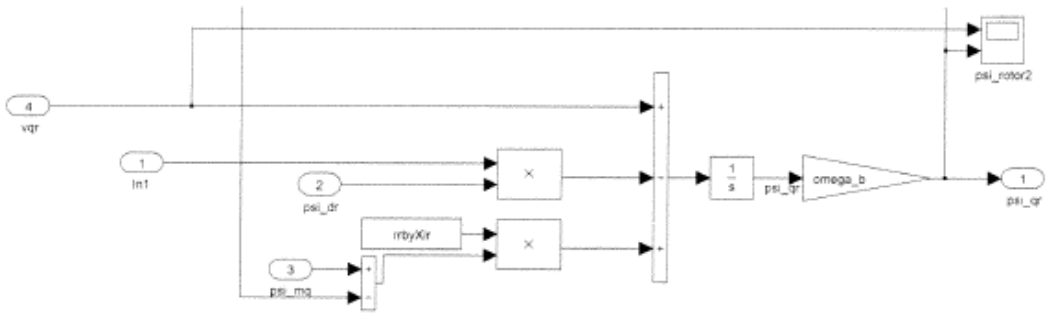

H:\thesis3\Dbl_Fed_Ind_6.mdl

printed 13-May-2009 18:40 | page 42/54

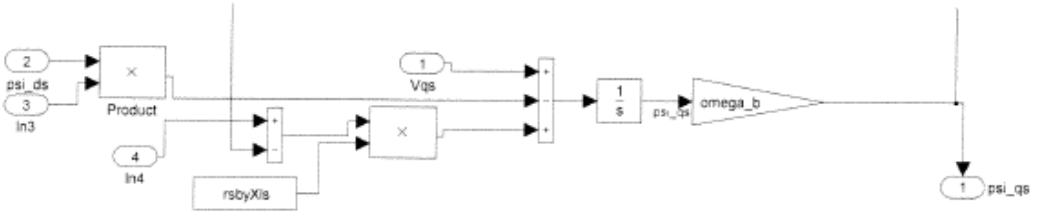
2
psi_ds
3
In3
Product
4
In4
rsbyXls
1
Vqs
1
s
psi_qs
omega_b
1
psi_qs

Dbl_Fed_Ind_6/DFIG Model/DFIG/torque

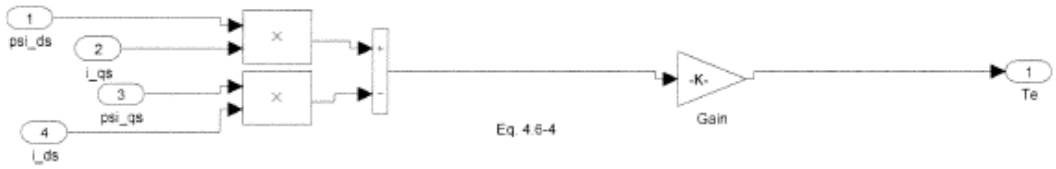

H:\thesis3\Dbl_Fed_Ind_6.mdl

printed 13-May-2009 18:40

page 44/54

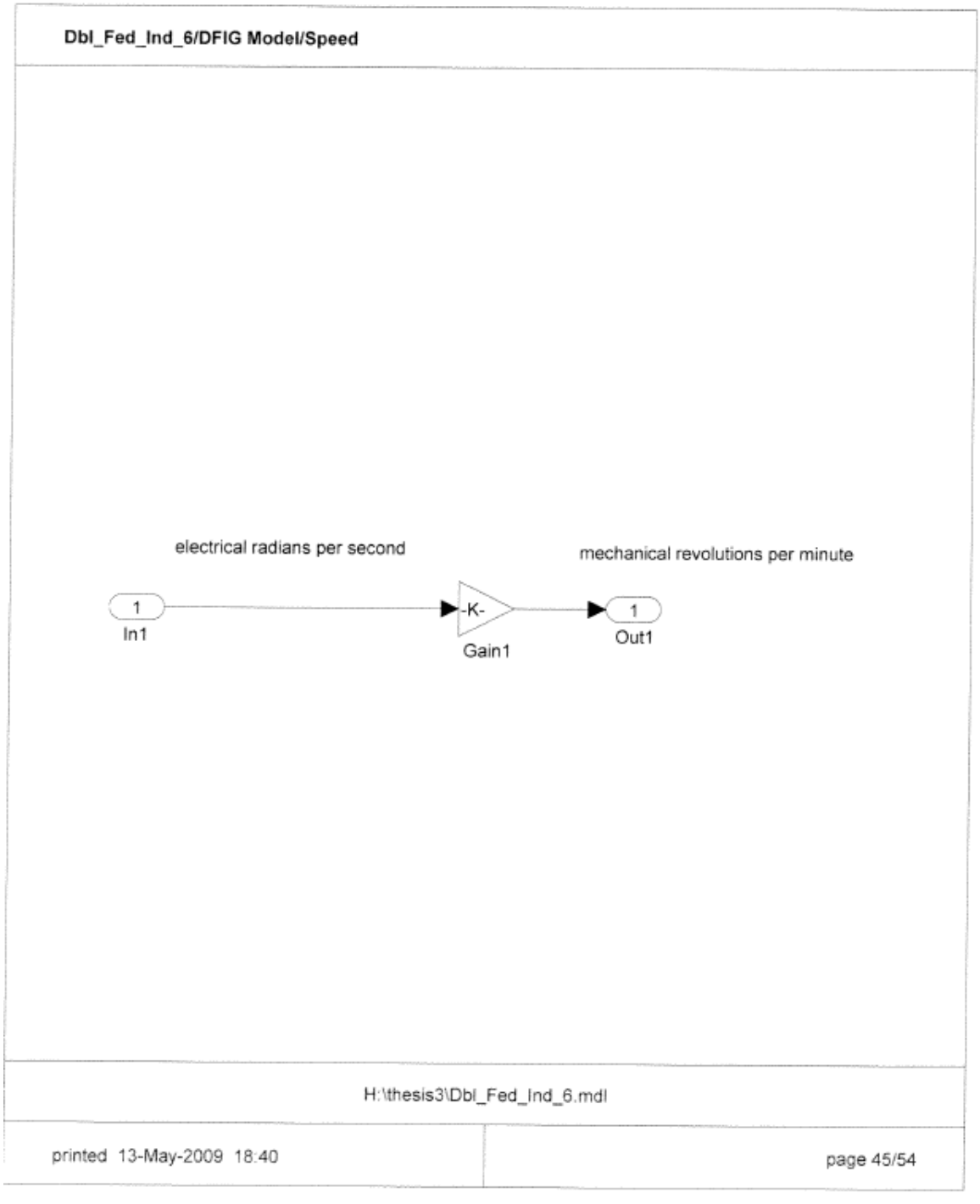
Dbl_Fed_Ind_6/DFIG Model/Speed
electrical radians per second
mechanical revolutions per minute
1
In1
-K-
Gain1
1
Out1
H:\thesis3\Dbl_Fed_Ind_6.mdl
printed 13-May-2009 18:40
page 45/54

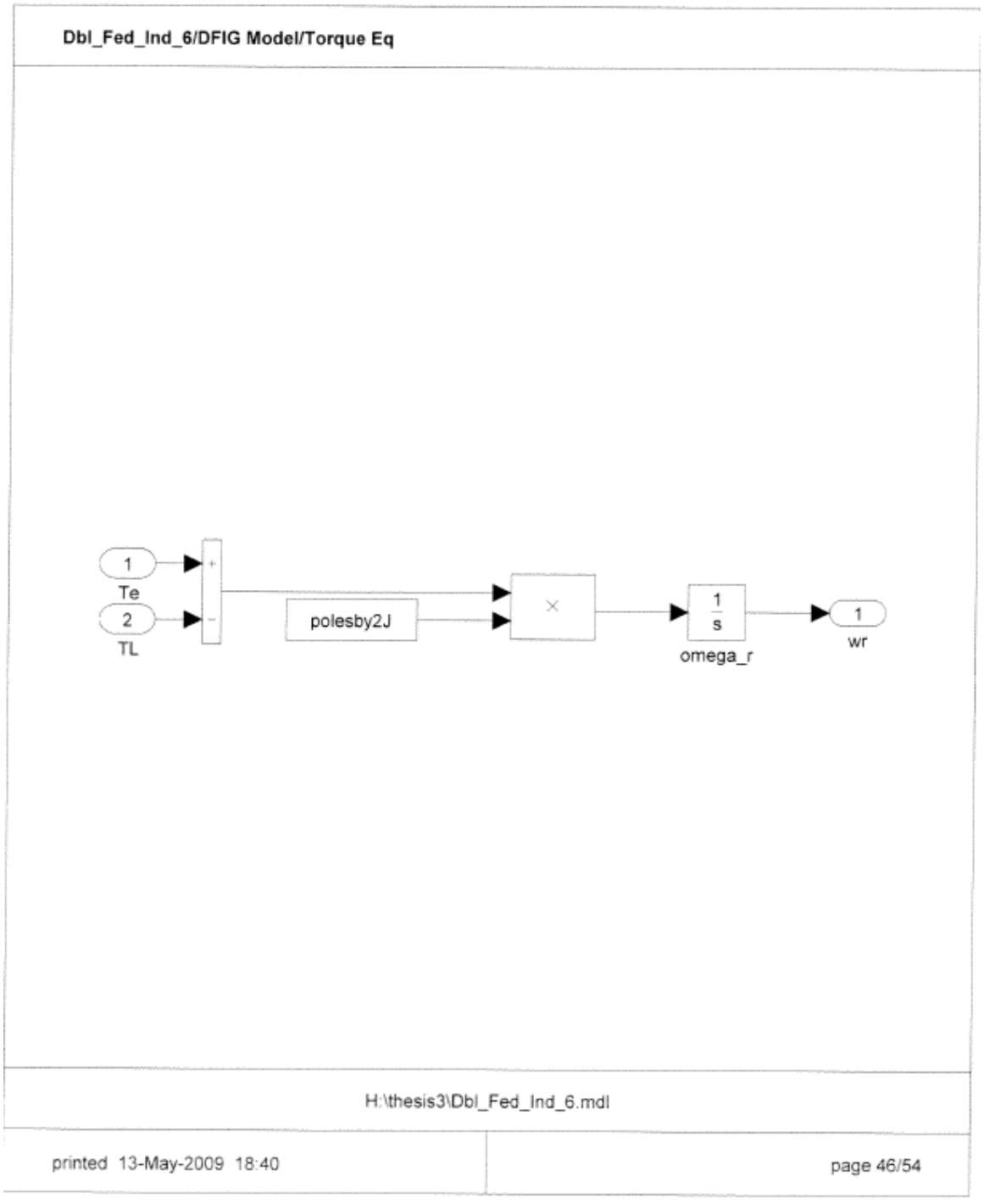
Dbl_Fed_Ind_6/DFIG Model/Torque Eq
1
Te
2
TL
+
-
polesby2J
×
1
s
omega_r
1
wr
H:\thesis3\Dbl_Fed_Ind_6.mdl
printed 13-May-2009 18:40
page 46/54

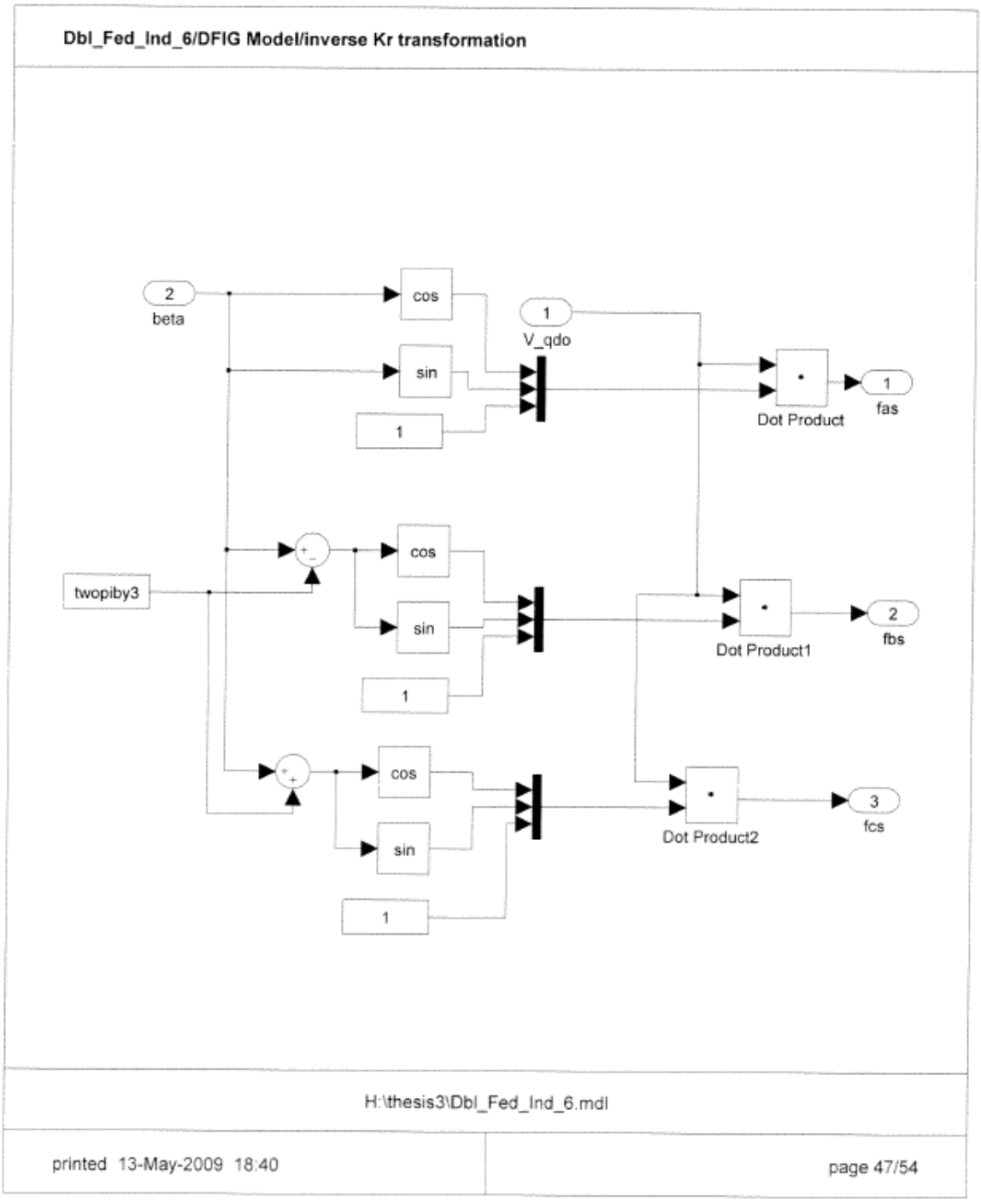
Dbl_Fed_Ind_6/DFIG Model/inverse Kr transformation
2
beta
cos
sin
1
1
V_qdo
Dot Product
1
fas
twopiby3
cos
sin
1
Dot Product1
2
fbs
cos
sin
1
Dot Product2
3
fcs
H:\thesis3\Dbl_Fed_Ind_6.mdl
printed 13-May-2009 18:40
page 47/54

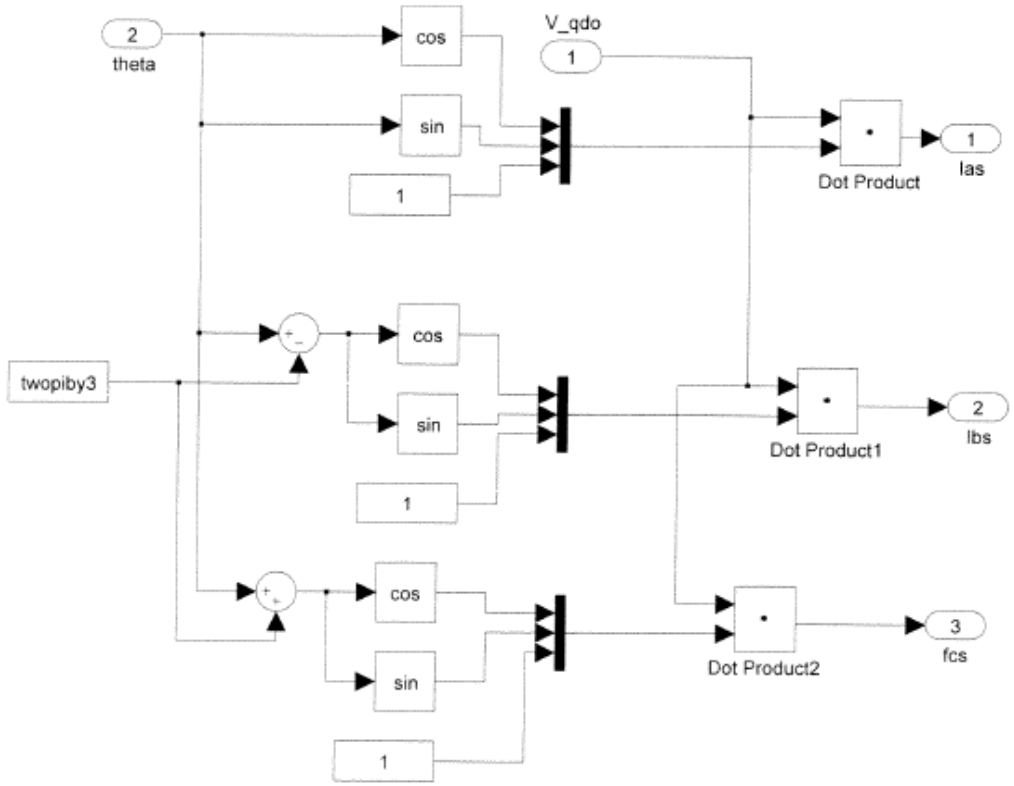
2
theta
cos
sin
1
V_qdo
1
Dot Product
1
Ias
twopiby3
cos
sin
1
Dot Product1
2
Ibs
cos
sin
1
Dot Product2
3
Ics

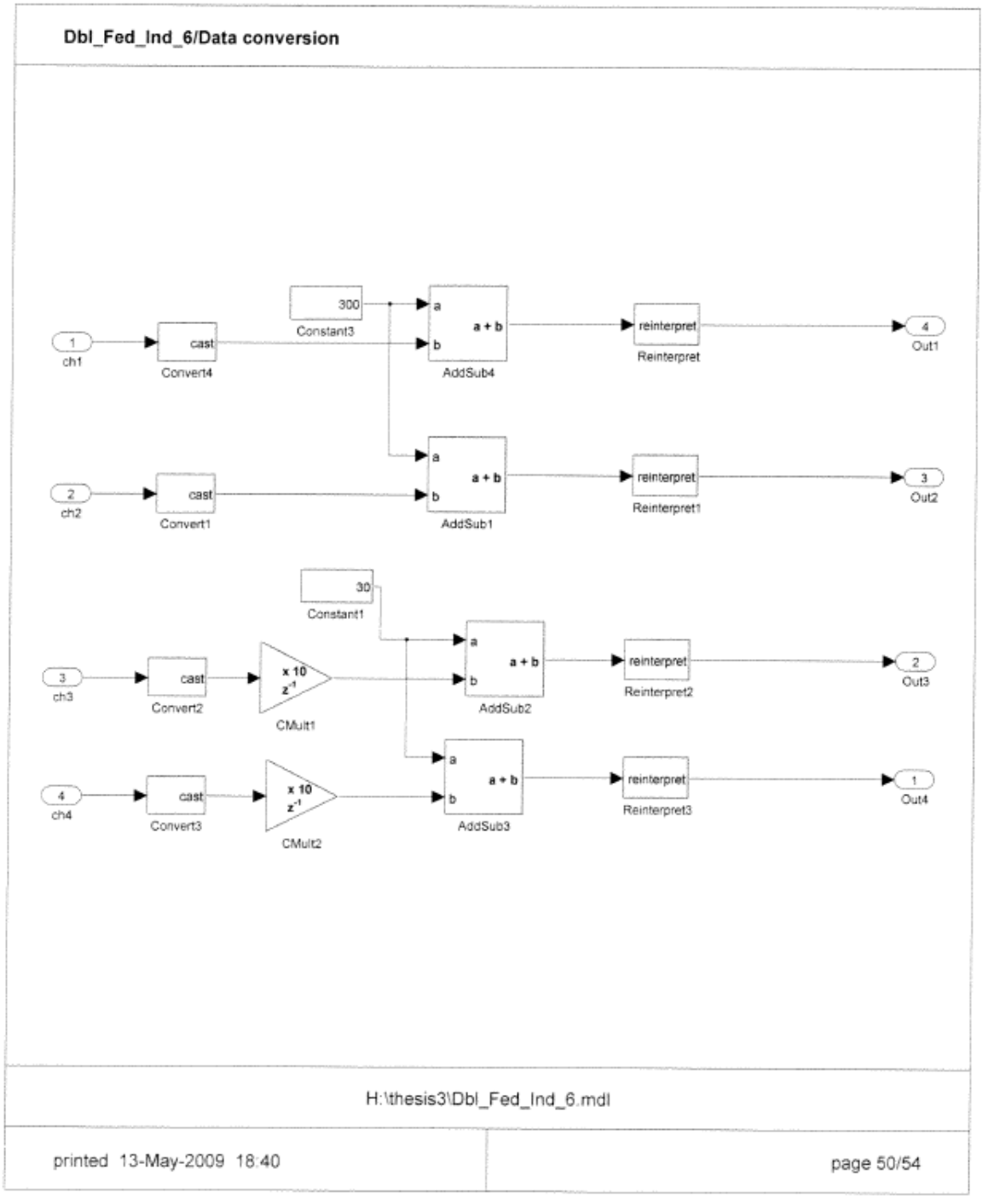
Dbl_Fed_Ind_6/Data conversion
1
ch1
cast
Convert4
300
Constant3
a
b
a + b
AddSub4
reinterpret
Reinterpret
4
Out1
2
ch2
cast
Convert1
a
b
a + b
AddSub1
reinterpret
Reinterpret1
3
Out2
30
Constant1
3
ch3
cast
Convert2
x 10
z-1
CMult1
a
b
a + b
AddSub2
reinterpret
Reinterpret2
2
Out3
4
ch4
cast
Convert3
x 10
z-1
CMult2
a
b
a + b
AddSub3
reinterpret
Reinterpret3
1
Out4
H:\thesis3\Dbl_Fed_Ind_6.mdl
printed 13-May-2009 18:40
page 50/54

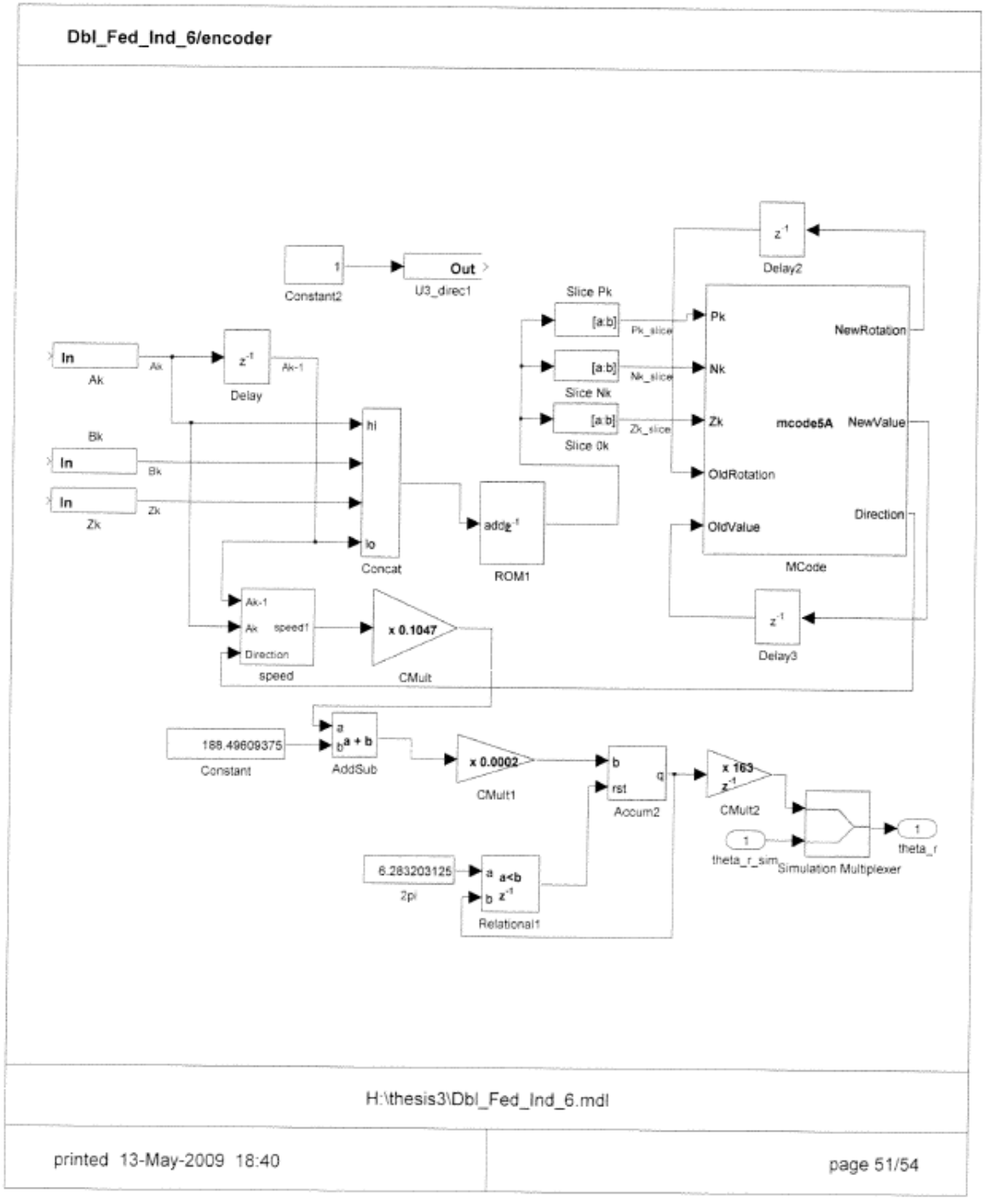
Dbl_Fed_Ind_6/encoder
Constant2
1
Out
U3_direct1
Delay2
Slice Pk
[a:b]
Pk_slice
Pk
NewRotation
In
Ak
Ak
Delay
Ak-1
Slice Nk
Nk_slice
Nk
Bk
In
Bk
Slice 0k
Zk_slice
Zk
mcode5A
NewValue
In
Zk
Zk
hi
lo
Concat
OldRotation
Direction
OldValue
MCode
add
ROM1
Ak-1
Ak
speed1
Direction
speed
x 0.1047
CMult
Delay3
188.49609375
Constant
a
b
a + b
AddSub
x 0.0002
CMult1
b
rst
q
Accum2
x 163
CMult2
1
theta_r_sim
Simulation Multiplexer
1
theta_r
6.283203125
2pi
a
b
a<b
Relational1
H:\thesis3\Dbl_Fed_Ind_6.mdl
printed 13-May-2009 18:40
page 51/54

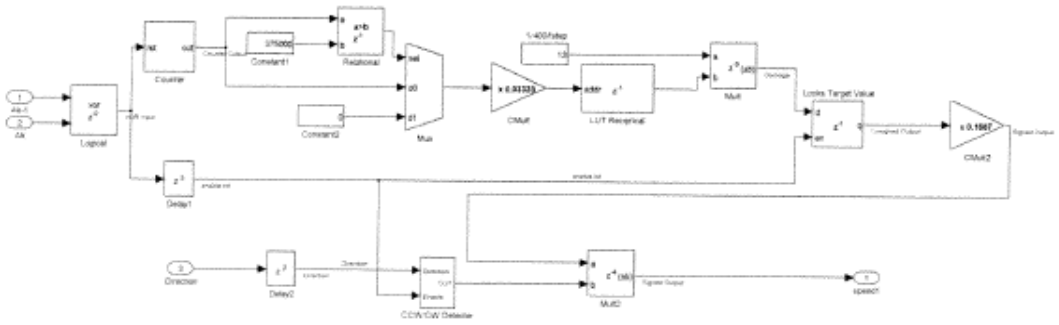
Counter
Constant1
Relational
Constant2
Mux
CMult
LUT Reciprocal
Mult
Looks Target Value
CMult2
Logical
Delay1
Delay2
CCW/CW Detector
MultD

Dbl_Fed_Ind_6/encoder/speed/CCW/CW Detector

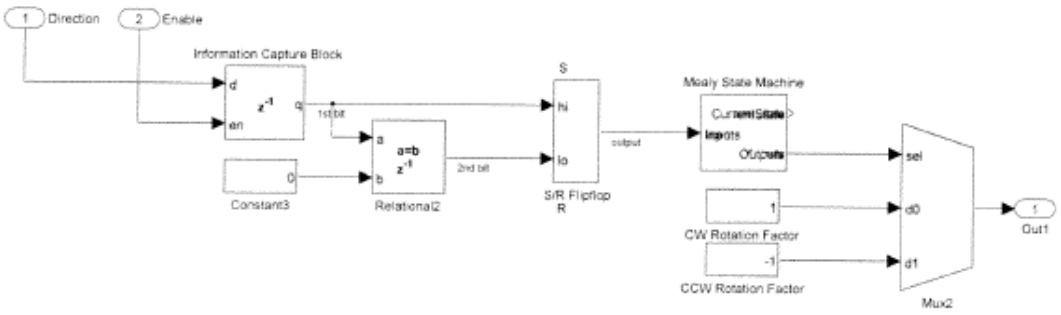

H:\thesis3\Dbl_Fed_Ind_6.mdl

printed 13-May-2009 18:40

page 53/54

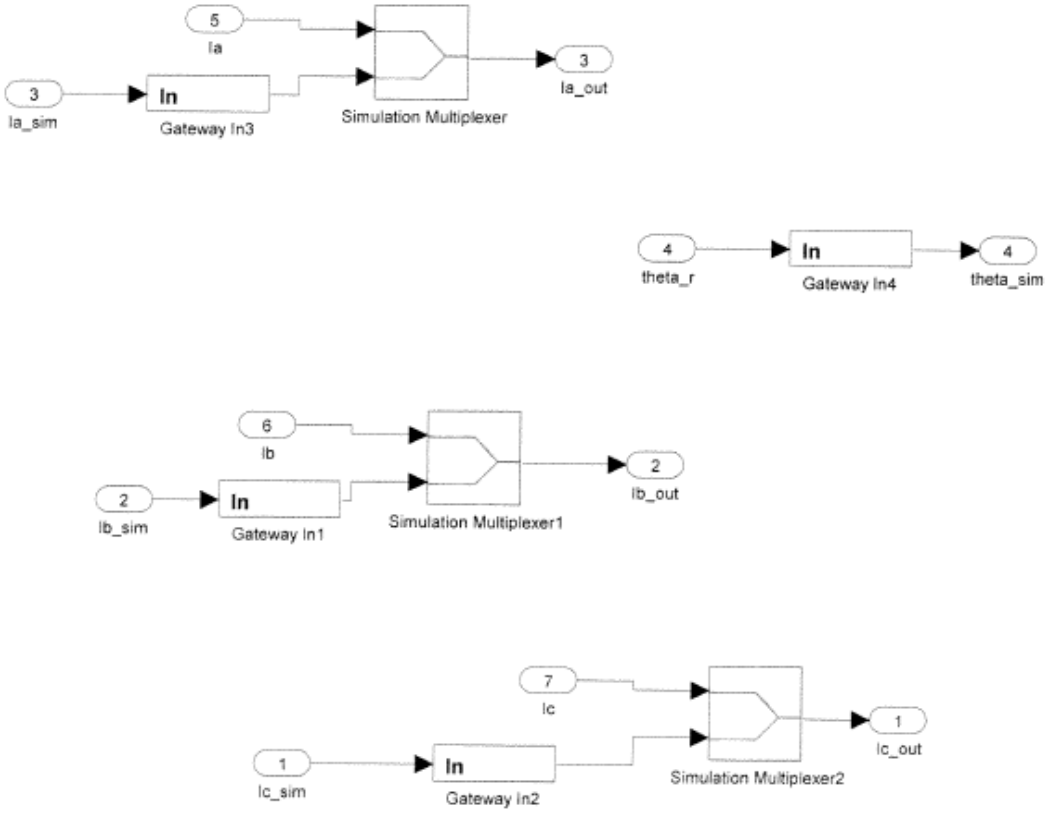
5
Ia
3
Ia_sim
In
Gateway In3
Simulation Multiplexer
3
Ia_out
4
theta_r
In
Gateway In4
4
theta_sim
6
Ib
2
Ib_sim
In
Gateway In1
Simulation Multiplexer1
2
Ib_out
7
Ic
1
Ic_sim
In
Gateway In2
Simulation Multiplexer2
1
Ic_out

APPENDIX D: TRANSFORMATION DERIVATION

$v_{ab} = v_a - v_b; v_{bc} = v_b - v_c = v_b - (-v_a - v_b);$ where $v_a + v_b + v_c = 0$ for a wye connected capacitor bank (with the neutral floating)
Note also that $i_a + i_b + i_c = 0$ for a wye connected transformer winding set.

$$\begin{bmatrix} v_{ab} \\ v_{bc} \end{bmatrix} = \begin{bmatrix} 1 & -1 \\ 1 & 2 \end{bmatrix} \begin{bmatrix} v_a \\ v_b \end{bmatrix} \Rightarrow \begin{bmatrix} v_a \\ v_b \end{bmatrix} = \frac{1}{3} \begin{bmatrix} 2 & 1 \\ -1 & 1 \end{bmatrix} \begin{bmatrix} v_{ab} \\ v_{bc} \end{bmatrix}$$

$v_q = \frac{2}{3}\left[v_a \cos(\theta) + v_b \cos\left(\theta - \frac{2\pi}{3}\right) + v_c \cos\left(\theta + \frac{2\pi}{3}\right)\right]$; ref. Krause text

$= \frac{2}{3}\left[v_a \cos(\theta) + v_b \cos\left(\theta - \frac{2\pi}{3}\right) + (-v_a - v_b) \cos\left(\theta + \frac{2\pi}{3}\right)\right]$

$= \frac{2}{3}\left[v_a \left(\cos(\theta) - \cos\left(\theta + \frac{2\pi}{3}\right)\right) + v_b \left(\cos\left(\theta - \frac{2\pi}{3}\right) - \cos\left(\theta + \frac{2\pi}{3}\right)\right)\right] = \boxed{\frac{2}{\sqrt{3}}\left(v_a \sin\left(\theta + \frac{\pi}{3}\right) + v_b \sin(\theta)\right)}$

$v_d = \frac{2}{3}\left[v_a \sin(\theta) + v_b \sin\left(\theta - \frac{2\pi}{3}\right) + v_c \sin\left(\theta + \frac{2\pi}{3}\right)\right]$; ref. Krause text

$= \frac{2}{3}\left[v_a \sin(\theta) + v_b \sin\left(\theta - \frac{2\pi}{3}\right) + (-v_a - v_b) \sin\left(\theta + \frac{2\pi}{3}\right)\right]$

$= \frac{2}{3}\left[v_a \left(\sin(\theta) - \sin\left(\theta + \frac{2\pi}{3}\right)\right) + v_b \left(\sin\left(\theta - \frac{2\pi}{3}\right) - \sin\left(\theta + \frac{2\pi}{3}\right)\right)\right] = \boxed{\frac{2}{\sqrt{3}}\left(-v_a \cos\left(\theta + \frac{\pi}{3}\right) - v_b \cos(\theta)\right)}$

$$\begin{bmatrix} v_q \\ v_d \end{bmatrix} = \frac{2}{\sqrt{3}} \begin{bmatrix} \sin\left(\theta_e + \frac{\pi}{3}\right) & \sin(\theta_e) \\ -\cos\left(\theta_e + \frac{\pi}{3}\right) & -\cos(\theta_e) \end{bmatrix} \frac{1}{3} \begin{bmatrix} 2 & 1 \\ -1 & 1 \end{bmatrix} \begin{bmatrix} v_{ab} \\ v_{bc} \end{bmatrix} = \frac{2}{3\sqrt{3}} \begin{bmatrix} \sin\left(\theta_e + \frac{\pi}{3}\right) & \sin(\theta_e) \\ -\cos\left(\theta_e + \frac{\pi}{3}\right) & -\cos(\theta_e) \end{bmatrix} \begin{bmatrix} 2 & 1 \\ -1 & 1 \end{bmatrix} \begin{bmatrix} v_{ab} \\ v_{bc} \end{bmatrix}$$

$$\boxed{\begin{bmatrix} v_q \\ v_d \end{bmatrix} = \frac{2}{3} \begin{bmatrix} \cos(\theta_e) & \sin\left(\theta_e + \frac{\pi}{6}\right) \\ \sin(\theta_e) & -\cos\left(\theta_e + \frac{\pi}{6}\right) \end{bmatrix} \begin{bmatrix} v_{ab} \\ v_{bc} \end{bmatrix}}$$; transformation used for measured line-to-line voltages

THIS PAGE INTENTIONALLY LEFT BLANK

LIST OF REFERENCES

[1] Karimi-Davijani, Sheikholeslami, Ahmadi, and Livani, "Active and Reactive Power Control of DFIG Using SVPWM Converter," Universities Power Engineering Conference, 2008. UPEC 2008. 43rd International.

[2] Energy & Environment, Last accessed April 2009 <http://change.gov/agenda/energy_and_environment_agenda/>.

[3] Paul C. Krause, Oleg Wasynczuk, and Scott D. Sudhoff. "Analysis of Electric Machinery and Drive Systems," John Wiley & Sons, 2002.

[4] Joseph E. O'conner, "Field Programmable Gate Array Control of Power Systems in Graduate Student Laboratories," Master's thesis, Naval Postgraduate School, 2008.

[5] Ayasun, Saffet and Chika O Nwankpa, "Induction Motor Test Using Matlab/Simulink and Their Integration Into Undergraduate Electric Machinery Courses," IEEE Transactions 48.1 (2005).

[6] Alexander. L. Julian, Notes for EC4130 (Advanced Electrical machinery Systems), Naval Postgraduate School, 2007 (unpublished).

[7] Andrew M. La Valley, "Design and Implementation of a Motor Incremental Shaft Encoder," Master's thesis, Naval Postgraduate School, 2008.

[8] Wikipedia, Space Vector Modulation, Last accessed 06 May 2009 <http://en.wikipedia.org/wiki/Space_vector_modulation>.

[9] Alexander L. Julain, "Digital Implementation of Naturally Sampled Space Vector Modulation," (unpublished).

THIS PAGE INTENTIONALLY LEFT BLANK

INITIAL DISTRIBUTION LIST

1. Defense Technical Information Center
   Ft. Belvoir, Virginia

2. Dudley Knox Library
   Naval Postgraduate School
   Monterey, California

3. Dr. Jeffrey Knorr
   Electrical Engineering and Computer Department
   Code EC/Ko
   Naval Postgraduate School
   Monterey, California

4. Dr. Alexander Julian
   Electrical Engineering and Computer Department
   Code EC/J1
   Naval Postgraduate School
   Monterey, California

5. Dr. Roberto Cristi
   Electrical Engineering and Computer Department
   Code EC/C1
   Naval Postgraduate School
   Monterey, California